

THESIS ON MECHANICAL ENGINEERING E91

**Aero-Acoustic Studies and Innovative  
Noise Control with Application to  
Modern Automotive Gas Exchange System**

RAIMO KABRAL

**TUT**  
**PRESS**

Tallinn University of Technology  
Faculty of Mechanical Engineering  
Department of Machinery

**This dissertation was accepted for the defence of the degree of Doctor of Philosophy in Engineering on May 25, 2015.**

**Supervisor:** Prof. Jüri Lavrentjev, Department of Machinery,  
Tallinn University of Technology, Estonia

**Opponents:** Prof. Antonio J. Torregrosa, Department of Thermal Engines and  
Machines, Polytechnical University of Valencia, Spain

Associate prof. Villu Mikita, Department of Technology,  
Estonian University of Life Sciences, Estonia

Defence of the thesis: June 25, 2015

Declaration:

*Hereby I declare that this doctoral thesis, my original investigation and achievement, submitted for the doctoral degree at Tallinn University of Technology has not been submitted for any academic degree.*



European Union  
European Social Fund



Investing in your future

Copyright: Raimo Kabral, 2015  
ISSN 1406-4758  
ISBN 978-9949-23-787-6 (publication)  
ISBN 978-9949-23-788-3 (PDF)

MEHHAOTEHNIKA E91

**Kaasaegse automootori gaasivahetussüsteemide  
aeroakustilised uuringud ja müra vähendamise  
innovaatilised meetodid**

RAIMO KABRAL



*Pühendatud maailma parimale reaalinete õpetajale,  
vanaemale ja minu suurimale kaasaelajale.*

*Tiiu*  
1932 – 2012



## Contents

List of publications .....	8
Abbreviations and symbols.....	9
Introduction.....	11
1 Experimental Aero-acoustic Investigation of Centrifugal Compressor.....	16
1.1 Experiments .....	18
1.2 Coupling between aerodynamic and acoustic fields .....	20
1.2.1 Method .....	20
1.2.2 Results and discussion .....	21
1.3 Reflection-free sound generation .....	22
1.3.1 Method .....	22
1.3.2 Results and discussion .....	24
2 Optimization of Compact Flow Duct Silencer .....	27
2.1 Finite element model.....	29
2.2 Proposed method.....	31
2.3 Sound attenuation mechanisms in optimized design .....	33
2.4 Results and discussion .....	34
3 Development of Absorptive Flow Duct Element .....	39
General conclusions.....	44
References.....	46
Acknowledgements.....	50
Abstract.....	52
Kokkuvõte.....	53
Appendix.....	55
Paper I.....	57
Paper II.....	65
Paper III .....	75
Paper IV .....	85
Curriculum Vitae .....	97
Elulookirjeldus.....	99

## List of publications

The present doctoral dissertation is based on the following peer reviewed publications:

- Paper I* Kabral, R., Rammal, H., Abom, M.  
Acoustical methods for investigating turbocharger flow instabilities.  
*SAE Technical Paper Series*, 2013, Paper no. 2013-01-1879,  
doi:10.4271/2013-01-1879.
- Paper II* Kabral, R., Du, L., Åbom, M., and Knutsson, M.  
A Compact silencer for the control of compressor noise.  
*SAE International Journal of Engines*, 2014, 7(3), 1572-1578,  
doi:10.4271/2014-01-2060.
- Paper III* Kabral, R., Auriemma, F., Knutsson, M., Åbom, M.  
A new type of compact silencer for high frequency noise.  
*Proceedings of 9th International DAAAM Baltic Conference,  
Tallinn, Estonia, April 24-26, 2014.*
- Paper IV* Kabral, R., Rammal, H., and Lavrentjev, J.  
Acoustic studies of micro-perforates for small engine silencers.  
*SAE Technical Paper Series*, 2012, Paper no. 2012-32-0107,  
doi:10.4271/2012-32-0107.

Copies of these articles are included in the Appendix.

## Approbation

1. 17th SAE/JSAE Small Engine Technology Conference, 8-10 November, Sapporo, Hokkaido, Japan (2011);
2. 18th SAE/JSAE Small Engine Technology Conference, 16-18 October, Madison, Wisconsin, USA (2012);
3. Euroscience Open Forum, 11-15 July, Dublin, Ireland (2012);
4. SAE 2013 Noise and Vibration Conference and Exhibition, 20-23 May, Grand Rapids, Michigan, USA (2013);
5. 9th International DAAAM Baltic Conference on Industrial Engineering, 24-26 April, Tallinn, Estonia (2014);
6. Baltic Nordic Acoustic Meeting, 2-4 June, Tallinn, Estonia (2014); and
7. 8th International Styrian Noise, Vibration and Harshness Congress, 2-4 July, Graz, Austria (2014).

## Abbreviations and symbols

BPF	– Blade Passing Frequency
CCGEx	– The Competence Center for the Gas Exchange
IC	– Internal Combustion
MPP	– Micro-Perforated Panel
SAE	– International Society of Automotive Engineers
Mic.	– Microphone
OP	– Operating point
S-matrix	– Acoustic Scattering Matrix
SA	– Sound Absorbed
SR	– Sound Reflected
TL	– Transmission Loss
$A$	– area of the flow channel cross-section, $m^2$
$D$	– diameter of the flow channel, m
$E$	– two by two unitary matrix
$G$	– one sided cross-spectrum
$G_s$	– acoustic source cross-spectrum matrix, $Pa^2$
$H$	– frequency response function
$H_m^{(n)}$	– Hankel function of n:th kind and m:th order
$K_0$	– acoustic wave propagation constant
$L_p$	– sound pressure level, dB
$M$	– mean flow Mach number
$M_g$	– the grazing flow Mach number of the micro-perforate
$N$	– Fast Fourier Transform of the measured pressure signal, Pa
$O$	– Fast Fourier Transform of the loudspeaker driving signal, V
$Q_m$	– acoustic monopole source, $s^{-2}$
$P$	– acoustic power, W
$R$	– acoustic reflection coefficient
$R_e$	– the radius of the expansion chamber, m
$R_s$	– the surface resistance of the micro-perforated panel, $Pa \cdot s \cdot m^{-1}$
$R$	– the reflection matrix of test rig terminations

- $\mathbf{S}$  – acoustic scattering matrix  
 $\mathbf{S}_p$  – acoustic power scattering matrix  
 $T$  – acoustic transmission coefficient  
 $\mathbf{T}$  – transformation matrix of acoustic wave  
 $Z$  – normalized acoustic impedance  
 $Pr$  – Prandtl number
- $a$  – the cross-section height of the rectangular channel, m  
 $c$  – the speed of sound,  $\text{m}\cdot\text{s}^{-1}$   
 $d$  – the slit width of the micro-perforated panel, m  
 $f$  – frequency,  $\text{s}^{-1}$   
 $i$  – unit imaginary number ( $i^2 = -1$ )  
 $k$  – wavenumber,  $\text{m}^{-1}$   
 $k_s$  – the shear wave number of the aperture  
 $\mathbf{n}_r$  – the normal unit vector of the flow channel surface  
 $p$  – acoustic pressure, Pa  
 $\mathbf{p}^S$  – acoustic source strength vector, Pa  
 $q_d$  – acoustic dipole source,  $\text{N}\cdot\text{m}^{-3}$   
 $r$  – the radius of the flow channel, m  
 $r_s$  – the normalized acoustic resistance of slit type micro-perforated panel  
 $s$  – share wave number  
 $t$  – the thickness of the micro-perforated panel, m  
 $x$  – axial co-ordinate, m  
 $x_s$  – the normalized acoustic reactance of slit type micro-perforated panel
- $\beta$  – the grazing flow coefficient of the micro-perforated panel  
 $\gamma$  – the ratio of specific heats  
 $\lambda$  – eigenvalue  
 $\mu$  – dynamic viscosity,  $\text{Pa}\cdot\text{s}$   
 $\nu$  – kinematic viscosity,  $\text{m}^2\cdot\text{s}^{-1}$   
 $\rho_0$  – density,  $\text{kg}\cdot\text{m}^{-3}$   
 $\sigma$  – the perforation ratio of the micro-perforated panel  
 $\omega$  – angular frequency,  $\text{s}^{-1}$

## Introduction

In modern automotive engine design, large part is determined by the European Commission emission limits known as Euro 6 [1] and customer demand for continuously reduced fuel consumption while still preserving the power output. The achievement of these contradictory goals requires conceptual changes in the classical internal combustion (IC) engine design. Therefore, today the concept of engine downsizing or right sizing, as it is known in truck engineering, is well adapted industry standard [2, 3, 4, 5]. The essence of the concept relays on reducing the IC engine capacity while increasing the charge air pressure [6]. As a consequence indicated fuel conversion efficiency is improved by increasing the indicated mean pressure. Although, the same result can also be achieved by rising the volumetric compression ratio, it is not preferable choice because of the higher combustion temperature, and thus increased  $\text{NO}_x$  emissions.

The idea of implementing unexploited enthalpy of hot exhaust gases for driving the inlet charger dates from early 20th century aviation where the loss of air density in high altitudes resulted in the loss of the IC engine power output. Devices of such principle are referred to as turbochargers (Fig. 1) and generally they consist of turbine coupled to centrifugal compressor. While turbine transforms recovered enthalpy into mechanical energy, the centrifugal compressor utilizes this energy to provide high pressure charge air delivery. Nowadays in the IC engine industry, turbochargers are used for efficiency reasons, and thus they carry a key role in the engine downsizing concept [7, 8].

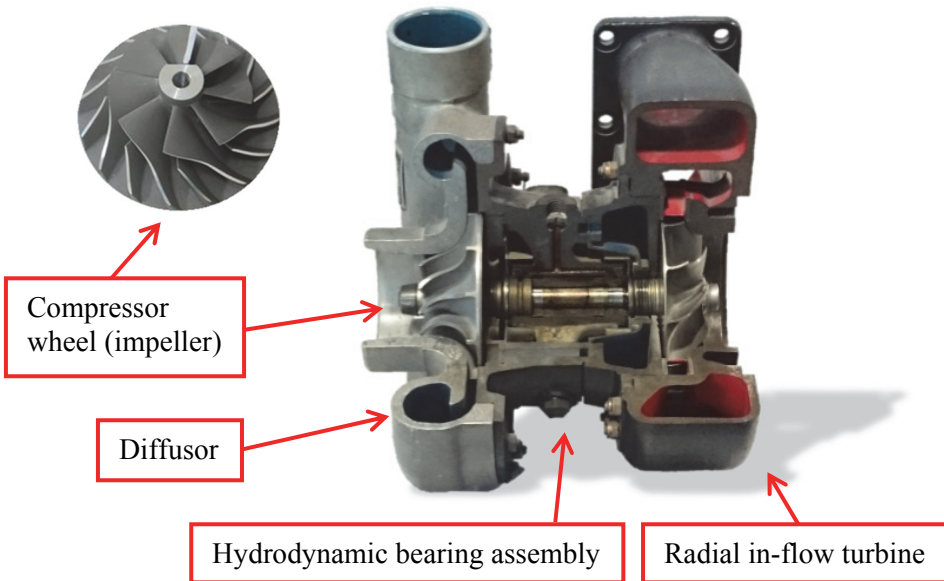


*Figure 1. A photo of an automotive turbocharger cutaway and an unassembled compressor impeller.*

A strong majority of automotive IC engines currently in the production are based on the downsizing concept and are equipped with turbocharger. Therefore, the number of turbochargers manufactured has increased during recent years tremendously. Nevertheless, the problem of having mass flux range of the compressor narrower than the engine demand, yet remained [8, 9 and 10]. In case of substantially downsized engine, the operation without high pressure charge results in the significant and unaccepted deficiency in power output. Moreover, future perspective is ultra-downsized engines [11] where the IC engine capacity is reduced even further, and thus the charge pressure must be even higher – three stages of turbochargers are planned in the concept!

The operating range of the centrifugal compressor is given by the 2D graph referred to as compressor map (Fig. 2). In the graph, horizontal axis denotes mass flow that is corrected according to the inlet temperature and pressure, while the vertical axis represents the ratio of total outlet pressure over the total inlet pressure. Consequently, the designed operating range is given as an “island” in the compressor map. Contours within the island indicate different efficiency levels of the compressor and solid lines across the map correspond to the constant rotational frequency of the rotor (Fig. 1). In addition, the island of the designed operating range is bounded by so called “surge line” at left hand side and a “choke line” at the right.

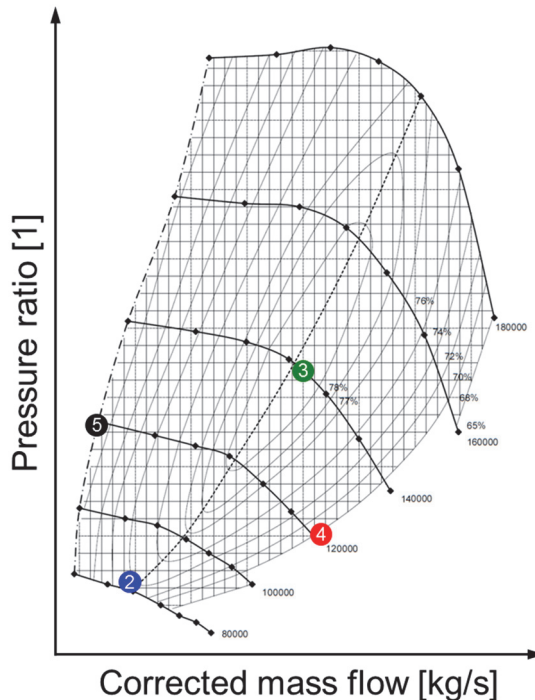


Figure 2. The compressor map determining the designed operating range of the centrifugal compressor.

In the designed operating range the compressor can provide continuous pressurized air delivery with acceptable efficiency. Exceeding the mass flow range, bounded by the choke line, the efficiency of the machine drops. On the contrast, the whole system is driven into destructive unstable state as the flow is reduced beyond the barrier posed by the surge line. Therefore, current industrial practice is to add preventive safety margins on the compressor map which can be as large as 20%. This unexploited part of the mass flow range could be efficiently implemented if the inception of the surge phenomena could be precisely predicted or if appropriate counteractions could be taken.

The centrifugal compressor surge pathology was recognized directly after it was invented [see e.g. 12]. When the back pressure of the coupled system becomes too high, for a given mass flow, the compressor cannot maintain stable discharge pressure and flow reversal occurs. This results in the large and often violent mass flow oscillation in the whole system, thus making the surge a system phenomenon [13, 14 and 15]. Although, the initiation of the surge is not fully understood, it is agreed that before global surge condition, local flow instability called rotating stall occurs [16, 17, and 18].

The phenomena of rotating stall in centrifugal compressor was first observed in 1945 by Cheshire [12]. In case of the rotating stall in the compressor, the stalled flow cell propagates along the circumference of the impeller in the reverse direction. Therefore, the resulting rotational frequency of the rotating stall is a fraction of shaft frequency, commonly observed close to the half of shaft frequency [see e.g. 16, 17]. In case of axial machines, a rotating stall is the initiation mechanism of full compressor stall [19]. Therefore, Oakes et al. investigated the nature of these self-induced circumferential flow distortions and possible relation with the surge initiation in the centrifugal compressors [17]. They observed growing flow distortion approximately at 0.6 of the shaft frequency while approaching to, as well as during the surge, with the exclusion of the phase of the pressure recovery. Despite that, they could not confirm that local stall initiates the global axisymmetric phenomena of surge.

It is believed herein that not only the surge is a system phenomenon, but also the initiation of the surge is related to the dynamics of the whole system, possibly involving acoustical properties of the compressor and the coupled system. Although the surge has been studied by many authors and institutions, the role of the acoustic field in the surge initiation has not been investigated. In addition, acoustics of the turbochargers generally have not received that much attention regardless the fact that related problems have been reported by the industry [see e.g. 4, 20, and 21]. Therefore, it is of importance to investigate the in-duct acoustic field of the centrifugal compressor in detail.

An approach based on circumferentially distributed microphone array, at one cross-section of the inlet duct and at the diffuser, was used by Lawless and Fleeter in [22] to identify the spatially coherent modes of the rotating stall. The location of these microphone arrays were relatively close to the impeller (1.8 cm at the inlet) i.e. the pressure was measured in incompressible acoustic near field.

Moreover the contribution of additional noise, originating from duct system discontinuities and other possible sources, affected the measurements. A rotatable circumferential microphone array was used by Raitor and Neise in [23] to resolve spatial distribution of acoustic modes at the inlet duct of the centrifugal compressor. In addition, they used another circumferential microphone array further upstream to determine the averaged sound power level according to the ISO 5136 standard [24]. Although this paper treats the full audible frequency range and presents new findings regarding the dominating noise sources at different regimes, all the results presented are measured under the assumption of dominating sound field from the machine. In case of low frequency sound, this assumption is arguable. Figurella et al. measured in-duct time resolved pressure fluctuations by means of wall mounted piezoelectric pressure transducer upstream of the compressor inlet [21]. Additionally, they measured sound pressure level radiated by the bell mouth inlet of the compressor in the semi-anechoic room. Even though, the intention of this measurement setup was reproducing the realistic application, which is not perfect in perspective of fundamental research, they observed that the blade passing frequency (BPF) dominates the generated sound field only at high flow rates. In addition, at the mid to low flow rates the contribution from BPF was significantly reduced and low frequency content started to dominate. While the methods used in previously discussed works are based on the reduction of reflections in different extents, the detailed decomposition of acoustic field was performed in [25] in order to determine the transmission of the incident acoustic power through the centrifugal compressor. Although, currently, the detailed decomposition cannot be performed in the entire audible frequency range, it has the advantage of providing more accurate results as all the contributions of the acoustic field are identified. This makes the approach adequate for the in detail and accurate aero-acoustic investigation of the centrifugal compressor.

All the results from previously discussed investigations indicate a very high level of noise generated by the centrifugal compressors. Moreover, the problem of high level of compressor noise at the IC engine inlet have been reported also by the passenger car as well as truck manufacturers. Noise control techniques currently applied are mainly based on the principle of the Helmholtz resonator, i.e. the generated sound is reflected back to the compressor. In this solution the dissipation of the sound depends on the source absorbing ability. Moreover, the resonators are relatively sensitive to the varying flow rates and the location in the system. In addition, the attenuation provided is often of narrow band type which makes the design complicated when noise sources of varying frequency, such as compressors, are considered. Therefore, substituting reflective resonators with dissipative noise control solutions could provide an advantage in terms of robustness and simplicity in the design process.

Traditionally dissipative flow duct silencers are based on fibrous materials. Nevertheless, several problems can occur when this type of materials are integrated in the gas exchange system. For instance, the fibers can pollute

environment or cause failure of the engine and other essential components. Therefore, it is of interest to produce acoustic energy absorption by utilizing other innovative materials. Alternatively, the acoustic energy dissipation can be produced by means of small apertures whose dimensions are in the order of acoustic boundary layer [26]. Such innovative noise control materials are referred to as micro-perforated panels (MPP) and recent development of these materials have led to the mass-production sheet material, branded as Acustimet™ [27]. The core material of this MPP is aluminum, hence making it appropriate for the IC engine inlet noise control applications. On another hand, the hot temperature and possible particles in the exhaust gas prevent the use of this material at exhaust. Although, the unit prize in the small series production is relatively high, in certain cases the custom made MPP can fulfill challenging design constraints, thus justifying higher production cost.

### **Objectives of the study**

In this study the main objectives are:

- 1) to identify if acoustic field plays role in the initiation of global and axisymmetric flow phenomena referred to as centrifugal compressor surge;
- 2) to develop optimization method for innovative flow channel silencer based on the micro-perforated element; and
- 3) to develop custom micro-perforated flow channel element for high temperature conditions and apply the element in the exhaust silencer of Formula SAE race car prototype.

# 1 Experimental Aero-acoustic Investigation of Centrifugal Compressor

In general, the accurate and detailed investigation of acoustic field in flow-duct can be performed by implementing well established methods for duct networks. However, because of the experimental limitations, such methods are limited to 0th duct mode frequency range. In this mode the acoustic pressure over the cross-section of the duct is nearly constant i.e. acoustic waves are planar. In case of circular duct, the frequency of the first non-planar propagation is determined by the relation:

$$f_{01}^c = \frac{1.841c}{\pi D} \sqrt{1 - |M|^2}, \quad (1.1)$$

where  $D$  is the diameter of the flow channel,  $c$  and  $M$  are the speed of sound and mean flow Mach number respectively [28]. Hence, below that frequency (Eq. (1.1)) the one dimensional acoustic field can be assumed to consist of superposition of two opposite propagating waves. Such acoustic field is sketched in the centrifugal compressor inlet and outlet branches in the Fig. 1.1.

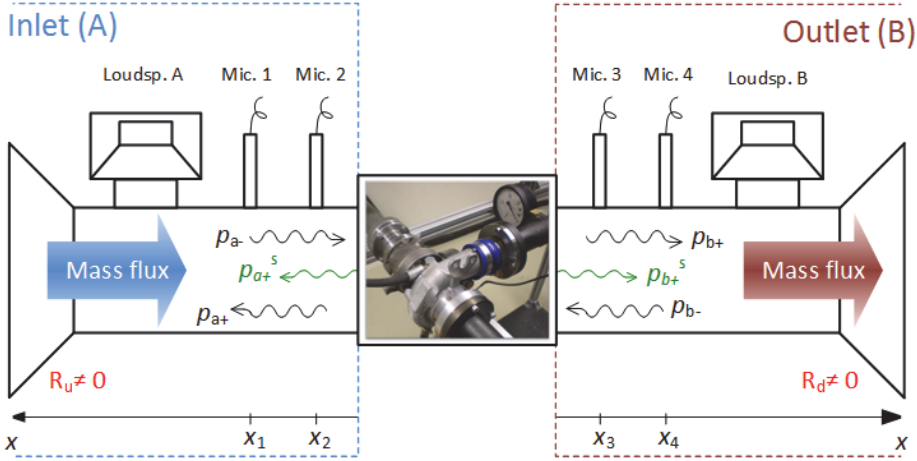


Figure 1.1. The simplified sketch of experimental setup, where  $p$  is acoustic pressure,  $R$  is the acoustic reflection coefficient, superscript  $S$  denotes the acoustic source term and mass flux refers to the mean flow.

In order to perform the wave decomposition of planar acoustic field in flow-duct (Fig. 1.1), the acoustic pressure has to be known in at least two axial positions. In addition, the information regarding the wave propagation between these two positions is essential. By assuming acoustic pressure time dependence of  $i\omega t$  and isentropic wave propagation in the flow-duct, the complex opposite propagating acoustic pressure wave amplitudes can be found by means of well-known Two-microphone technique (see e.g. [29] or [30]):

$$\begin{bmatrix} p_1 \\ p_2 \end{bmatrix} = \begin{bmatrix} e^{-ik_+x_1} & e^{ik_-x_1} \\ e^{-ik_+x_2} & e^{ik_-x_2} \end{bmatrix} \begin{bmatrix} p_+ \\ p_- \end{bmatrix}, \quad (1.2)$$

where plus and minus signs are referring to the propagation direction,  $k$  is the isentropic axial wave number,  $p$  is the acoustic pressure in frequency domain, and  $x$  is the axial co-ordinate (Fig. 1.1). The wave number in Eq. (1.2) is defined as:

$$k_{\pm} = \frac{\omega}{c(1 \pm M)}, \quad (1.3)$$

where  $\omega$  is the angular frequency.

Generally, the dissipation of the acoustic energy occurring in the long propagation distance and in presence of mean flow cannot be neglected. Therefore, the assumption of isentropic propagation is not valid and model for dissipation has to be applied. As was suggested by Dokumaci in [31], the visco-thermal damping in the wave propagation can be accounted by altering the isentropic wave number  $k$  (Eq. (1.3)):

$$k_{\pm} = \frac{\omega K_0}{c(1 \pm K_0 M)}, \quad (1.4)$$

where  $K_0$  is the propagation constant. Based on the well-known Kirchhoff dispersion relation, the propagation constant is expressed as:

$$K_0 = 1 + \left( \frac{1-i}{s\sqrt{2}} \right) \left( 1 + \frac{\gamma-1}{\sqrt{Pr}} \right), \quad (1.5)$$

where  $s$  is the shear wave number,  $\gamma$  is the ratio of specific heats and  $Pr$  is the Prandtl number. The shear wave number is defined as:

$$s = r \sqrt{\frac{\rho_0 \omega}{\mu}}, \quad (1.6)$$

where  $r$  is the duct radius,  $\rho_0$  and  $\mu$  are the density and dynamic viscosity of undisturbed gas.

The implementation of previously described method enables to decompose the overall airborne sound field in the inlet as well as in the outlet branches of centrifugal compressor. Furthermore, if the compressor operation is stable throughout the measurement, and therefore time invariant, the acoustic transmission and reflection properties can be determined.

Acoustic n-port models have been used for decades to characterize the separate elements and predict the overall duct network acoustical properties. Depending on the purpose, the n-port characterization of a duct network element can be represented by either in transmission matrix or in scattering matrix (S-matrix) form. The latter is preferable herein, as it describes the wave interaction problem explicitly [30].

The S-matrix [30] of acoustic 2-port is formulated by means of determined pressure wave amplitudes (Eq. (1.2)), in the inlet and outlet branches of the centrifugal compressor, as:

$$\begin{bmatrix} p_{a+} \\ p_{b+} \end{bmatrix} = \underbrace{\begin{bmatrix} R_a & T_b \\ T_a & R_b \end{bmatrix}}_S \begin{bmatrix} p_{a-} \\ p_{b-} \end{bmatrix}, \quad (1.7)$$

where  $R$  and  $T$  are complex reflection and transmission coefficients respectively,  $S$  is the acoustic S-matrix, subscripts  $a$  and  $b$  are referring to the inlet and outlet branches of the compressor.

In order to determine the four unknown coefficients in Eq. (1.7) (e.g. via matrix inverse operation), at least two linearly independent test cases have to be performed. It results in the reformulation of Eq. (1.7) as:

$$\begin{bmatrix} p_{a+}^I & p_{a+}^{II} \\ p_{b+}^I & p_{b+}^{II} \end{bmatrix} = \underbrace{\begin{bmatrix} R_a & T_b \\ T_a & R_b \end{bmatrix}}_S \begin{bmatrix} p_{a-}^I & p_{a-}^{II} \\ p_{b-}^I & p_{b-}^{II} \end{bmatrix}, \quad (1.8)$$

where superscripts  $I$  and  $II$  denote the first and the second test cases which can be realized by providing external acoustic excitation at different branches (Fig. 1.1) by using the Two-source measurement technique [32].

In case of high velocity turbulent flow, the pressure transducers will record the pressure fluctuation caused by the turbulence in addition to the sound. In order to suppress this contribution the correlation techniques can be applied. If the external excitation is used, the driving signal can be utilized as a reference signal and the best estimate of the acoustic pressure, in the least square sense, is obtained by the frequency response function [33], as:

$$H_{no}(f) = \frac{G_{no}(f)}{G_{oo}(f)} = \frac{N(f)^* O(f)}{O(f)^* O(f)}, \quad (1.9)$$

where subscript  $n$  and  $o$  refer to the driving and pressure signal respectively, capital letters  $N$  and  $O$  denote the Fast Fourier Transforms of respective signals,  $G$  is one sided cross-spectrum and superscript “\*” denotes complex conjugated quantity. As a consequence, the uncorrelated contribution in the pressure measurements will be suppressed and the acoustic S-matrix can be computed by implementing frequency response functions directly in Eq. (1.8). Nevertheless, if the unit of pressure is desired, it can be restored by further multiplying the frequency response function by the reference signal.

## 1.1 Experiments

The acoustic pressure data involved in present investigation have been provided by Tiikoja et al. [25]. Measurements have been carried out in the dedicated facility [34] of Competence Centre for Gas Exchange (CCGEx) [35] located in the KTH Royal Institute of Technology (Fig. 1.2).



*Figure 1.2. A photo of the test-rig in the facility for turbocharger acoustic measurements of the CCGEx.*

In the rig, a typical automotive turbocharger with vanless diffuser have been operated at five realistic operating points (OPs). The values of physical quantities determining these OPs are provided in Table 1.1 and graphical representation on the compressor map in the Fig. 2.

*Table 1.1. The operating conditions of the turbocharger.*

	<b>Pressure ratio</b>	<b>Corrected mass flow, kg/s</b>	<b>Rotational frequency, min<sup>-1</sup></b>
<b>OP 1</b>	1	-	-
<b>OP 2</b>	1.28	0.054	82 304
<b>OP 3</b>	1.85	0.119	141 643
<b>OP 4</b>	1.37	0.126	123 012
<b>OP 5</b>	1.71	0.050	120 168

The in-duct acoustic pressure data have been measured at six transducer positions along the compressor contour while the external excitation have been provided by means of loudspeakers at both branches. In addition, the acoustic pressure data have also been measured in the absence of external excitation.

## 1.2 Coupling between aerodynamic and acoustic fields

If a stable flow field in the centrifugal compressor is considered, the coupling is expected to occur in a form of strong dissipation of incident acoustic waves in small scale turbulence. However, when the mass flow is reduced beyond the surge line, the flow in different parts of the compressor will stall. While this abnormal compressor flow causes the occurrence of local flow instabilities, the global mass flow in the system still remains constant. Therefore, it is expected that these local flow instabilities can modulate incident acoustic waves resulting in the amplification of out-going waves.

### 1.2.1 Method

One of the frequently encountered problem, caused by the aero-acoustic coupling phenomena, is the whistling of the flow channel valves and orifices. In this case the whistling is caused by the modulation of in-going acoustic waves and the system response leading to the acoustic energy build up. In the studies of this phenomena the acoustic S-matrix have been proven to be a very useful information (see e.g. [36]). By setting up the acoustic power balance based on the experimental S-matrix, the acoustic energy dissipation or production can be identified [37] i.e. all the flow acoustic coupling effects are included in this matrix [36]. Therefore, it is believed that the coupling in centrifugal compressor, can also be identified by studying the experimental S-matrix (Eq. (1.7)).

In order to set up acoustic power balance by means of incident acoustic waves, and to provide clear and explicit equations, it is appropriate to introduce a new acoustic state variable  $\mathbf{x}$  which is related to the acoustic power as:

$$\mathbf{x}_{\pm}^{\dagger} \mathbf{x}_{\pm} = \langle P_{\pm} \rangle, \quad (1.10)$$

where  $P$  is the acoustic power and superscript  $\dagger$  denotes self-adjoint matrix (Hermitian transpose). In case of time averaged in-going sound power of the compressor, the variable is defined as:

$$\mathbf{x}_{-} = \begin{bmatrix} (1 + M_a) \sqrt{\frac{A_a}{\rho_{0a} c_{0a}}} \cdot p_{a-} \\ (1 - M_b) \sqrt{\frac{A_b}{\rho_{0b} c_{0b}}} \cdot p_{b-} \end{bmatrix}, \quad (1.11)$$

where  $A$  is the cross-section area of respective branch. Now by implementing the new acoustic state variable (Eq. (1.10)) together with previously determined S-matrix, the acoustic power output of the compressor for a given incident acoustic field can be expressed in following form:

$$\langle P_{out} \rangle = \mathbf{x}_{-}^{\dagger} (\mathbf{S}_P^{\dagger} \mathbf{S}_P) \mathbf{x}_{-} - \mathbf{x}_{-}^{\dagger} \mathbf{x}_{-}, \quad (1.12)$$

where  $\mathbf{S}_P$  is so called acoustic power scattering matrix and it is defined as:

$$\mathbf{S}_P = \begin{bmatrix} \frac{(1 - M_a)}{(1 + M_a)} \cdot R_a & \frac{(1 - M_a)}{(1 - M_b)} \sqrt{\frac{\rho_{0b} c_{0b} A_a}{\rho_{0a} c_{0a} A_b}} \cdot T_b \\ \frac{(1 + M_b)}{(1 + M_a)} \sqrt{\frac{\rho_{0a} c_{0a} A_b}{\rho_{0b} c_{0b} A_a}} \cdot T_a & \frac{(1 + M_b)}{(1 - M_b)} \cdot R_b \end{bmatrix}. \quad (1.13)$$

Furthermore, the incident acoustic power (Eq. (1.12)) can be normalized to 1 without the loss of generality [37]. Thus, the acoustic power balance of the compressor for a given incident acoustic field, normalized to 1 W, can be written as:

$$\langle P_{out} \rangle = \mathbf{x}_-^\dagger (\mathbf{S}_P^\dagger \mathbf{S}_P) \mathbf{x}_- - 1. \quad (1.14)$$

In addition, the acoustic power output, in Eq. (1.12), depends on the phase and amplitude relation between incident waves. Thus all the possible combinations must be considered and maximum potential power output can be obtained as [38]:

$$\langle P_{out}^{max} \rangle = \lambda_{max} - 1, \quad (1.15)$$

where  $\lambda_{max}$  is the positive and real maximum eigenvalue of the matrix  $(\mathbf{S}_P^\dagger \mathbf{S}_P)$ . The eigenvalue smaller than unity, in the Eq. (1.15), indicates the dissipation of incident acoustic power and the value larger than unity indicates the amplification.

### 1.2.2 Results and discussion

The method has been applied on the experimental acoustic pressure data of the automotive centrifugal compressor operating under realistic conditions (Fig. 1.2). The maximum potential power output (Eq. (1.15)) have been determined in five OPs and resulting eigenvalue spectrums are presented in the Fig. 1.3.

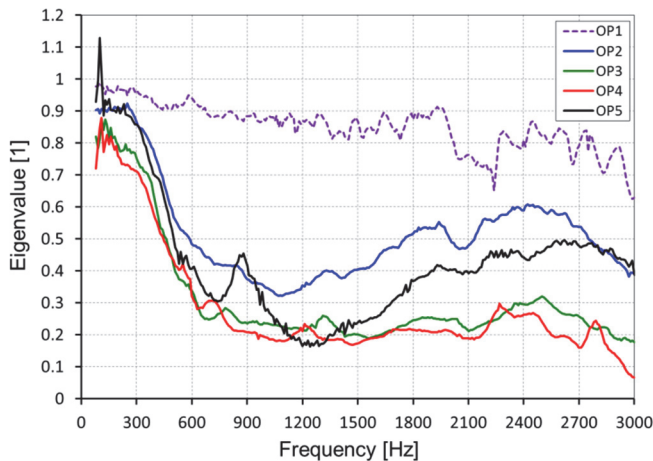


Figure 1.3. The maximum ratio of scattered acoustic power over incident acoustic power determined in five operating points (see Tab. 1.1).

In general, eigenvalues remain smaller than unity across the frequency range i.e. there is no net amplification of the incident acoustic power. In addition, three trends, linked with the mass flow rate (Tab. 1.1), can be distinguished. The constant low level of dissipation, i.e. eigenvalue close to one, expectedly corresponds to the stationary machine (OP1), while all other OPs show significantly higher level of flow induced acoustic losses. Moreover, there is a deviation in a form of well pronounced peak approximately at 900 Hz in case of the OP5 close to surge. This frequency corresponds to the shaft (impeller) rotational frequency multiplied by 0.45, i.e. where often flow instability of rotating stall has been observed by other authors [e.g. 16 and 17].

Based on these observations (Fig. 1.3), it is believed that the amplification of the incident acoustic power caused by the rotating stall (~900 Hz) at the OP5, appears as a sharp reduction of the dissipation because the amplification is insufficient for dominating overall losses. Hence, in perspective of initiating a surge condition, this amplification is irrelevant. However, the losses are very small at the low frequency range, and in particularly small when operating close to surge (OP5).

### 1.3 Reflection-free sound generation

In a plane wave frequency range (Eq. (1.1)) reflections from duct discontinuities are highly significant and absolutely reflection free terminations in experimental setups are rare (Fig. 1.1). Thus the overall sound field in compressor branches consists of several contributions including the reflections of the generated sound. In order to determine the sound generation characteristics of the compressor, the reflection-free sound has to be extracted.

#### 1.3.1 Method

The problem of determining the accurate aero-acoustic source data of ducted-fans is not new. Cremer suggested to treat such devices as two-port sources, already in 1971 [39]. This was followed by the development of experimental methods by Terao et.al [40] and Lavrentjev et al. [41] in 1990s. Although investigated fans in these works were mainly axial and of low pressure type, the same methods will be adapted to the centrifugal compressor herein.

The active properties, i.e. the contribution of sound generation, can be included in the passive two-port formulation (Eq. (1.7)) by means of superposition principle. Thus the resulting full two-port model takes the following form:

$$\begin{bmatrix} p_{a+} \\ p_{b+} \end{bmatrix} = \underbrace{\begin{bmatrix} R_a & T_b \\ T_a & R_b \end{bmatrix}}_S \begin{bmatrix} p_{a-} \\ p_{b-} \end{bmatrix} + \underbrace{\begin{bmatrix} p_{a+}^s \\ p_{b+}^s \end{bmatrix}}_{\mathbf{p}_s}, \quad (1.16)$$

where superscript  $s$  denotes the source term (Fig. 1.1) and  $\mathbf{p}_s$  is the source strength vector. However, it should be observed that in such formulation (Eq. (1.16)), the reflection-free conditions are assumed at the test rig terminations. Since this is rarely the case, the terminations have to be characterized and accounted for.

In order to describe the acoustic effects of test rig terminations, the acoustic one-port model is convenient choice as it originates from the same acoustic n-port theory. In addition, by assuming passive behavior i.e. no additional sound generation behind test rig terminations (Fig. 1.1), the reflection coefficients

$$R_u = \frac{p_{a-}^I}{p_{a+}^I} \quad \text{and} \quad R_d = \frac{p_{b-}^I}{p_{b+}^I} \quad (1.17)$$

are completely adequate for the characterization. Subscripts  $u$  and  $d$  in Eq. (1.17) refer to up- and downstream direction respectively.

Although, the reflection coefficients (Eq. (1.17)) can readily be obtained from previously determined complex pressure wave amplitudes, the approach is limited to the Two-source measurement technique [32]. Because of the assumption of passive terminations, the external excitation must not be provided in respective branch while characterizing the termination (Fig. 1.1). This requirement is fulfilled if at least two linearly independent test cases, necessary to compute the acoustic scattering matrix (Eq. (1.8)), are realized by providing the external excitation sequentially in both branches.

After determination of passive properties of the test rig, the second acoustic pressure measurement have to be conducted in absence of external excitation. By utilizing this pressure data and known passive properties of the test rig, the reflection-free source strength vector can be extracted from the overall airborne sound field according to following formulation [41]:

$$\mathbf{p}_s = (\mathbf{E} - \mathbf{S}\mathbf{R})(\mathbf{E} + \mathbf{R})^{-1}\mathbf{p}, \quad (1.18)$$

where  $\mathbf{p}$  is vector that contains the acoustic pressures measured in absence of external excitation,  $\mathbf{E}$  is a square unitary matrix and

$$\mathbf{R} = \begin{bmatrix} R_u & 0 \\ 0 & R_d \end{bmatrix}. \quad (1.19)$$

Since the acoustic pressure is measured at the microphone locations, the acoustic S-matrix and the reflection matrix of test rig terminations have to be transformed from reference cross-section ( $x = 0$  in the Fig. 1.1) to respective axial location  $x$  of the microphone. This is performed by means of transformation matrixes as:

$$\mathbf{S}^x = \mathbf{T}_+ \mathbf{S} \mathbf{T}_+^{-1} \quad \text{and} \quad \mathbf{R}^x = \mathbf{T}_+^{-1} \mathbf{R} \mathbf{T}_+, \quad (1.20)$$

where

$$\mathbf{T}_-(x) = \begin{bmatrix} e^{ik_a x_a} & 0 \\ 0 & e^{ik_b x_b} \end{bmatrix} \quad \text{and} \quad \mathbf{T}_+(x) = \begin{bmatrix} e^{-ik_a x_a} & 0 \\ 0 & e^{-ik_b x_b} \end{bmatrix}. \quad (1.21)$$

Furthermore, determined source strength vector can be transformed back to the original reference cross-section ( $x = 0$ ) by implementing the transformation matrix of positive propagation direction (Eq. (1.21)). This yields the expression of source strength vector of following form:

$$\mathbf{p}_s = \mathbf{T}_+^{-1}(x)(\mathbf{E} - \mathbf{S}^x \mathbf{R}^x)(\mathbf{E} + \mathbf{R}^x)^{-1}\mathbf{p}^x. \quad (1.22)$$

The flow velocities in the centrifugal compressor branches can reach high level and, as mentioned earlier, such a turbulent flow field causes the contamination of acoustic pressure measurement. Therefore, it is of interest to apply the correlation techniques also in case of Eq. (1.22). For the sake of the explicit expression a new constant

$$\mathbf{C}^x = \mathbf{T}_+^{-1}(\mathbf{x})(\mathbf{E} - \mathbf{S}^x \mathbf{R}^x)(\mathbf{E} + \mathbf{R}^x)^{-1} \quad (1.23)$$

is introduced in Eq. (1.22) and the source cross-spectrum matrix [41], based on source strength vectors, can be formulated as:

$$\mathbf{G}_s = \mathbf{p}_s^{x_{1,4}} (\mathbf{p}_s^{x_{2,3}})^\dagger = \mathbf{C}^{x_{1,4}} \begin{bmatrix} G_{x_2 x_1} & G_{x_3 x_1} \\ G_{x_2 x_4} & G_{x_3 x_4} \end{bmatrix} (\mathbf{C}^{x_{2,3}})^\dagger, \quad (1.24)$$

where  $x_1$  to  $x_4$  denotes the pressure transducer axial positions (Fig. 1.1). Since the correlation length of turbulence pressure perturbation compared to sound wave is small, the cross-spectrum estimated between different axial locations in Eq. (1.24) enables the suppression of turbulence related measurement error. Furthermore, such cross-spectrum source strength estimate is valid for both the periodic and random signals [41]. In addition, the auto-spectrums of reflection-free sound generation are obtained directly from the main diagonal of source cross-spectrum matrix, and the sound pressure level (SPL) can be computed according to the classical definition:

$$L_p = 10 \log_{10} \left( \frac{G_{xx}}{\tilde{p}_{ref}^2} \right), \quad (1.25)$$

where  $\tilde{p}_{ref} = 2 \cdot 10^{-5}$  [Pa] .

### 1.3.2 Results and discussion

The auto-spectrums of reflection-free sound generation of centrifugal compressor have been determined in case of four realistic operating points (Tab. 1.1 and Fig. 2). In the Fig. 1.4 and 1.5 the corresponding SPL spectrums for the inlet and outlet branches are presented respectively.

Considering very harsh measurement conditions in the presence of high pressure, temperature and velocity gradients, the overall quality of the obtained results in the Fig. 1.4 and 1.5 is remarkably good. In general, the spectrums consist of broadband contribution, which is  $\sim 7$  dB higher at the outlet, and characteristic high level tones. It is of common belief that the sound generated by the centrifugal compressor in the plane wave frequency range merely consists of broad band flow noise, since the BPF is higher. Based on these results (Fig. 1.4 and 1.5), it is proven to be misconception. In addition, while the broadband level can be associated to the turbulent flow noise characteristics, the origin of the high level tones is not obvious.

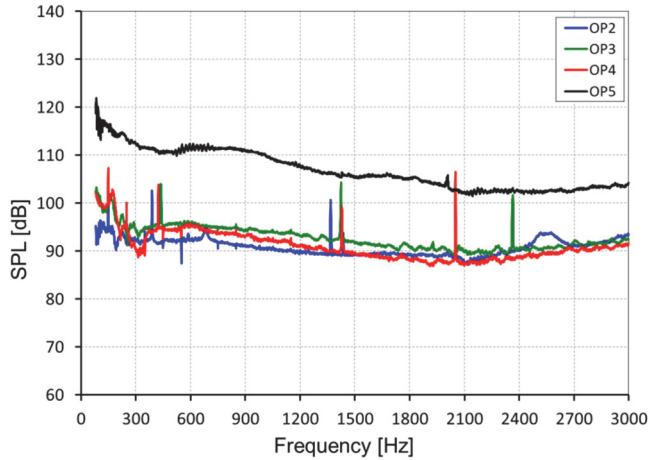


Figure 1.4. The generated sound pressure level at the inlet channel (low pressure) of the compressor at different operating conditions (Tab. 1.1).

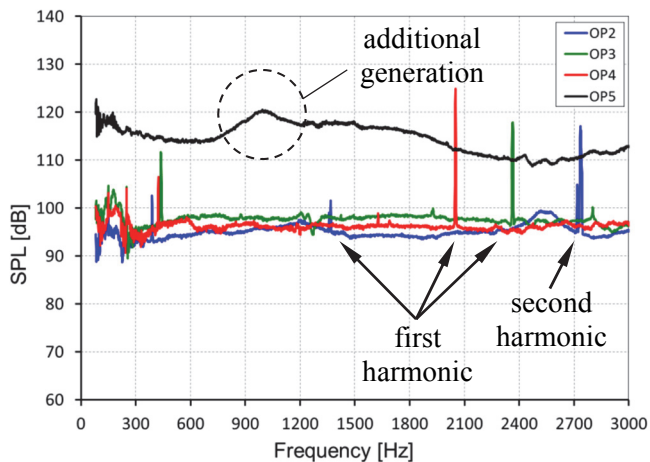


Figure 1.5. The generated sound pressure level at the outlet channel (high pressure) of the compressor at different operating conditions (Tab. 1.1).

The frequency of the characteristic tones in the Fig. 1.4 and 1.5 corresponds to impeller rotational frequency harmonics, and in general, the level is higher at the outlet branch. Furthermore, the level and also difference between the inlet and outlet are also increasing with mass flow rate. Based on the previous observations, it can only be concluded that these rotor harmonics are caused by the periodical flow phenomena (pressure fluctuation) at the high pressure side which is related with shaft rotational frequency. However, Figurella et al. in [21] recently suggested that the origin of rotor harmonic sound is related to geometrical imperfections. Nevertheless, based on the detailed results of sound generation presented herein (Fig. 1.4 and 1.5) or cursory results presented in [21], this cannot be confirmed.

The reduction of mass flow down to the designed operating limit i.e. the OP5 (Tab. 1.1 and Fig. 2) is causing a large broadband increase of the SPL in both inlet (Fig. 1.4) and outlet (Fig. 1.5) branch of the compressor. In addition, the broadband increase is masking characteristic harmonics completely at the outlet branch (Fig. 1.5). This is believably related to the flow separation in the impeller vanes as the reduction of mass flow will increase the angle of attack at impeller blades and, therefore, blades are operating near the stalled flow conditions. Furthermore, an additional contribution appears in the outlet sound generation spectrum (Fig. 1.5) approximately at frequency where previously the local amplification of incident sound was observed (Fig. 1.3). Arguably, it is the same flow instability of rotating stall that is manifested in both the sound scattering and generation.

It should be observed that a very high level of sound is generated in very low frequency range in case of the OP5 (Fig. 1.4 and 1.5). The level is approximately 120 dB at the outlet branch i.e. the pressure at that frequency is fluctuating with amplitude of  $\sim 30$  Pa. Furthermore, the dissipation of sound in this frequency range is almost negligible (Fig. 1.3). Therefore, it is believed that if certain boundary conditions are provided to the compressor, generated acoustic energy starts to accumulate in a system which eventually leads to the significant disturbance of aerodynamic field and thus can trigger a compressor surge.

The previous hypothesis is also consistent with the experimental findings in [42] where they found that a large volume, i.e. low natural frequency, at the compressor outlet branch is necessary to initiate the deep surge.

## 2 Optimization of Compact Flow Duct Silencer

The concept of compact flow duct silencer, treated herein, is the result of several works investigating the possibility of using mass production micro-perforated sheet material Acustimet™ for vehicle applications. A new type of flow duct silencer, based on the micro-perforated tube, made of Acustimet™ panels, was proposed by Allam and Åbom in [43]. The simplified sketch of this silencer is presented in the Fig. 2.1.

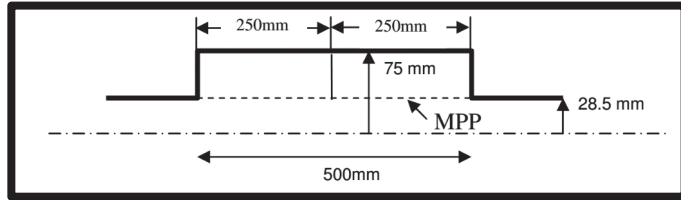


Figure 2.1. Geometry for the MPP muffler proposed in ref. [43]. Circular symmetry is assumed and the outer chamber is sub-divided into two or several cavities by rigid walls.

It was concluded in [43] that such silencer (Fig. 2.1) can provide non-fibrous alternative to the classical dissipative silencer. However, the expected drawback of having negligible sound damping at frequencies where the chamber length equals half wave length multiples, was recognized. Therefore the implementation of impenetrable separating baffles inside the cavity was suggested (Fig. 2.1), and as a consequence, the minima in sound damping is shifted to the higher frequency. In order to eliminate the minima completely, the locally reacting limit was formulated by Åbom and Allam in [44]. Essentially, the cavity is locally reacting up to the frequency where the length of the cavity is smaller than the half of wavelength. In addition, a custom Acustimet™ panel with larger apertures was also considered in [44] and it was concluded that the higher damping of sound in such silencer (Fig. 1.2) is achievable in case of larger apertures i.e. smaller acoustic resistance.

The starting point of the optimization herein is the silencer based on previously described development. The initial design constraints, determined by the application in the Volvo Car Corporation, are tabulated in the Tab. 2.1 and geometrical constraints are sketched in the Fig. 2.2.

Table 2.1. Design constraints for the compressor noise problem studied.

Parameter	Inlet/outlet duct radius, m	Average Mach number	Temperature, °C	Target frequency, kHz
Value	0.03	0.05	20	2.0

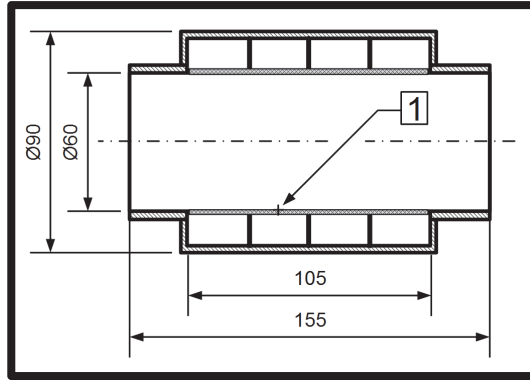


Figure 2.2. Geometry of the prototype MPP silencer studied. The arrow, marked 1, points at the micro-perforated sheet tube (Acustimet™), separating the main duct from the outer cavities.

In order to predict and compare the acoustic performance of different compact silencer configurations modeling has to be performed. In the 0th duct mode frequency range (Eq. (1.1)) and under the assumption of uniform mean flow profile, the silencer (Fig. 2.2) represents a two dimensional acoustic field problem, i.e. the analytical solution can be obtained by means of existing knowledge. However, for the sake of straightforward and robust implementation in the industrial applications, the commercial FEM software Comsol Multiphysics® [45] is utilized herein. In addition, the prototype built in the Volvo Car Corporation by means of rapid prototyping and employing a standard Acustimet panel™, is used for validation purposes. Moreover, the cavity of the prototype is also used to experimentally evaluate the results of the optimization. The photo of this prototype silencer is presented in the Fig. 2.3.

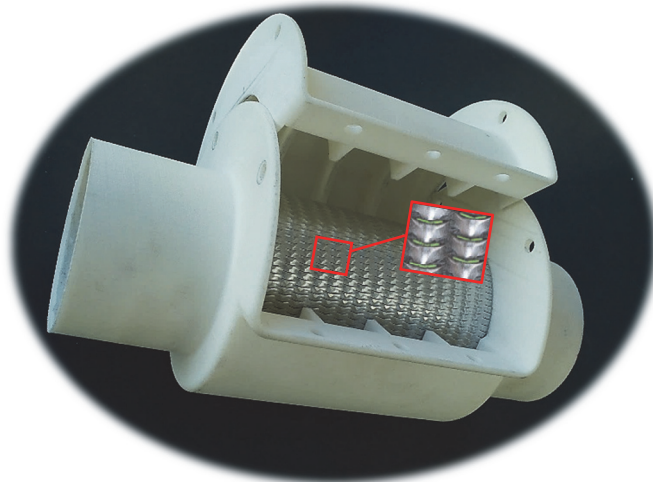


Figure 2.3. Photo of the compact silencer rapid prototype with magnified view of the micro-perforated (Acustimet™) sheet tube. Dimensions as in Figure 2.2.

## 2.1 Finite element model

The modeling in [43] was carried out by means of the FEM. In the model, the MPP was substituted by the pre-computed acoustic transfer impedance boundary condition. Thus, the resulting model consisted of two separate domains connected by this pre-defined boundary condition (Fig. 2.1). In addition, the convective flow effects were neglected in the main flow path while the grazing flow effects on the MPP were accounted for in the computation of the boundary condition. Such approach is reasonable for low mean flow Mach number applications [43].

In the present work, the mean flow velocity is relatively small compared to speed of sound (Tab. 2.1). Therefore, the approach used also in [43] is adequate to be applied herein. Moreover, as the cavity of the compact silencer considered is locally reacting, it can be modeled analytically and included in the boundary condition. It results in the complete acoustic boundary condition of flow path inside the cavity (Fig. 2.2). Consequently, the modeling domain is consisting only of the air volume in the flow channel of the silencer (Fig. 2.4).

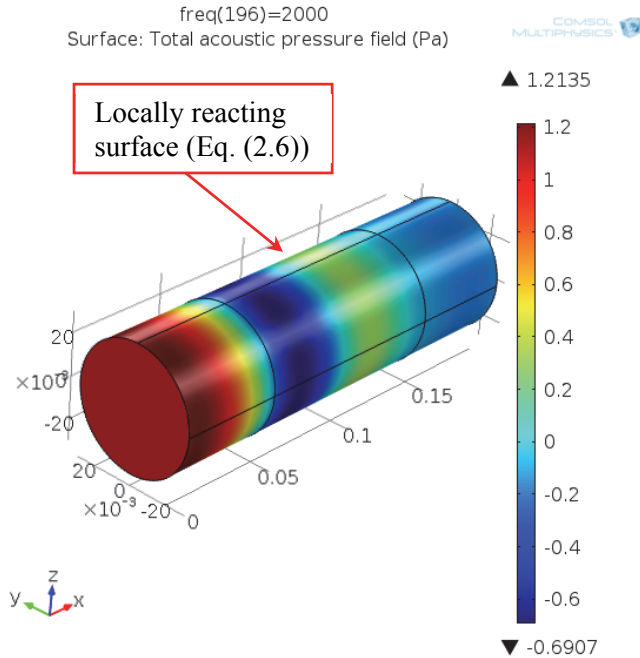


Figure 2.4. Acoustic pressure distribution at 2 kHz plotted on the FEM modeling domain for the prototype silencer with the standard MPP, i.e. not optimized configuration.

In the modeling domain, the inhomogeneous Helmholtz equation is solved in the lossless medium as:

$$\nabla \frac{1}{\rho} (\nabla p - \mathbf{q}_d) - \frac{k^2 p}{\rho} = Q_m, \quad (2.1)$$

where

$Q_m$  – monopole source; and

$q_d$  – dipole source.

The main duct is assumed to be impenetrable by sound waves i.e. the wall boundary condition is set as:

$$-\mathbf{n}_r \left[ -\frac{1}{\rho} (\nabla p - \mathbf{q}_d) \right] = 0, \quad (2.2)$$

where

$\mathbf{n}_r$  – the normal vector of the flow duct surface.

Along the cavity section (Fig. 2.2) the wall boundary is set as:

$$-\mathbf{n}_r \left[ -\frac{1}{\rho} (\nabla p - \mathbf{q}_d) \right] = -p \frac{i\omega}{Z_{wall}\rho c}, \quad (2.3)$$

where

$Z_{wall}$  – a normalized acoustic surface impedance.

In order to evaluate the acoustic performance of the silencer, the straightforward and widely implemented parameter is the transmission loss (TL):

$$TL = 10 \log_{10} \left( \frac{P_{in}}{P_{out}} \right), \quad (2.4)$$

where the subscripts *in* and *out* refers to the in-going direction at the inlet and out-going direction at the outlet of the silencer. This formulation considers one way propagation of sound, and thus it is convenient to use reflection-free terminations in the axial direction, which is realized by requiring that [46]:

$$-\mathbf{n}_a \cdot \left[ -\frac{1}{\rho} (\nabla p - \mathbf{q}_d) \right] + p \frac{ik}{\rho} + \nabla^2 p \frac{i}{2k\rho} = Q_m \quad (2.5)$$

at the modeling domain terminations (Fig. 2.4). By assuming that the reflected sound waves are negligible, the acoustic power ( $P_{out}$ ) at the outlet termination is obtained by integrating the sound intensity over the cross-section. At the inlet, an incident plane wave is prescribed using Eq. (2.5) i.e. the incident power ( $P_{in}$ ) can be directly computed.

## 2.2 Proposed method

In order to optimize the compact silencer (Fig. 2.3), it has to be realized that the acoustic performance is completely controlled by the acoustic impedance of the locally reacting surface ( $Z_{wall}$ ) inside the cavity (Fig. 2.2 and 2.4). This impedance is a consequence of the perforate and the adjoining cavity, acting together so that:

$$Z_{wall} = Z_{MPP} + Z_{cav} , \quad (2.6)$$

where

$Z_{MPP}$  – the normalized MPP impedance; and

$Z_{cav}$  – the normalized cavity impedance.

Guo et al. gave an overview in Ref. [47] on the semi-empirical modeling of micro-perforate transfer impedance. They also investigated the effect of flow and, based on experiments at KTH, they suggested correction terms for the acoustic impedance under grazing flow conditions. In addition, they showed that the acoustic mass end correction term for the slit types of MPP, e.g. as the Acustimet™ panel used here, can be neglected. The linear acoustic resistance  $\text{Re}(Z_{MPP})$  of the slit type MPP can be computed from:

$$r_s = \text{Re} \left\{ \frac{i\omega t}{\sigma c} \left[ 1 - \frac{\tanh(k_s \sqrt{i})}{k_s \sqrt{i}} \right]^{-1} \right\} + \frac{4R_s}{\sigma \rho c} + \beta \frac{M_g}{\sigma} , \quad (2.7)$$

and the reactance  $\text{Im}(Z_{MPP})$  from:

$$x_s = \text{Im} \left\{ \frac{i\omega t}{\sigma c} \left[ 1 - \frac{\tanh(k_s \sqrt{i})}{k_s \sqrt{i}} \right]^{-1} \right\} , \quad (2.8)$$

where

$k_s$  – the shear wave number of the aperture;

$t$  – the thickness of perforated panel;

$\sigma$  – the porosity of the perforated surface;

$\beta$  – a factor for grazing flow effects;

$R_s$  – surface resistance; and

$M_g$  – Mach number of grazing flow.

The shear wave number, which relates the aperture dimensions with the acoustic boundary layer thickness, is defined as:

$$k_s = d \sqrt{\frac{\omega}{4\nu}} , \quad (2.9)$$

where

$d$  – the slit width; and

$\nu$  – the kinematic viscosity of medium.

Finally, the surface resistance, which is a consequence of oscillating motion of the fluid on the surface of a perforated panel, can be found from:

$$R_s = \frac{1}{2} \sqrt{2\rho\omega\mu}. \quad (2.10)$$

The normalized linear resistance (Eq. (2.7)) is a sum of three terms. The first term analytically relates acoustic losses with viscous effects inside the apertures, whereas the last two terms empirically describe the acoustic losses outside the apertures. As also seen from Eq. (2.7) and Eq. (2.8) a grazing flow will affect (increase) the resistance but not affect the reactance.

The analytical model for the acoustic cavity impedance  $Z_{cav}$  has been derived and proposed in the [44] and is given by:

$$Z_{cav} = \frac{i \left[ H_0^{(1)}(kr) - \frac{H_1^{(1)}(kR_e)}{H_1^{(2)}(kR_e)} H_0^{(2)}(kr) \right]}{H_1^{(1)}(kr) - \frac{H_1^{(1)}(kR_e)}{H_1^{(2)}(kR_e)} H_1^{(2)}(kr)}, \quad (2.11)$$

where

$R_e$  – the radius of the expansion chamber, m; and

$H_m^{(n)}$  – the Hankel function of  $n$ :th kind and  $m$ :th order.

It was discovered in 1953 by L. Cremer that the maximum damping of pair of sound wave modes in the infinite rectangular duct with definite acoustic impedance on one side is obtained when they merge in the complex plane. The optimal wall impedance, so called Cremer impedance, was derived and expressed in the [48] as:

$$Z_{Cr} = (0.91 - 0.76i) \frac{ka}{\pi}, \quad (2.12)$$

where

$Z_{Cr}$  – the normalized surface impedance for theoretical maximum sound damping in an infinite rectangular duct; and

$a$  – the cross-section height of the rectangular duct.

By following the same principles as Cremer, B. J. Tester derived the optimal wall impedance expression for circular ducts in 1973. In addition, the mean flow correction was added under uniform mean flow assumption in the [49] as:

$$Z_{Cc} = (0.88 - 0.38i) \frac{kr}{\pi(1 + M)^2}, \quad (2.13)$$

where

$Z_{Cc}$  – the normalized surface impedance for theoretical maximum sound damping in a circular duct.

The essence of the optimization method proposed herein, is the matching of locally reacting surface impedance to the Cremer optimum (Eq. (2.13)). It should be noted that the reactance is produced by means of both the cavity (Eq. (2.11)) and the MPP (Eq. (2.8)) while the acoustic resistance is produced only by the MPP (Eq. (2.7)). Therefore, the resistance is matched first by determining corresponding MPP geometrical parameters. As a consequence, certain mass reactance is produced i.e. the reactance is positive and increasing with the frequency while the Cremer optimum suggests the negative reactance (Eq. (2.13)). This discrepancy is then eliminated by introducing corresponding cavity with required negative reactance (Eq. (2.11)).

While the concept of compact silencer as such is general, i.e. the acoustic resistance can be produced by any means, in the present work the resistance is produced by implementing the MPP. Since the resistance of the MPP can be approximated to a constant value across the frequency range, linearly increasing optimum resistance (Eq. (2.13)) can be realized only at the frequency where the maximum sound damping is desired (Tab. 2.1). (A detailed discussion regarding described issue can be found in the *Paper II* and *Paper III*.)

It should be noted that the optimal wall impedance expression (Eq. (2.13)) is derived by assuming infinite duct, i.e. in the 0th duct mode frequency range reflected waves cannot exist. Therefore, it is assumed that the proposed optimization technique will lead to the dissipative silencer. On another hand, the locally reacting surface in the compact silencer is with definite length. Thus the occurrence of reflections at the cavity interfaces are expected. In addition, the Cremer optimum impedance (Eq. (2.13)) equals zero in the trivial case of zero frequency ( $k = 0$ ) i.e. a perfect resonator with total reflection.

### 2.3 Sound attenuation mechanisms in optimized design

In the robust noise control solution of a duct network, the property of high attenuation should preferably be achieved in dissipative manner. Moreover, as was discussed previously (Fig. 1.3), the reflected sound waves in the inlet system of the modern IC engines can be responsible for triggering the surge condition. Therefore, it is also essential to reveal the sound damping mechanism to adequately evaluate the result of the optimization technique. To this aim, the distribution of sound power is followed by studying the acoustic S-matrix data. It is assumed that the differences in hydrodynamic pressure, temperature, air density and Mach number between the silencer branches are negligible. Consequently, the total acoustic power loss in the direction of sound propagation, i.e. the TL, can be computed as:

$$TL = 10 \log_{10} \left( \frac{1}{|T_a|^2} \right). \quad (2.14)$$

Now by considering the contribution of incident sound power that is not reflected and contribution that is transmitted, the sound absorbed (SA) is expressed in the logarithmic scale as:

$$SA = 10 \log_{10} \left[ \frac{1 - |R_a|^2 \frac{(1 - M)^2}{(1 + M)^2}}{|T_a|^2} \right]. \quad (2.15)$$

In addition, the contribution of sound power reflected (SR) is obtained in similar fashion as:

$$SR = -10 \log_{10} \left[ 1 - |R_a|^2 \frac{(1 - M)^2}{(1 + M)^2} \right]. \quad (2.16)$$

The set of these logarithmic parameters (Eq. (2.14), (2.15) and (2.16)) gives a detailed description of the silencer acoustic performance and the quantification of attenuated, absorbed and reflected sound power.

## 2.4 Results and discussion

The experimental validation of TL spectrum predicted by the simplified FEM model in absence of mean flow is presented in the Fig. 2.5. In addition, the theoretical TL spectrum computed by assuming the Cremer impedance (Eq. (2.13)) across all the frequency range is plotted for reference purposes.

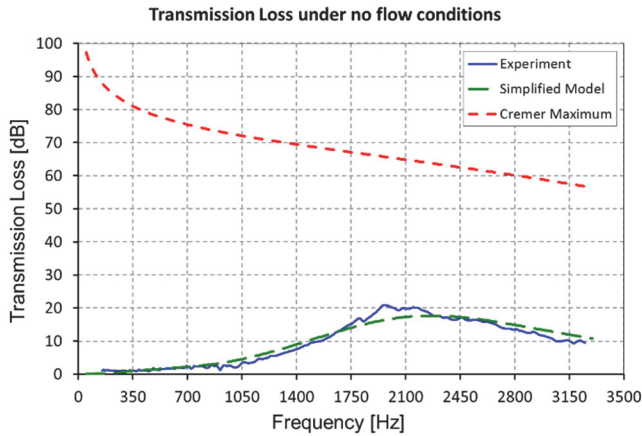


Figure 2.5. The results of experimental validation of sound transmission loss obtained by the simplified modeling approach (green and blue curves) for the prototype silencer (Figure 2.3). The red curve shows the theoretical maximum damping for the silencer using the so called Cremer impedance.

As can be observed in the TL graph (Fig. 2.5), the experimental spectrum is well captured by the simplified FEM model in absence of mean flow. Moreover, the predicted theoretical maximum TL curve shows that a much higher peak value at target frequency is obtainable by implementing the optimization method.

According to the proposed optimization technique, the appropriate set of the MPP geometrical parameters are determined by considering the initial design constraints (Tab. 2.1) and required resistance (Eq. (2.13)) while preserving the

original MPP thickness  $t$ . The resulting parameters are given and compared to the standard Acustimet™ MPP, used in the first prototype (Fig. 2.3), in the Table 2.2. Corresponding cavity radius  $R = 49$  mm, to match the reactance, is also determined.

Table 2.2. The geometrical parameters of the MPP studied. The optimized MPP is designed to match the Cremer resistance at 2 kHz for  $r = 30$  mm.

MPP panel	Thickness, mm	Perforation ratio	Averaged slit width, mm
Standard	1	0.043	0.095
Optimized	1	0.062	0.210

The predicted TL spectrums of silencer configuration of the new optimized design (Tab. 2.2), of the first prototype and also of theoretical Cremer impedance across the frequency range, in Mach 0.05 mean flow conditions, is presented in the Fig. 2.6.

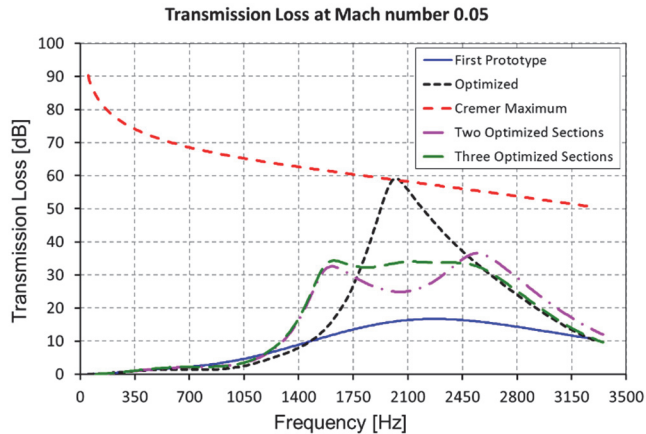


Figure 2.6. Predicted sound transmission loss for the prototype silencer for different configurations of MPP + cavity impedance. The optimized result is obtained by tuning the wall impedance based on Cremer's impedance at a target frequency 2000 Hz. By splitting the silencer in 2 or 3 sections tuned to 1500, 2500 Hz and 1500, 2000 and 2500 Hz, respectively, a more broad-band damping behavior is possible, see Table 2.3.

Expectedly, the much higher TL peak value of the optimized design (Fig. 2.6), compared to the first prototype, is laying on the theoretical reference curve at the target frequency of 2 kHz. Moreover, as the cavity is of locally reacting type, the total cavity length available can be divided into separately optimized sections at different target frequencies, thus producing close to a constant wideband dissipation. In addition, such a high attenuation, as  $> 60$  dB, would be challenging

to achieve in industrial applications because the in-duct air borne sound transmission is reduced in extent that other transmission mechanisms could dominate instead.

In order to produce wideband dissipation around the original target frequency (Table 2.1), the optimization has been reconsidered by splitting the total reacting length (Fig. 2.4) into separated optimized sections with different target frequencies. The new constraints are listed in the Tab. 2.3 and the corresponding predicted TL spectrums are presented in the Fig. 2.6.

Table 2.3. Design constraints for the optimized sections shown in Fig. 2.6.

Configuration name	Section 2		Section 1		Section 3	
	length, mm	freq., kHz	length, mm	freq., kHz	length, mm	freq., kHz
<b>Optimized</b>	-	-	96	2.0	-	-
<b>Two optimized sections</b>	48	1.5	-	-	48	2.5
<b>Three optimized sections</b>	48	1.5	20	2.0	28	2.5

As can be observed in the Fig. 2.6, by further dividing the compact silencer into separately optimized sections, a high TL in a wide frequency band (more than octave) is possible. Furthermore, close to constant TL ( $30 \pm 2$  dB), required in the noise control of sources with varying frequency signature, e.g. centrifugal compressors, is also achievable.

The cavity radius of the first prototype ( $R = 45$  mm) is not appropriate for experimental realization of optimized design for given initial design constraints. Nevertheless, the optimized design can be realized at different target frequency corresponding to the existing cavity radius. Therefore, a custom made Acustimet™ MPP (referred as Res. 0.25), whose transfer impedance matches closely the optimum condition, is utilized in the experimental evaluation of the optimization technique. In addition, another custom Acustimet panel (Res. 0.05) with relatively large apertures and producing a very small acoustic resistance (thus, not matching the Cremer optimum), is included for comparison purposes. On these modified prototype configurations, a standard experimental determination of the acoustic two-port data is carried out. The set of logarithmic parameters (Eq. (2.14), (2.15) and (2.16)), describing the sound power attenuation, dissipation and reflection, have been computed and presented in the Fig. 2.7. (Detailed information regarding prototype configurations can be found in the *Paper III*.)

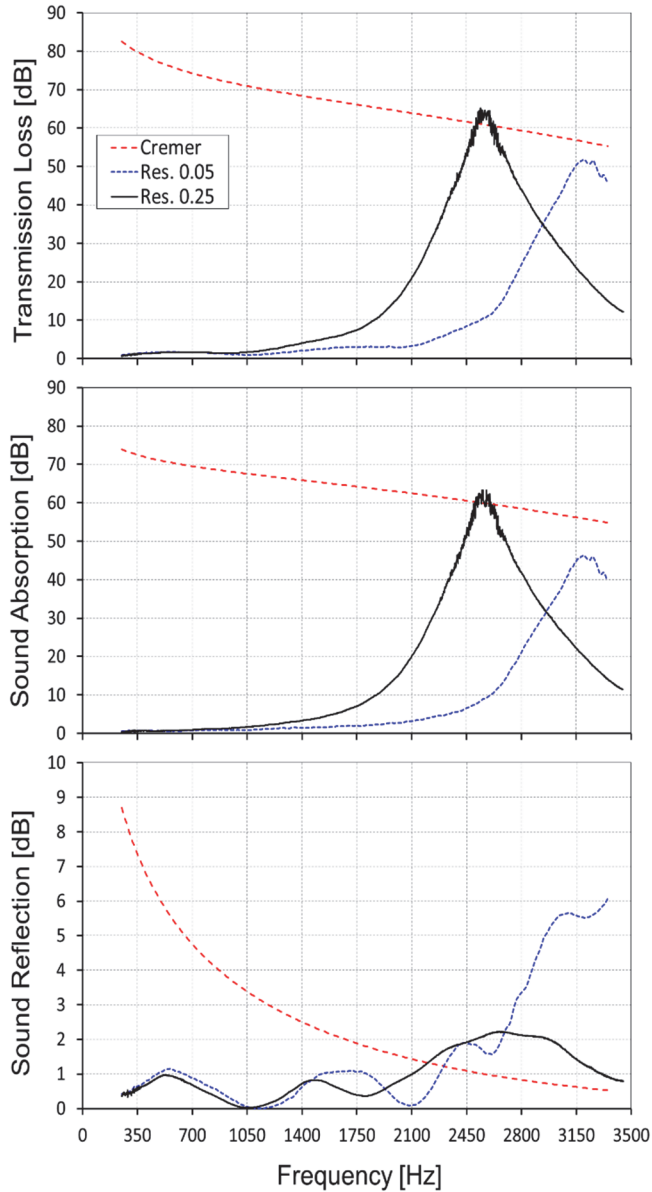


Figure 2.7. Acoustic performance parameters under 0.05 Mach mean flow conditions.

The experimental realization of optimized design (Res. 0.25) provides a very high and wide TL peak at predicted center frequency (the most upper graph in the Fig. 2.7). Nevertheless, the not optimized configuration with relatively small resistance provides a comparable TL performance, thus one configuration cannot be preferred over another based purely on the TL spectrums. In addition, it should be noted that the expected sharp TL peak is cut-off in case of the Res. 0.05. This

is believed to be a consequence of experimental difficulties with realizing completely sealed silencer cavity in the Res. 0.05 prototype configuration. Such imperfectly sealed cavity is expected to increase the indicated sound absorption and reduce reflection.

Now by further studying the sound power spectrums of absorption and reflection (Fig. 2.7), it is clear that the optimized prototype configuration Res. 0.25 provides absorptive type of sound attenuation with negligible reflected contribution i.e. the sound attenuation is achieved predominantly by the acoustic damping at the perforate. In addition, regardless of the imperfectly sealed cavity of the Res. 0.05 configuration, it provides more reflection compared to the Res. 0.25.

### 3 Development of Absorptive Flow Duct Element

Advanced computer aided technologies such as laser cutting, etching and jetting enable custom perforations to be applied not only on planar elements but also on tubular elements commonly used in flow-duct applications. Although this approach provides desired alternative when the standard MPPs cannot fulfill desired design criteria, often existing acoustic transfer impedance models are deficient because of their empirical nature in flow related terms. In addition, the process of interaction between sequential apertures of random geometrical shape is not fully clear. Therefore, an experimental approach has to be used for the evaluation of different custom perforations and also can be used for the determination of corresponding semi-empirical transfer impedance model.

In the development of the custom absorptive flow duct element herein, the application of Formula SAE (Fig. 3.1) silencer is considered. Since the temperature can reach up to 700 °C the use of aluminum based mass produced MPPs is not possible in this case. The dominating frequency of tailpipe noise is caused by the engine ignition frequency and its multiples, which means low frequency source. In general such low frequency sources can be attenuated most efficiently by means of the reflection. Hence, on one hand it is desirable to produce wideband losses by the dissipation of the MPP while on the other hand the perforation should provide an easy access to the expansion chamber for low frequency reflection purposes.

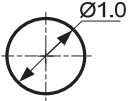
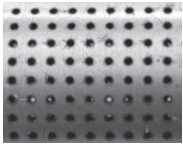
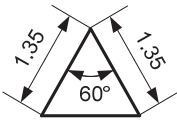
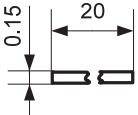
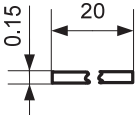
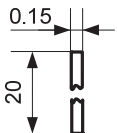


Figure 3.1. The Formula SAE race car prototype [50].

The main part of viscous losses in perforations are originating from acoustic boundary layer, thus it is expected that the aperture shape with longer perimeter and smaller area provides more wideband dissipation. Therefore, as the first approximation, the ratio of aperture perimeter over its area (PA ratio) is used as a characterizing parameter for aperture shapes. In this work the geometrical shapes of circle, triangle and slit with different PA ratios are used. In addition,

two different perforation ratios and slit orientations are considered. The resulting perforations are listed in the Tab. 3.1.

Table 3.1. A technical description of the perforated samples investigated.

Name	Aperture sketch, mm	P/A rat.	Photo	Porosity, %
Sample 1		4.0		10
Sample 2		5.1		10
Sample 3		13.4		10
Sample 4		13.4		2
Sample 5		13.4		2

Acoustical properties of tubular test samples are compared in the highly reflective measurement chamber sketched in the Fig. 3.2. The resulting acoustical properties are then compared in case of all the samples (Tab. 3.1) i.e. a so called black box approach by means of Two-port formulation is used. In addition to the five test samples, the reference case with conventional perforation provided of circular apertures of 3 mm in diameter and wrapped into 20 mm thick natural wool, is also included in the investigation.

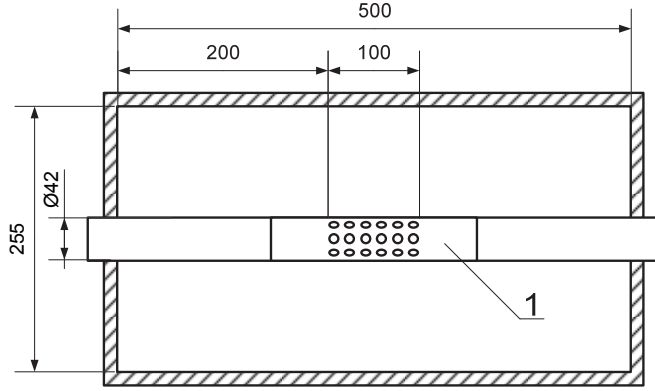


Figure 3.2. A measurement chamber incorporating a centrally positioned perforated test sample (1) (measurements are given in mm).

The appropriate parameter to evaluate the samples in this experimental setup (Fig. 3.2) is the absorption coefficient based on the experimental Two-port data and defined as:

$$A_a = 1 - \left[ |R_a| \frac{(1 - M_a)}{(1 + M_a)} \right]^2 - \left[ |T_a| \frac{(1 + M_b)}{(1 + M_a)} \right]^2. \quad (3.1)$$

In Eq. (3.1) the cross-sectional area, the speed of sound and the density of the fluid are assumed to be the same in both ports. Such absorption coefficient spectrum describes the acoustic power contribution that is not reflected nor transmitted, in case of incident sound power in port  $a$  normalized to 1 W. It includes the effects of dissipation at the perforate as well as the wave interference inside the cavity.

In the Fig. 3.3 the spectrums of experimentally determined absorption coefficients (Eq. (3.1)) of the high perforation ratio test samples are compared to the dissipative reference setup containing natural wool. In the graph, three distinguishable trends can be observed. The expected highest value wideband absorption coefficient spectrum of the reference configuration is caused by the dissipation in the natural wool. The relatively low value of wideband absorption can be observed in case of the sample 1 and 2, while the sample 3 provides a noticeable more wideband absorption believed to be originated from the dissipation at the perforate. Furthermore, the level of the characteristic peaks is also preserved, i.e. the incident acoustic waves can penetrate the perforation, and thus the potential attenuation of the expansion chamber can be implemented. In addition, it should be noted that the PA ratio of the sample 3, which provided significantly higher wideband absorption, is larger compared to the relatively similar values of the sample 1 and 2. Based on the results in the Fig. 3.3, it can be concluded that the PA ratio can be used as the first approximation to quantify the potential dissipation of the perforate. (More experimental results regarding all the test samples in the Tab. 3.1 can be found in the *Paper IV*)

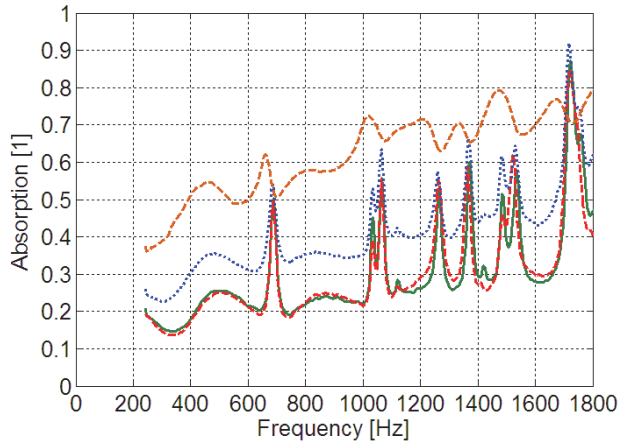


Figure 3.3. The absorption coefficient of sample 1 (red dashed), sample 2 (green solid), sample 3 (blue dotted) and reference setup with wool (orange dashed).

Based on the experimental results obtained by the black box approach, the lateral slit type perforation with perforation ratio of 10 percent is found to be suitable for the formula SAE straight-flow exhaust silencer prototype. The expansion chamber geometry is designed to maximize low frequency reflections by implementing all the space determined by the geometrical constraints. In addition, the chamber is irrationally divided in order to avoid attenuation minima at half wave length multiples of chamber length. The resulting prototype silencer is compared to the natural wool based conventional straight-flow silencer designed for the same vehicle. Characteristic technical data of the silencers are given in the Tab. 3.2.

The acoustic performance of the silencers (Tab. 3.2), in terms of TL (Eq. (2.14)) in realistic mean flow conditions, is compared in the Fig. 3.4. In general, the prototype silencer provides similar level of TL. Although at 1 kHz the conventional silencer has higher TL, a noticeably better low frequency attenuation is achieved by the prototype silencer. The resonant character of the prototype silencer TL curve is believed to be caused by its shell vibrations which is made of thin material. In addition to the comparable or higher TL, one should note the significant weight reduction of the prototype unit over the conventional silencer (Tab. 3.2).

Table 3.2. A technical description of the micro-perforated prototype silencer and the conventionally perforated silencer filled with fibrous material.

Name	Prototype	Conventional Silencer
<b>Simplified Sketch</b>		
<b>Photo</b>		
<b>Aperture Sketch</b>		
<b>Porosity</b>	10%	35%
<b>Mass</b>	1.43kg	1.81kg

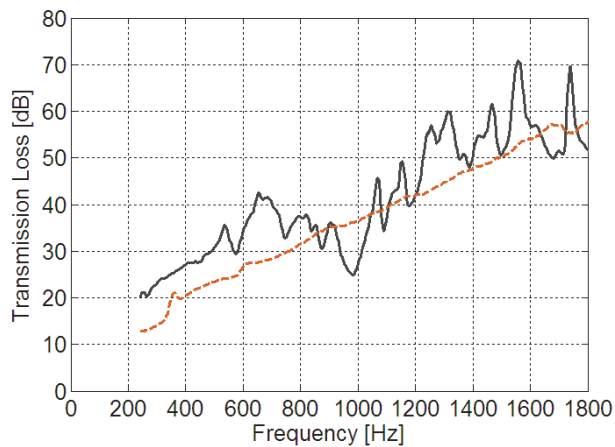


Figure 3.4. The transmission loss of the prototype silencer (gray solid) and conventional straight-flow silencer (orange dashed) in 20 m/s mean flow conditions.

## General conclusions

- 1) A significantly reduced dissipation of incident sound power at approximately half of shaft rotational frequency is observed in case of close to surge operation. It is believed that the local flow instability, known as rotating stall, modulates the incident acoustic waves and thus causes amplification. Nevertheless, the overall losses in the compressor flow field are higher and, as a consequence, there is no net amplification. Based on these observations, it is concluded that, from the perspective of acoustic initiation of surge, the amplification is found to be irrelevant.

In case of close to surge operation, a large broadband increase of flow generated sound (>10 dB) at both compressor branches is observed. In particular, high sound generation ~120 dB at very low frequency is also noticed. Considering the high level of sound generation and negligible dissipation of incident sound at low frequency, it is concluded that the compressor surge could be initiated by the accumulating acoustic energy which causes a significant disturbance of the aerodynamic field.

- 2) The compact silencer optimization technique, based on the Cremer optimum impedance concept, is proposed herein. It is demonstrated numerically and also experimentally that, by following the proposed optimization technique, a very high level of dissipative attenuation is achieved at desired target frequency. Moreover, almost constant high level of damping in a wide frequency band can be realized by splitting the silencer into separately optimized sections. Considering the numerical and experimental results, it can be concluded that such modular and wideband silencer is convenient for noise control in limited space conditions and can also handle sources with varying frequency signature, e.g. automotive compressors. In addition, as this type of optimized compact silencer is of dissipative type, it provides robust noise control which could also be relevant from the perspective of surge initiation.
- 3) A custom absorptive flow duct element is experimentally developed considering the requirements for exhaust silencer of a Formula SAE race car prototype. It is demonstrated that the prototype silencer provides similar or better transmission loss performance compared to the classical dissipative silencer while being significantly lighter in weight and not employing fibrous materials. In addition, the Formula SAE car, equipped with the silencer prototype, successfully passed the noise emission test and participated in the endurance race competition. Considering all the previous, it can be concluded that such element can be successfully used in the high-temperature flow duct applications.

## Scientific novelty

The first part of the present work represents, according to the author's knowledge, the first successful attempt to use accurate and detailed methodology to investigate the centrifugal compressor sound generation and surge initiation by

the acoustic field. The experimental results regarding the coupling between instable aerodynamic and incident acoustic fields in the centrifugal compressor, operating under realistic conditions, are presented. Moreover, the in-duct reflection-free sound is extracted from overall acoustic field at inlet and outlet branches i.e. the sound generation of the compressor is accurately determined.

The centrifugal compressor carries a key role in the modern IC engine technology and currently the phenomena of surge restricts the efficient use of this device. In the literature, the phenomena have received attention from many authors. However, all the works are focused on the aerodynamic field investigation while neglect the acoustic field. In addition, a limited number of publications consider the noise generation of the centrifugal compressors. Nevertheless, the methods used so far are, in essence, assuming completely reflection-free terminations.

In the second part of the work, the optimization technique for a compact silencer, based on micro-perforated panels, is proposed and validated by means of FEM modeling as well as experiments on dedicated prototype. While such innovative materials can provide a good alternative to the traditional fibrous materials, they need to be accurately designed for specific applications, making the optimization process essential.

The third part of the present work is dedicated to the experimental development of custom made absorptive flow-duct element. Based on the resulting element, a prototype silencer is build and compared with classical dissipative silencer incorporating fibrous materials. Moreover, the Formula SAE car equipped with the silencer prototype passed the noise emission test and the prototype silencer was used successfully during the competition. According to the knowledge of the author such type of silencers has not been used at the IC engine exhaust before.

### **Further work**

In order to further confirm the phenomena related to the flow instabilities of the centrifugal compressor observed herein, a new test campaign could be performed, i.e. approaching to the real limit of surge by following the constant rotational frequency line on the compressor map. In addition to the maximum eigenvalue, also the minimum eigenvalue as well as corresponding eigenvectors could be studied to further determine the compressor sensitivity to the boundary conditions in the system.

The experimental development of the absorptive flow duct element applied in the exhaust of Formula SAE race car, should be continued by determining the appropriate transfer impedance model for such elements. As a start, the planar elements could be used to determine the transfer impedance in the standard impedance tube. This could be then compared to the analytical solutions of different transfer impedance models currently available in the literature.

## References

1. Regulation No. 715/2007 of the European Parliament and of the Council of 20 June 2007 on type approval of motor vehicles with respect to emissions from light passenger and commercial vehicles (Euro 5 and Euro 6) and on access to vehicle repair and maintenance information. – *Official Journal of the European Union*, 2007, L171, 1-16.
2. Krebs, R. The new Audi 2.0l T-FSI motor – The first direct injection turbo gasoline engine at Audi. – *Proceedings of the 25th International Vienna Motor Symposium, Vienna, Austria. Vienna University of Technology, 2004, 247-254.*
3. Nishida, M., Isobe, R., Goto, T., Hanzawa, H., Aiga, S. The new 2.3l direct injection turbo gasoline engine from Mazda. – *Proceedings of the 14th Aachen Colloquium Automobile and Engine Technology, Aachen, Germany. Institute for Automotive Engineering of RWTH Aachen University, 2005, 939-960.*
4. Welter, A., Bruener, T., Unger, H., Hoyer, U., Brendel, U. The new BMW turbocharged six-cylinder inline petrol engine. – *MTZ worldwide*, 2007, 68, 2-6.
5. Meloni, M., Cacciatore, D., Dohmen, J., Ring, F., Hermsen, F.-G. Lamborghini Approach to Engine Downsizing – Engine Friction Modeling. – *SAE technical Paper Series*, 2013, Paper no. 2013-24-0088.
6. Stokes, J., Lake, T. H., Osborne, R. J., A gasoline engine concept for improved fuel economy – the lean boost system. – *SAE Technical Paper Series*, 2000, Paper no. 2000-01-2902.
7. Wirth, M., Mayerhofer, U., Piock, W. F., Fraidl, G. K. Turbocharging the DI gasoline engine. – *SAE Technical Paper Series*, 2000, Paper no. 2000-01-0251.
8. Ricardo, M.-B., Apostolos, P., Yang, M. Y. Overview of boosting options for future downsized engines. – *Science China Technological Sciences*, 2011, 54, 318-331.
9. Fraser, N., Blaxill, H., Lumsden, G., Bassett, M. Challenges for increased efficiency through gasoline engine downsizing. – *SAE International Journal of Engines*, 2009, 2(1), 991-1008.
10. Turner, J. W. G., Popplewell, A., Patel, R., Johnson, T. R., Darton, N. J., Richardson, S., Bredda, S. W., Tudor, R. J., Bithell, C. I., Jackson, R., Remmert, S. M., Cracknell, R. F., Fernandes, J. X., Lewis, A. G. J., Akehurst, S., Brace, C. J., Copeland, C., Martinez-Botas, R., Romagnoli, A., Burluka, A. A. Ultra boost for economy: extending the limits of extreme engine downsizing. – *SAE International Journal of Engines*, 2014, 7(1), 387-417.
11. Gheorghiu, V. Ultra-downsizing of internal combustion engines. – *Proceedings of the 1st International Conference on Engine Processes, Berlin, Germany. IAV Automotive Engineering, 2013, 2-35.*

12. Chesire L. J. The Design and development of the centrifugal compressors for aircraft gas turbines. – *Proceeding of the Institution of Mechanical Engineers*, 1945, 153(War Emergency Issue No. 12), 426-442.
13. Japikse, D. Stall, stage stall, and surge. – *Proceedings of the tenth turbomachinery symposium, College Station, Texas, USA. Texas A&M Engineering Experiment Station, 1981, 1-8.*
14. Oakes, W. C., Lawless, P. B., Fagan, J. R., Fleeter, S. High-speed centrifugal compressor surge initiation characterization. – *Journal of Propulsion and Power*, 2002,18(1), 1012-1018.
15. Galindo, J., Serrano, J. R., Climent, H., Tiseira, A. Experiments and modeling of surge in small centrifugal compressor for automotive engines. – *Experimental Thermal and Fluid Science*, 2008, 32(1), 818-826.
16. Stenning, A. H. Rotating stall and surge. – *Journal of Fluids Engineering (by The American Society of Mechanical Engineers)*, 1980, 102(1), 14-20.
17. Oakes, W. C., Lawless, P. B., Fleeter, S. A characterization of rotating stall behaviors in high and low speed centrifugal compressors. – *Proceedings of the International Compressor Engineering Conference, West Lafayette, Indiana, USA. Purdue University Press 1998, 773-778.*
18. Ishimoto, L., Silva, R. T., Rangel, J. S., Miranda, M. A., Audehove, F. N., Marques, B. S., Baldassarre, L., Puaut, C. Early detection of rotating stall phenomenon in centrifugal compressor by means of ASME PTC 10 type 2 test. – *Proceedings of the 41st Turbomachinery Symposium, Houston, Texas, USA. Texas A&M Engineering Experiment Station, 2012, 1-14.*
19. McDougall, N. M., Cumpsty, N. A., Hynes, T. P. Stall inception in Axial Compressors. – *Journal of Turbomachinery*, 1990, 112(1), 116-125.
20. Feld, H.-J., Aschenbrenner, S., Girsberger, R. Investigation of acoustic phenomena at the inlet and the outlet of a centrifugal compressor for pressure ratio 4.5. – *Proceedings of the ASME Turbo Expo, New Orleans, Louisiana, USA. The American Society of Mechanical Engineers Transactions, 2001.*
21. Figurella, N., Dehner, R., Selamet, A., Tallio, K., Miazgowicz, K. Wade, R. Noise at the mid to high flow range of a turbocharger compressor. – *Noise Control Engineering Journal*, 2014, 62(5), 306-312.
22. Lawless, P. B., Fleeter, S., Rotating Stall Acoustic Signature in a Low-Speed Centrifugal Compressor: Part 1 – Vanless diffuser. – *Journal of Turbomachinery*, 1995, 117(1), 87-96.
23. Raitor, T., Neise, W. Sound generation in centrifugal compressors. – *Journal of Sound and Vibration*, 2008, 314(3), 738-756.
24. Determination of sound power radiated into a duct by fans and other air-moving devices, ISO/TC 43 - Acoustics : ISO 5136:2003. Geneva : International Organization for Standardization, 2003.
25. Tiikoja, H., Rammal, H., Åbom, M., Bodén, H. Sound transmission in automotive turbochargers. – *SAE technical Paper Series*, 2011, Paper no. 2011-01-1525.

26. Maa, D.-Y. Theory and design of micro-perforated panel sound-absorbing construction. – *Science China Mathematics*, 1975, 18, 55-71.
27. Knipstein, D. Sound absorbing element and procedure for manufacture of this element and use of this element: European patent no. EP0876539, 1997. [Online] (05.05.2015)
28. Mason, V. Some experiments on the propagation of sound along a cylindrical duct containing flowing air. – *Journal of Sound and Vibration*, 1969, 10(2), 208-226.
29. Seybert, A. F., Ross, D. F. Experimental determination of acoustic properties using a two-microphone random-excitation technique. – *Journal of Acoustical Society of America*, 1977, 61(5), 1362-1370.
30. Åbom, M. Measurement of the scattering-matrix of acoustical two-ports. – *Mechanical Systems and Signal Processing*, 1991, 5(2), 89-104.
31. Dokumaci, E. A note on transmission of sound in a wide pipe with mean flow and viscothermal attenuation. – *Journal of Sound and Vibration*, 1997, 208 (4), 653-655.
32. Munjal, M. L., Doige, A. G. Theory of two source-location method for direct experimental evaluation of the four-pole parameters of an aeroacoustic element. – *Journal of Sound and Vibration*, 1990, 141(2), 323-333.
33. Bendat, J. S., Piersol, A. G. Random data: Analysis and measurement procedures. New York : Wiley, 2011.
34. Tikoja, H., Rämmal, H., Åbom, M., Bodén, H. Test-rig for complete acoustic characterization of turbochargers. – *Proceedings of 16th AIAA/CEAS Aeroacoustics Conference, Stockholm, Sweden. AIAA, 2010, Paper no. 2010-4012.*
35. Competence Center for Gas Exchange. [WWW] <https://www.ccgex.kth.se> (05.05.2015)
36. Karlsson, M., Åbom, M. On the use of linear acoustic multiports to predict whistling in confined flows. – *Acta Acustica United with Acustica*, 2011, 97(1), 24-33.
37. Aurégan, Y., Starobinski, R. Determination of acoustical energy dissipation/production potentiality from the acoustical transfer functions of a multiport. – *Acustica*, 1999, 85, 788-792.
38. Starobinski, R. Theory and synthesis of mufflers for the intake and exhaust systems of internal combustion engines: PhD dissertation, Togliatti, Togliatti State University, 1983.
39. Cremer, L. The second annual Fairey lecture: The treatment of fans as black boxes. – *Journal of Sound and Vibration*, 1971, 16 (1), 1-15.
40. Terao, M., Sekine, H. Fan acoustic characteristics required for reliable HVAC duct sound prediction. – *Proceedings of the 1st Fan Noise Symposium, Senlis, France. CETIM Technical Center for Mechanical Industry, 1992, 342-350.*
41. Lavrentjev, J., Åbom, M., Bodén, H. A measurement method for determining the source data of acoustic two-port sources. – *Journal of Sound and Vibration*, 1995, 183 (3), 517-531.

42. Fink, D. A., Cumpsty, N. A., Greitzer, E. M. Surge dynamics in a free-spool centrifugal compressor systems. – *Journal of Turbomachinery*, 1992, 114(1), 321-332.
43. Allam, S., Åbom, M. A new type of muffler based on the microperforated tubes. – *Journal of Vibration and Acoustics*, 2011, 133(3), Paper No. 031005. [Online] ASME Digital Collection (02.02.2015)
44. Åbom, M., Allam, S. Dissipative Silencer Based on the micro-perforated plates. – *SAE Technical Paper Series*, 2013, Paper No. 2013-24-0071.
45. Comsol Multiphysics. [WWW] <https://www.comsol.com/products> (05.05.2015)
46. Givoli, D., Neta, B. High-order non-reflecting boundary scheme for time-dependent waves. – *Journal of Computational Physics*, 2004, 186(1), 24-46.
47. Guo, Y., Allam, S., Åbom, M. Microperforated plates for vehicle applications. – *Proceedings of the 37th International Congress and Exposition on Noise Control Engineering: INTER-NOISE 2008. International Institute of Noise Control Engineering, 2008, 773-791.*
48. Cremer, L. Theory regarding the attenuation of sound transmitted by air in a rectangular duct with an absorbing wall, and the maximum attenuation constant produced during this process. – *Acustica*, 1953, 3, 249-263.
49. Tester, B. J. The propagation and attenuation of sound in lined ducts containing uniform or “plug flow”. – *Journal of Sound and Vibration*, 1973, 28(2), 151-203.
50. Formula Student Team Tallinn. [WWW] <https://www.formulastudent.ee> (05.05.2015)

## Acknowledgements

There are so many people to whom I am grateful for being able to write this thesis. I would like to start from the beginning of this journey that brought me here. The year is 1999, I am 16 years old and recently been thrown out from the secondary school of Tallinna Liivalaia Gümnaasium for being inventive on making trouble. Teachers and principal “kindly” have said to my mother and me that I never graduate and eventually end up of being a criminal. On the contrast, they were the teachers of the Tallinna Vanalinna Täiskasvanute Gümnaasium, which continuously encouraged me throughout the studies in the new secondary school and never lost the faith on me. Hereby, I would like to express my sincere gratitude to them all for making the graduation of the secondary school possible and for motivation they provided me during these confusing times.

During our ordinary discussions with my dear friend Oona-Maria, she once mentioned that one of her course mate in the Tallinn University of Technology was coming from my new school and the idea now seemed to be so reachable also for me, was planted to my head. That was one (and there is another) determining moment in my life for what I would like to thank her sincerely.

My respectful grandparents Hillar and Ölme, I would like to thank especially for showing the strong respect for the engineering sciences including the most important moments of university selection. Our long discussions on the world, where we live in, have been the most inspiring. While being surrounded by so inspiring people, it was no coincidence that eventually I was accepted to study in Tallinn University of Technology instead of being a criminal and a cherry on the cake was the school's third exam result in the mathematics.

I will never forget my passed away grandmother Tiiu, a school principle and world best physics and mathematics teacher. She was my greatest fan throughout the university studies but never had a possibility to see my PhD graduation. That is one of the reasons why the present work is dedicated to her. I will also never forget my passed away grandfather Elmar who was a caring and protecting grandfather to me whom I never had chance to know for real.

My gratitude also goes to my supervisors from academia: Priit Põdra for the support during the writing of bachelor thesis, without him I would never graduate within nominal time, perhaps at all; prof. Tauno Otto, the supervisor of master thesis, for the great support and for finding me a PhD study position; the professor Mats Åbom from KTH Royal Institute of Technology for support and making large share of present work possible; Fabio Auriemma for fruitful discussions and the review of the present work.

Furthermore, I would like to thank my supervisors also from industry: Magnus Knutsson from Volvo Car Corporation for the good supervision and great lunches during my stay in the corporation headquarters in Gothenburg; Thomas Mönkediek for making my stay at Audi AG in Ingolstadt very interesting and for

the enthusiastic car talks during lunches with him and his PhD student Sara-Joohwa Lee.

I been also blessed with having good friends. I would like to thank Kermo and Marie for all the help you gave and great times we have had. The one of a kind of friend, that not everybody are lucky to have in their life, is my best friend Siim. I would like to express my sincere appreciation to him for being on my side through all the adventures, with capital A, that life has set to us and I certainly believe it will always remain like that.

It is natural that mothers care about their children the most, but amount of worry that I, unintentionally, have caused to my mother and self-rejected love that I received cannot be described by words. I doubt if any mother could love her child as much as my mother does. You are the best!

There are simply no words that could express my feelings to my dearest wife Cherlin. Thank you for appearing to my life almost 9 years ago, and still hanging on regardless of these lonely times of my studies in Stockholm. You are the reason of me!

Finally, the financial support provided by the European Commission within Marie Curie initial training network of FlowAirS ([www.flowairs.com](http://www.flowairs.com)) and by the Competence Center for Gas Exchange at KTH Royal Institute of Technology is greatly acknowledged. This research was also supported by European Social Fund's Doctoral Studies and Internationalization Program DoRa, which is carried out by Foundation Archimedes.

## **Abstract**

### **Aero-acoustic Studies and Innovative Noise Control with Application to Modern Automotive Gas Exchange System**

In modern IC engine design turbochargers are implemented to increase the fuel conversion efficiency and reduce emissions. Regardless the fact that almost all of the IC engines, manufactured today, are equipped with turbochargers, the problem of narrower mass flow range of the turbo-compressor than it is required by the engine, jet remained. Flow phenomena posing a barrier to the low end mass flow is referred to as compressor surge. Since the initiation mechanism of this destructive phenomena is not clear, the current industrial practice is to implement preventative safety margins, thus restricting the effective use of turbochargers. If the compressor surge could be predicted or appropriate counteractions taken, the unexploited mass flow range could be enabled. In addition to the problem of surge, the compressors are also recognized as a strong sources of sound.

It is supposed herein that acoustic field could play a significant role in the initiation of low frequency phenomena of compressor surge. Moreover, all the investigations found from literature focusing on the aerodynamic field while neglecting the acoustic field. Therefore, in detail investigation of the acoustic field in the centrifugal compressor is carried out in first part of the present doctoral thesis. As a result, the coupling between the aerodynamic and the acoustic fields have been successfully characterized. Furthermore, the generated sound spectra are also determined accurately by extracting generated sound from overall sound field in the compressor inlet and outlet branches.

The current noise control of the IC engine inlet is based on the reflective resonators. In general, the substitution of reflective resonators in flow channel applications with absorptive noise control solutions, can provide advantages in terms of system robustness and design process. Innovative mass-produced noise control materials, such as micro-perforated panels, can be effectively used to substitute the traditional fibrous materials in the absorptive noise control. Nevertheless, designs based on these materials have to be precisely fine-tuned to fit the specific application, thus making the optimization process essential.

In the second part of the thesis the optimization method for innovative silencer, based on the micro-perforated panels, is proposed. The optimization for the application in the Volvo Car Corporation have successfully been done by simplified FEM approach. Moreover, the acoustic performance of the resulting design have been experimentally determined and analyzed.

On the contrast to a mass produced materials, in challenging environmental conditions the custom micro-perforated elements can justify the higher manufacturing price. Therefore, the custom micro perforated flow channel element is experimentally developed in the third part of the thesis. Moreover the element has been successfully applied in the silencer of Formula SAE race car.

## Kokkuvõte

### **Kaasaegse automootori gaasivahetussüsteemide aero-akustilised uuringud ja müra vähendamise innovaatilised meetodid**

Tänapäeval kasutatakse turbolaadureid sise põlemismootorite tehnoloogias selleks, et tõsta kütuse muundamise efektiivsust ja vähendada kahjulike saasteainete emissiooni. Hoolimata asjaolust, et pea kõik sise põlemismootorid, mis tänapäeval toodetakse on varustatud turbolaaduritega, on turbokompressorite kitsa tööpiirkonna probleem jäänud ikka aktuaalseks.

Üldiselt on turbokompressorite tööpiirkond massivoolu teljel kitsam, kui seda on sise põlemismootori oma, ja väiksem massivool on piiritletud ülerõhu perioodiliste tagasilöökide (i.k. *compressor surge*) ilmnemisega. Nimetatud ülerõhu tagasilöögid põhjustavad laaderõhu, ja seetõttu ka massivoolu, perioodilist varieerumist kogu kompressorikontuuri ulatuses, mis on ohtlik nii kompressorile endale kui ka kogu veoagregaadile tervikuna. Kuna füüsikaline mehhanism, mis potentsiaalselt hävitavaid ülerõhu tagasilööke algatab, ei ole täielikult teada, rakendatakse praktikas tööpiirkonnale varutegeureid. Kui kirjeldatud ülerõhu tagasilöökide ilmnemist oleks võimalik täpselt ette näha või ennetada, võimaldaks see kogu kompressori tööpiirkonda edukalt rakendada. Lisaks eelnevalt kirjeldatud tööpiirkonna probleemile, on sisselaskekompressorid tuntud ka kui väga võimsad müraallikad. Kompressorimüraga seotud probleemide ilmnemisest on teada antud nii veo- kui ka sõiduauto tööstustest.

Käesolevas töös eeldatakse, et tsükliliste ülerõhu tagasilöökide algatusmehhanism võib olla seotud akustilise väljaga. Erinevates allikates kajastatud eelnevad teadustööd on nimetatud probleemi uurimisel olnud suunatud aerodünaamilise välja uurimisele, mille juures on jäetud akustiline väli tähelepanuta. Sellest tulenevalt on käesoleva doktoritöö esimeses peatükis läbiviidud detailne akustilise välja uurimine autotehnilises tsentrifugaalkompressoris. Uurimuse tulemusena iseloomustati akustilise ja aerodünaamilise välja omavahelist seotust kompressoris ning täpselt määrati ka genereeritud heli spektrid nn. peegeldusvaba heli eraldamise kaudu kompressori sisse- ja väljalaskekanalis.

Tulemustest selgub, et kompressori töötamisel madalaima võimaliku massivoolu piirkonnas madalsagedusliku heli neeldumine puudub ja määratud heli spektritest nähtub, et genereeritud madalsagedusliku heli võimsus on suurenenud drastiliselt. Nimetatud leide arvesse võttes on alust arvata, et sobivate piiritingimuste olemasolul kompressorikontuuris on akustilise energia akumulatsioon süsteemis tõenäoline ning voolutingimuste mõjutamise kaudu võib see esile kutsuda ülerõhu tagasilöögi kompressoris.

Modernse sise põlemismootori müra emissiooni vähendamiseks on tänapäeval kasutusel sisselaskekompressori müra tagasi peegeldavad resonaatorid. Kanalite süsteemis, kus genereeritud helilained peegeldatakse tagasi nende allikasse,

sõltub helivõimsuse vähenemine lainete neeldumisest allikas. Eelnevalt kirjeldatud süsteemi ja selle projekteerimisprotsessi on võimalik muuta oluliselt robustsemaks, asendades peegeldavad resonaatorid neelduvate lahendustega.

Traditsiooniliselt baseeruvad neelduvad lahendused erinevat tüüpi kiudmaterjalidel, mis aja jooksul võivad laguneda, põhjustades kiudude eraldumist ja materjali neeldumisvõime vähenemist. Eralduvad kiud on ohtlikud sisepõlemismootorile ning keskkonda sattudes võivad kiud põhjustada inimestele ja loomadele tõsiseid hingamisteede haigusi. Seetõttu üritatakse tänapäeval hoiduda kiuliste materjalide kasutamisest vooluga seotud rakendustes.

Kiuliste materjalide asemel saab edukalt rakendada innovaatilisi mass-toodetavaid materjale, näiteks nn. mikroperforeeritud paneele. Selleks et nimetatud materjale saaks müra vähendamisel efektiivselt kasutada, peavad nendel baseeruvad lahendused olema konkreetse rakenduse põhiselt ja täpselt projekteeritud. Eelnevalt kirjeldatud asjaolu muudab innovaatilistel materjalidel põhinevate lahenduste optimeerimisprotsessi võtmetähtsusega etapiks kogu kanalisüsteemi projekteerimisel.

Käesoleva doktoritöö teises peatükis on käsitletud innovaatilise mikroperforeeritud paneelidel baseeruva voolukanali summuti optimeerimist. Välja on pakutud meetod nimetatud tüüpi summuti optimeerimiseks, mis lähtub voolukanali pinna optimaalse akustilise näivtakistuse mudelist (nn. Cremer'i näivtakistus) ja seisneb selle reprodutseerimises mikroperforeeritud paneelide ja lokaalselt reageerivate paisukambrite abil. Eelnevalt kirjeldatud optimeerimis-meetodit kasutades on võimalik kompaktselt geomeetriaga saavutada väga efektiivne heli neelduvus voolukanalis.

Kasutades lihtsustatud lõplike elementide meetodi mudelit ja kirjeldatud optimeerimis-meetodit, on käesoleva doktoritöö raames sõiduauto tootja Volvo Car Corporation juures edukalt optimeeritud teatud rakenduses kasutatav summuti prototüüp. Lisaks määrati optimeerimistulemusena saadud summuti prototüübi akustilised omadused eksperimentaalselt, mille käigus analüüsiti täiendavalt ka summutust põhjustavaid füüsikalisi mehhanisme. Tulemustest nähtub, et koostatud mudel on piisavalt täpne kõnealust tüüpi summuti modelleerimiseks ja modelleeritud efektiivne heli neelduvus optimeeritud summutis on realiseeritav.

Masstoodetavate akustilist neelduvust pakkuvate materjalide valmistamis-maksumus on suhteliselt madal. Üldiselt ei vasta aga need rasketes keskkonna-tingimustes rakendamiseks vajalikele nõuetele. Selliste rakenduste puhul on vajalikud erilahendused, mille kõrgem maksumus on niisugusel juhul õigustatud. Eelnevast asjaolust tulenevalt on käesoleva töö kolmandas peatükis eksperimentaalselt erilahendusena välja arendatud mikroperforeeritud voolukanali element. Projekteeritud on ka nimetatud elemendil baseeruv sisepõlemismootori väljalaskesummuti Formula SAE võistlussõidukile, millel see täitis edukalt kõik sellele püstitatud ülesanded nii tehnilise kontrolli läbimisel kui ka kogu võistluse vältel.

## Appendix



## Paper I

Kabral, R., Rammal, H., Abom, M.  
Acoustical methods for investigating turbocharger flow instabilities.  
*SAE Technical Paper Series*, 2013, Paper no. 2013-01-1879,  
doi:10.4271/2013-01-1879.

Reprinted with permission from SAE paper 2013-01-1879 Copyright © 2013  
SAE International. This paper may not be reprinted, copied, distributed, or  
saved on any retrieval system without prior permission from SAE





## Acoustical Methods for Investigating Turbocharger Flow Instabilities

2013-01-1879

Published  
05/13/2013

Raimo Kabral  
KTH Royal Institute of Technology, CCGEx

Hans Rammal  
Tallinn University of Technology

Mats Abom  
KTH Royal Institute of Technology

Copyright © 2013 SAE International

doi:[10.4271/2013-01-1879](https://doi.org/10.4271/2013-01-1879)

### **ABSTRACT**

In order to increase the internal combustion engine efficiency turbocharging is today widely used. The trend, in modern engine technology, is towards higher boost pressures while keeping the combustion pressure raise relatively small. The turbocharger surge occurs if the pressure at the outlet of the compressor is greater than it can maintain, i.e., a reverse flow will be induced. In presence of such flow conditions instabilities will occur which can couple to incident acoustic (pressure) waves and amplify them.

The main objective of the present work is to propose a novel method for investigation of turbocharger flow instabilities or surge precursors. The method is based on the determination of the acoustic two-port data. The active part of this data describes the sound generation and the passive part the scattering of sound. The scattering data will contain information about flow-acoustic interaction and amplification of sound that could occur close to surge.

Here the existence of such amplification will be investigated for a compressor operating at different operating points including points near the surge line. In addition the generated sound for reflection-free conditions is also investigated on both the up- and downstream side. All the measurements have been carried out in the unique CCGEx test rig for two-port testing of turbo-compressors.

### **INTRODUCTION**

The concept of supercharging the internal combustion engine by extracting “wasted” energy from exhaust gases, to drive the charger, dates from early 20<sup>th</sup> century. Although, the original purpose of the turbocharging was to improve aviation engines performance at high altitudes, nowadays it is widely implemented for efficiency reasons.

In principle the high indicated fuel conversion efficiency (IFCE) of an internal combustion engine is obtained by increasing its indicated mean pressure (IMEP). While this can be done by increasing the volumetric compression ratio (VCR), it is not preferable due to higher combustion temperature and therefore increased NO<sub>x</sub> emission and thermal load of engine components. Another way is to increase the charge air pressure by introducing a concept of turbocharging, and if necessary reducing the VCR. However, to maintain acceptable output torque characteristic, such an engine would need high pressure charge air delivery in a wide mass flow range.

Turbocharger surge occurs when the compressor outlet pressure ratio over the inlet pressure for a given (low-end) mass flux exceeds the pressure it can maintain. In general, at least four type of surge, according to flow and pressure fluctuations, are distinguished today [1]: mild, classic, modified and heavy surge where even flow reversal can occur.

All these, except mild surge, are considered to be hazardous to the compressor. Therefore, surge margins implemented today are relatively high ( $\sim 10\text{...}20\%$ ) which limits the efficient use of such devices. In order to broaden the operating range the phenomenon of surge has to be investigated and preferably the inception predicted.

The acoustical two-port model is well known and commonly implemented for the characterization of acoustical performance of flow-duct elements including turbochargers e.g. in [2]. Nevertheless, in the present work, a novel method for investigation of turbocharger surge based on the acoustic two-port data will be proposed.

This investigation represents a first attempt to apply the proposed method on a turbocharger operating in realistic conditions. Also to the author's knowledge, it is a first successful determination of a compressors complete two-port data, i.e., both the passive and active parts.

## METHOD

The acoustical impact of a linear and time invariant flow-duct element can be characterized by means of multi-port models [3]. Depending on the number of ports, the majority of flow-duct elements studied are treated as acoustic two-ports (e.g. turbocharger's compressor and turbine).

In the plane wave frequency range, the convenient choice of state variables are acoustic pressure waves propagating in the downstream and upstream direction [4] i.e. the acoustic impact of a two-port is completely described by the scattering matrix (passive properties) and source strength vector (active properties):

$$\begin{bmatrix} p_{a+} \\ p_{b+} \end{bmatrix} = \begin{bmatrix} R_a & T_b \\ T_a & R_b \end{bmatrix} \begin{bmatrix} p_{a-} \\ p_{b-} \end{bmatrix} + \begin{bmatrix} p_a^s \\ p_b^s \end{bmatrix}, \quad (1)$$

where  $p$  stands for complex acoustic pressure wave amplitude, subscript  $a$  and  $b$  refers to the respective branch of the two-port, superscript  $s$  denotes source term,  $R$  and  $T$  are the reflection and the transmission coefficients forming the scattering matrix (S-Matrix). Note the source term represents the wave amplitudes under reflection-free conditions.

In order to determine the pressure wave amplitudes from the acoustic field in flowing media at the inlet and outlet of the two-port, the fields have to be decomposed into opposite propagating acoustic waves. This can be done by implementing the well-known two-microphone method [5].

While there are four unknown coefficients in Eq. 1, it contains only two independent relations. Therefore, to determine the S-Matrix, the acoustic field has to be modified and two independent test scenarios generated i.e. four independent relations are obtained. This can be realized with

the Two Source-Location method [6] where the location of an external acoustic source (e.g. loudspeaker) is varied.

Commonly, flow-duct elements that are experiencing high flow velocities during the operation and determination of passive acoustic data, e.g. turbochargers, are generating high level of aero-acoustic noise (active properties see Eq. 1). In addition, there will be broad band flow-noise in the duct. For accurate determination of the S-Matrix data in such conditions, where the aero-acoustic source and a flow-noise have to be suppressed, the loudspeaker driving signal is used as a reference. By averaging frequency response functions measured between the loudspeaker driving signal and the microphone pressure signal, the uncorrelated noise will be suppressed [4].

As discussed by Karlsson and Åbom [7] any coupling between the acoustic and flow fields will appear in the S-matrix. This implies that damping as well as amplification of sound due to flow instabilities can be found by studying the S-matrix.

Concerning the hostile environment for turbo-compressor acoustic measurements and the need for accurate S-matrix data, the two-microphone method should be extended into over determination with weighted residuals to improve the accuracy of the measurements, as formulated by Jones et al. in [8] and recently successfully implemented by Holmberg et al. in [9]. Therefore, it is necessary to implement more than two microphones at both branches of a two-port.

Once the S-matrix data is measured and computed, it enables to determine the minimum and maximum values of the difference between the scattered acoustic power and the incident acoustic power, including all the possible excitation combinations [10]. In order to obtain the minimum and maximum, a power balance has to be set up over the acoustic flow-duct element. By normalizing the total energy of the arbitrary incident waves to unity [10], one can express the output time averaged acoustic power in the following fashion (Eq. 2):

$$\langle P_{out} \rangle = \mathbf{x}_-^\dagger (\mathbf{S}^\dagger \mathbf{S}) \mathbf{x}_- - 1, \quad (2)$$

where  $\mathbf{S}$  is the acoustic S-matrix of a two-port,  $\mathbf{x}$  is a state variable related to the acoustic power as  $\langle P_\pm \rangle = \mathbf{x}_\pm^\dagger \mathbf{x}_\pm$  and  $\dagger$  denotes Hermitian transpose.

Since the positive definitive matrix expression in Eq. 2 can be reduced into a sum of squares, one can determine the maximum possible time averaged power output as:

$$\langle P_{out}^{max} \rangle = \lambda_{max} - 1, \quad (3)$$

where  $\lambda_{max}$  is maximum real and positive eigenvalue of the matrix ( $S^*S$ ).

The maximum eigenvalue determined (See Eq. 2 and 3) represent the maximum value of acoustic power ratio potentially scattered over the incident acoustic power i.e. amplification in case of a value larger than unity and dissipation otherwise.

Since turbocharger surge related flow instabilities inside the compressor are coupled with an acoustic field, an additional aero-acoustic source will be formed which will contribute to the overall sound field generated by the machine. This source is expected to be affected by the incident sound waves because of the coupling between the hydrodynamic and acoustic fields i.e. the incident acoustic waves will be amplified or less dissipated compared to the neighboring frequency range.

To summarize, it is assumed that the occurrence of flow instabilities inside the compressor is possible to detect with the method described. Also the flow instability interacting with the moving compressor blades will produce sound that is expected to be seen in source cross spectrum matrix (Eq. 5).

In order to extract the source strength components from the overall sound field in a flow-duct, the transmission and reflection properties has to be known at each branch of the element under investigation. These properties can be computed from propagating complex pressure wave amplitudes obtained from sound field decomposition described earlier.

Once the passive properties are determined, the source strength vector can be expressed as follows [9]:

$$\mathbf{p}_s = (\mathbf{E} - \mathbf{SR})(\mathbf{E} + \mathbf{R})^{-1}\mathbf{p}, \quad (4)$$

where  $\mathbf{p}_s$  and  $\mathbf{p}$  are the vectors of complex pressure wave amplitudes of source and microphone pressures respectively.  $\mathbf{E}$  is a unitary matrix and  $\mathbf{R}$  denotes a diagonal matrix containing the reflection coefficients of the test rigs terminations.

Since the formulation (Eq. 4) is inadequate for random sources, the more general source cross spectrum matrix should be implemented instead [9]:

$$\mathbf{G}^s = \mathbf{p}_s(\mathbf{p}_s)^\dagger. \quad (5)$$

The diagonal elements of the source cross spectrum matrix, i.e.  $G_{11}$  and  $G_{22}$  in case of a two-port, are the single sided auto spectra of the source strength elements at respective branch which can be utilized to compute the generated sound pressure level (SPL).

## EXPERIMENTS

The acoustic data used here are from measurements carried out by H. Tiikoja et al. [2] using the turbo-charger test facility available at the CCGEx center at Royal Institute of Technology (See Fig. 1).



Figure 1. A photo of the test-rig in the facility for turbocharger acoustic measurements at CCGEx.

The acoustic two-port data has been measured for a typical automotive turbo-compressor in 5 operating points (OP) covering rotor speed variation from standing still up to 140k RPM. The values of physical quantities determining the OPs measured have been concentrated into Tab. 1. In addition, the graphical representation of the OPs on the compressor map is given in Fig. 2.

Table 1. The operating conditions of the turbocharger.

	Pressure Ratio, 1	Corrected Mass Flow, kg/s	Rotational frequency, RPM
OP 1	1	-	-
OP 2	1.28	0.054	082 304
OP 3	1.85	0.119	141 643
OP 4	1.37	0.126	123 012
OP 5	1.71	0.050	120 168

While the OP1, OP2 and OP3 (See Tab. 1) are representing rotational frequency variation with constant throttle valve opening, the OP4 and OP5 have been chosen to investigate

the acoustic behavior in the vicinities of choke (OP4) and surge lines (OP5) on the compressor map (see Fig. 2).

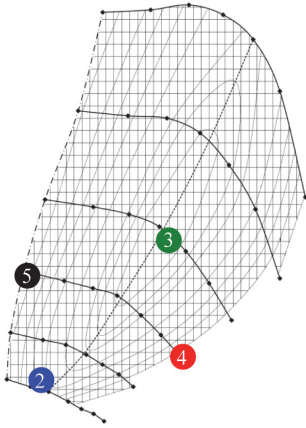


Figure 2. The non-stationary operating points of the turbocharger on the compressor map.

## RESULTS AND ANALYSIS

In Fig. 3 the maximum eigenvalue of the acoustic power balance (see Eq. 3) is presented.

It can be observed (Fig. 3) that the ability to absorb acoustic energy (eigenvalue less than unity) is highly affected by operating conditions (e.g. the OP1 vs. the OP4) and on the graph, three different trends directly linked with mass flux (See Tab. 1) can be distinguished.

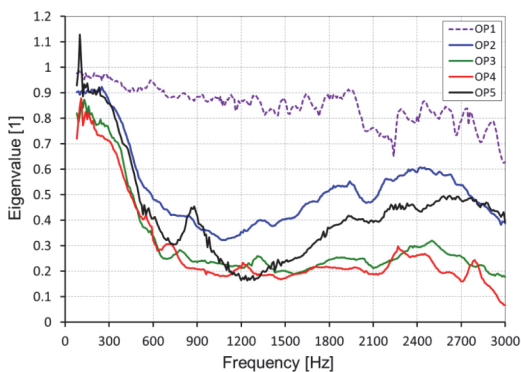


Figure 3. The maximum ratio of scattered acoustic power over incident acoustic power determined in five operating points (See Tab. 1).

The constant high level (small losses) trend is represented by the OP1 (stationary machine). The other OPs show considerable more losses related to, as discussed in Ref. 2,

flow induced acoustic losses. But OP5 the point closest to surge shows an interesting deviation i.e. a local reduction in the losses around 900 Hz. This could be an onset of mild surge via rotating instabilities or stall.

The frequency of 900 Hz (Fig. 3), corresponds to the rotational frequency of the impeller (2003 Hz) with multiplier of 0.45 i.e. the frequency range where rotating instabilities have been found in [11]. But to prove this point a set of systematic measurements following a fixed RPM line on the turbo map approaching surge must be performed.

In addition, the curve of the OP5 in Fig. 3 shows a sharp peak with value larger than one i.e. the amplification of sound. In this frequency region one could expect the surge related flow oscillations to appear. However, unfortunately the measurement data quality at this frequency point is considerably low. Therefore, the conclusions regarding the peak have to be validated in further systematic investigations.

In the following figures (Fig. 4 and 5) the SPL generated by the compressor in its inlet and outlet ducts is presented.

In general the generated sound spectra (Fig. 4 and 5) consist of a broad band level and very sharp peaks (tones), except OP5 with no narrow peaks.

The broadband level of the generated SPL is generally higher (~5dB) at the outlet side and remains similar in all the OPs except OP5 (i.e. close to surge) where a large increase of ~15dB can be observed (Fig. 4 and 5) at both junctions of the compressor.

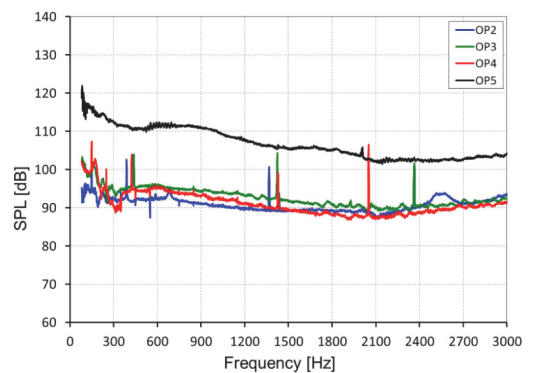
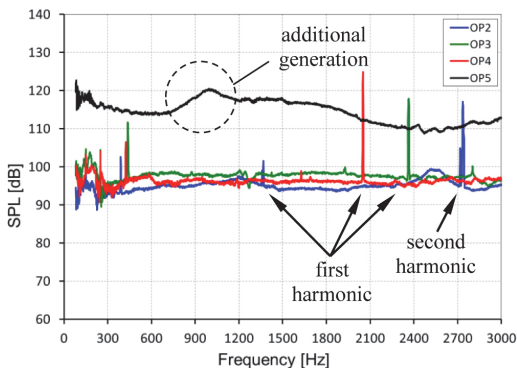


Figure 4. The generated sound pressure level at the inlet channel (low pressure) of the compressor at different operating conditions (Tab. 1).

Tonal components of the generated SPL spectrums (Fig. 4 and 5) can be directly linked with the rotational frequency of the impeller and its harmonics. These tones are caused by the supersonic flow velocity inside the compressor impeller

vanes inducing shock waves while interacting with the diffuser. The resulting noise is commonly referred to as “buzz-saw” noise [11].



**Figure 5. The generated sound pressure level at the outlet channel (high pressure) of the compressor at different operating conditions (Tab. 1).**

The level of the harmonics is lower at inlet side since the upstream wave propagation through the transonic flow is restricted. Because of the flow velocity dependence inside the vanes, the larger mass flux fill results in higher level of these tones as can be observed in Fig. 4 and 5. In addition, the disappearing of these tonal peaks in the OP5 (Fig. 4 and 5), while operating close to surge, can be related to the restricted flow through the impeller vanes creating a more unsteady “chaotic” flow and therefore more broadband sound.

There is a noticeable hump, occurring approximately at 900 Hz, on the curve for the compressor SPL at the outlet (Fig. 5) in case of OP5. The frequency is close to the maximum eigenvalue peak (See Fig. 2) discussed earlier. Therefore, it can be argued that it is the same flow instability that is being manifested via both sound scattering and generation.

## SUMMARY AND CONCLUSION

In the present work a novel acoustical method for turbocharger surge investigation has been proposed. The method has been tested on an automotive turbocharger operating in realistic conditions close to surge.

It was found that under such conditions the compressor can start amplification of sound due to flow-acoustic coupling. The frequency, where this phenomena is observed, is approximately half (0.45) of the impellers rotational frequency i.e. the frequency range where rotating instabilities are commonly found [11].

The work also represents the first successful determination of the complete two-port data, i.e., both source cross spectrum

and scattering matrix of a compressor at different operating points.

A large broadband increase of the generated SPL close to surge operation was also observed. In addition, a noticeable hump on the sound generation curve was noticed at the same frequency range where amplification was observed. The additional generation is believed to indicate to the flow separation taking place inside the compressor.

The ideas presented still need more experimental data to be fully validated. Therefore, more tests running compressors at a constant RPM approaching surge is planned.

## REFERENCES

1. de Jager, B., “Rotating Stall and Surge Control: A survey,” presented at Proceedings of the 34<sup>th</sup> Conference on Decision & Control, USA, December 13-15, 1995.
2. Tiikojä, H., Rämäl, H., Abom, M., and Bodén, H., “Investigations of Automotive Turbocharger Acoustics,” *SAE Int. J. Engines* 4(2):2531-2542, 2011, doi:10.4271/2011-24-0221.
3. Bodén, H., Åbom, M., “Modelling of Fluid Machines as Sources of Sound in Duct and Pipe Systems,” *Acta Acustica* 3:549-560, 1995.
4. Åbom, M., “Measurement of the Scattering-Matrix of Acoustical Two-Ports,” *Mechanical Systems and Signal Processing* 5(2):89-104, 1991.
5. Seybert, A., F., Ross, D., F., “Experimental Determination of Acoustic Properties Using a Two-Microphone Random-Excitation Technique,” *Journal of Acoustical Society of America* 61(5):1362-1370, 1977, doi:10.1121/1.381403.
6. Munjal, M., L., Doige, A., G., “Theory of a Two Source-Location Method for Direct Experimental Evaluation of the Four-Pole Parameters of an Aeroacoustic Element,” *Journal of Sound and Vibration* 141(2):323-333, 1990, doi:10.1016/0022-460X(90)90843-O.
7. Karlsson, M., Åbom, M., “On the Use of Linear Acoustic Multiports to Predict Whistling in Confined Flows,” *Acta Acustica united with Acustica* 97(1):24-33, 2011, doi:10.3813/AAA.918383.
8. Jones, M., G., Parrot, T., L., “Evaluation of a multi-point method for determining acoustic impedance” *Mechanical Systems and Signal Processing* 3(1):15-35, 1989, doi:10.1016/0888-3270(89)90020-4.
9. Holmberg, A., Åbom, M., Bodén, H., “Accurate experimental two-port analysis of flow generated sound,” *Journal of Sound and Vibration* 330(26):6336-6354, 2011, doi:10.1016/j.jsv.2011.07.041.
10. Aurégan, Y., Starobinski, R., “Determination of Acoustical Energy Dissipation/Production Potentiality from

the Acoustical Transfer Functions of a Multiport,” *Acta Acustica united with Acustica* 85(6):788-792, 1999.

11. Raitor, T., Neise, W., “Sound generation in centrifugal compressors,” *Journal of Sound and Vibration* 314(3-5): 738-756, 2008, doi:[10.1016/j.jsv.2008.01.034](https://doi.org/10.1016/j.jsv.2008.01.034).

## **CONTACT INFORMATION**

Raimo Kabral  
Competence Center for Gas Exchange  
The Royal Institute of Technology  
Teknikringen 8, Stockholm, SE-10044, Sweden  
[kabral@kth.se](mailto:kabral@kth.se)

Mats Åbom  
Marcus Wallenberg Laboratory  
The Royal Institute of Technology  
Teknikringen 8, Stockholm, SE-10044, Sweden  
[matsabom@kth.se](mailto:matsabom@kth.se)

## **ACKNOWLEDGMENTS**

The authors of this work would like to acknowledge the Heiki Tiikoja for providing the measured data used in investigation. Also the financial support from European Union (7th Framework program) through Marie Curie actions initial training network FlowAirS ([www.flowairs.eu](http://www.flowairs.eu)) is acknowledged.

## **ABBREVIATIONS**

**IFCE** - indicated fuel conversion efficiency

**IMEP** - indicated mean pressure

**VCR** - volumetric compression ratio

**S-matrix** - scattering matrix

**SPL** - sound pressure level

**OP** - operating point

---

The Engineering Meetings Board has approved this paper for publication. It has successfully completed SAE's peer review process under the supervision of the session organizer. This process requires a minimum of three (3) reviews by industry experts.

All rights reserved. No part of this publication may be reproduced, stored in a retrieval system, or transmitted, in any form or by any means, electronic, mechanical, photocopying, recording, or otherwise, without the prior written permission of SAE.

ISSN 0148-7191

Positions and opinions advanced in this paper are those of the author(s) and not necessarily those of SAE. The author is solely responsible for the content of the paper.

**SAE Customer Service:**

Tel: 877-606-7323 (inside USA and Canada)

Tel: 724-776-4970 (outside USA)

Fax: 724-776-0790

Email: [CustomerService@sae.org](mailto:CustomerService@sae.org)

**SAE Web Address:** <http://www.sae.org>

**Printed in USA**

## Paper II

Kabral, R., Du, L., Åbom, M., and Knutsson, M.  
A Compact silencer for the control of compressor noise.  
*SAE International Journal of Engines*, 2014, 7(3), 1572-1578,  
doi:10.4271/2014-01-2060.

Reprinted with permission from SAE paper 2014-01-2060 Copyright © 2014 SAE International. This paper may not be reprinted, copied, distributed, or saved on any retrieval system without prior permission from SAE.





## A Compact Silencer for the Control of Compressor Noise

Raimo Kabral, Lin Du, and Mats Åbom  
KTH Royal Institute of Technology

Magnus Knutsson  
Volvo Car Corporation

### ABSTRACT

Current trends for IC-engines are driving the development of more efficient engines with higher specific power. This is true for both light and heavy duty vehicles and has led to an increased use of super-charging. The super-charging can be both in the form of a single or multi-stage turbo-charger driven by exhaust gases, or via a directly driven compressor. In both cases a possible noise problem can be a strong Blade Passing Frequency (BPF) typically in the kHz range and above the plane wave range.

In this paper a novel type of compact dissipative silencer developed especially to handle this type of problem is described and optimized. The silencer is based on a combination of a micro-perforated (MPP) tube backed by a locally reacting cavity. The combined impedance of micro-perforate and cavity is chosen to match the theoretical optimum known as the Cremer impedance at the mid-frequency in the frequency range of interest. Due to the high damping achieved at the Cremer optimum (hundreds of dB/m) it is easy to create a compact silencer with a significant damping (say > 30 dB) in a range larger than an octave. Both simulations and experimental tests of the novel silencer are presented based on a light duty vehicle application.

**CITATION:** Kabral, R., Du, L., Åbom, M., and Knutsson, M., "A Compact Silencer for the Control of Compressor Noise," *SAE Int. J. Engines* 7(3):2014, doi:10.4271/2014-01-2060.

### INTRODUCTION

In the field of internal combustion (IC) engines the marketing success depends on complying with the continuously increasing environmental regulations, e.g., EURO 6 [1], and fulfilling the market expectations for fuel efficiency and vehicle performance. Therefore, the industry main focus today is on developing more efficient IC engines side by side with other energy saving solutions, e.g., automatic engine start-stop or brake energy regeneration systems.

It is a well-known fact that in order to increase the IC engine efficiency, one approach is to increase the charge air pressure which results in a better fuel conversion efficiency and specific power of the IC unit while keeping the low level of nitrogen emission. There are two main types of such devices that can increase the charge air pressure: one which is mechanically driven by the IC engine itself or by an additional electric motor, and another which uses a turbine to extract otherwise wasted energy from the hot high pressure exhaust gases. On the modern IC engine, both solutions are commonly implemented for covering the high pressure charge air delivery demand in a wide mass flow range while ensuring a good transient response.

The expected dominating sound when such rotating devices are used, is the blade passing frequency tone (BPF) and its multiples. If in the audible range, such tones can be highly annoying. This can either happen for larger compressors on heavy duty vehicles or light duty vehicles when a combination of a directly driven compressor, for moderate load conditions, and a turbo-charger, for high power output operation, is used. In the latter case tones in the audible frequency range are caused by the compressor often of Roots type.

In order to address these noise issues, relatively robust and lightweight compact silencer solutions are needed. As a starting point to find such a silencer, the expansion chamber muffler with a micro-perforated sheet tube proposed by Allam and Åbom in Ref. [2] will be used here (See Fig. 1). It was demonstrated in Ref. [2] that such a configuration can provide a non-fibrous alternative to the traditional dissipative silencers, with the drawback of having transmission loss (TL) minima at half wave-length multiples of the cavity length.

The effects of mean flow and high sound pressure levels causing non-linear effects on the micro-perforate impedance were also investigated by Allam and Åbom in Ref. [2]. The modelling in Ref. [2] was based on FEM neglecting convective

flow effects but including flow effects for the micro-perforate impedance, which is reasonable for low Mach-numbers and will also be used here. The micro-perforate impedance was used as a boundary condition between the two domains, main duct and the outer cavities, see [Figure 1](#). In order to eliminate the minima at half-wave length multiples of the cavity length, a solution in the form of a locally reacting limit was recently suggested by Åbom and Allam [3]. Also two different MPPs were considered, and it was concluded that higher damping of the sound is achievable when the acoustic resistance is smaller than the optimum for room acoustic applications. The conclusion being that one cannot naively use standard MPPs for a silencer, which are optimized for applications involving 3D sound fields in rooms [4].

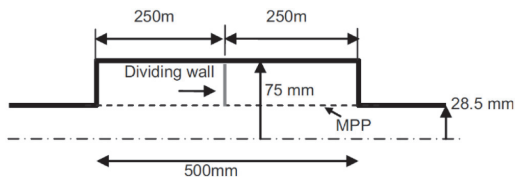


Figure 1. Geometry for the MPP muffler proposed in Ref. [2]. Circular symmetry is assumed and the outer chamber is sub-divided into two or several cavities by rigid walls.

In the present work, the dissipative silencer concept proposed in Refs. [2-3] is further studied in order to find an optimum design. Based on the proposed optimization a design for a Compact Silencer for a light-duty vehicle charger problem is considered. The design constraints for this case are summarized in [Table 1](#) and [Figure 2](#).

Table 1. Design constraints for the compressor noise problem studied.

Parameter	Inlet/outlet duct radius, m	Average Mach number	Temperature, °C	Target frequency, kHz
Value	0.03	0.05	20	2.0

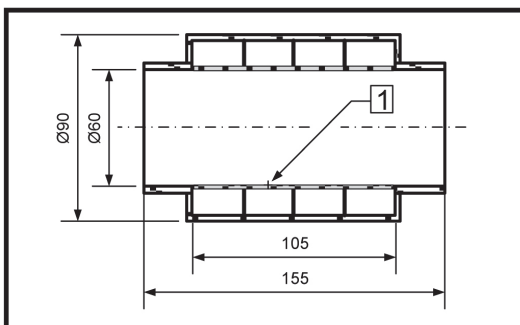


Figure 2. Geometry of the prototype MPP silencer studied. The arrow, marked 1, points at the micro-perforated sheet tube (Acustimet™), separating the main duct from the outer cavities. Note all outer dimensions [mm] except the chamber diameter are fixed during the optimization.

A photo of the prototype built by using rapid prototyping is presented in [Figure 3](#).

## MODELING

First a prototype silencer (See [Fig. 3](#)) will be evaluated. This silencer was built ensuring local reaction in the outer cavities in the frequency range of interest, but *not* using an optimized cavity plus micro-perforate impedance. After validating modelling procedures for this prototype an optimization will be carried out by varying the chamber diameter and the micro-perforate impedance. Through all the current work the 0<sup>th</sup> ("plane wave") duct mode with time dependence of  $\exp(i\omega t)$  is assumed and air ( $1.21 \text{ kg/m}^3$ ) with a sound speed of 343 m/s.

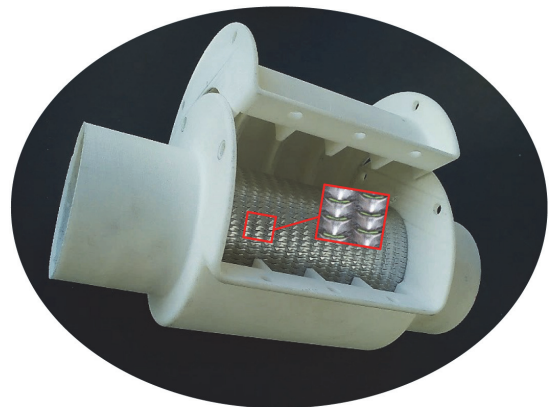


Figure 3. Photo of the compact silencer rapid prototype with magnified view of the micro-perforated (Acustimet™) sheet tube. Dimensions as in [Figure 2](#).

## Experimental Validation Data Determination

The prototype is constructed by implementing a standard MPP aluminum sheet (Acustimet™) under the constraints summarized in [Table 1](#) and [Figure 2](#). In order to evaluate its acoustic attenuation ability, the transmission loss was experimentally determined using a two-port test rig [5]. The obtained TL curve can be found in [Figure 5](#).

In principle, a flow-duct component as the compact silencer treated here can be completely modeled by a finite element method (FEM) approach. Nevertheless, the relatively small aperture dimensions and complicated surface geometry of the MPP would require very fine grid elements and therefore, is computationally expensive. Moreover, since wave propagation in the cavity can be neglected, except normal to the perforated surface, its acoustic effect can be described by an impedance. Hence, a more efficient approach is a simplified model, where a locally reacting surface will be entered into the FEM model using an impedance boundary condition representing the MPP and the outer cavity.

### Wall Impedance Determination

The wall impedance is a consequence of two parts a perforate (MPP) and an adjoining cavity, acting together so that:

$$Z_{wall} = Z_{MPP} + Z_{cav}, \quad (1)$$

where

$Z_{wall}$  - a normalized surface impedance,

$Z_{MPP}$  - the normalized MPP impedance; and

$Z_{cav}$  - the normalized cavity impedance.

Guo et al. gave an overview in Ref. [6] on the semi-empirical modeling of micro-perforate transfer impedance. They also investigated the effect of flow and based on experiments at KTH, they suggested correction terms for the acoustic impedance under grazing flow conditions. In addition, they showed that the acoustic mass end correction term for the slit types of MPP, e.g. as the Acustimet™ panel used here, can be neglected. The acoustic resistance  $\text{Re}(Z_{MPP})$  of the slit type MPP can be computed from:

$$r_s = \text{Re} \left\{ \frac{i\omega t}{\sigma c} \left[ 1 - \frac{\tanh(k_s \sqrt{i})}{k_s \sqrt{i}} \right]^{-1} \right\} + \frac{4R_s}{\sigma \rho c} + \frac{|u_h|}{\sigma c} + \beta \frac{M}{\sigma} \quad (2)$$

and the reactance  $\text{Im}(Z_{MPP})$  from:

$$x_s = \text{Im} \left\{ \frac{i\omega t}{\sigma c} \left[ 1 - \frac{\tanh(k_s \sqrt{i})}{k_s \sqrt{i}} \right]^{-1} \right\}, \quad (3)$$

where

$\omega$  - a radial frequency,  $\text{s}^{-1}$ ;

$\rho$  - the density of the medium,  $\text{kg} \cdot \text{m}^{-3}$ ;

$k_s$  - shear wave number,  $\text{m}^{-1}$ ;

$t$  - the thickness of perforated panel, m;

$\sigma$  - the porosity of the perf. surface;

$\beta$  - a factor for grazing flow effects;

$u_h$  - peak particle velocity in apertures,  $\text{m} \cdot \text{s}^{-1}$ ;

$R_s$  - surface resistance,  $\text{Pas} \cdot \text{m}^{-1}$ ; and

$M$  - Mach number of grazing flow.

The shear wave number, which relates the aperture dimensions with the acoustic boundary layer thickness, is defined as:

$$k_s = d \sqrt{\frac{\omega}{4\nu}}, \quad (4)$$

where

$d$  - the slit width, m; and

$\nu$  - the kinematic viscosity of medium,  $\text{m}^2 \cdot \text{s}^{-1}$ .

Finally, the surface resistance which is a consequence of oscillating motion of the fluid on the surface of a perforated panel, can be found from:

$$R_s = \frac{1}{2} \sqrt{2\rho\omega\eta}, \quad (5)$$

where

$\eta$  - the dynamic viscosity of the medium,  $\text{kgm}^2 \cdot \text{s}^{-1}$ .

The normalized resistance (Eq. 2) is a sum of four terms which relates acoustic losses with viscous effects inside the apertures, first term, and outside, the last three terms. The non-linear effects (the second last term in Eq. 2) proportional to the velocity in the holes  $u_h$ , can be important for applications on IC-engines but will for the present study be omitted. As also seen from Eq. 2 and Eq. 3 a grazing flow will affect (increase) the resistance but not affect the reactance.

The analytical model for the acoustic cavity impedance has been derived and proposed in the earlier paper [3] and is given by:

$$Z_{cav} = \frac{i \left[ H_0^{(1)}(k_a r) - \frac{H_1^{(1)}(k_a R)}{H_1^{(2)}(k_a R)} H_0^{(2)}(k_a r) \right]}{H_1^{(1)}(k_a r) - \frac{H_1^{(1)}(k_a R)}{H_1^{(2)}(k_a R)} H_1^{(2)}(k_a r)}, \quad (6)$$

where

$k_a$  - the axial wave number,  $\text{m}^{-1}$ ;

$R$  - the radius of the expansion chamber, m;

$r$  - the radius of main duct, m; and

$H_m^{(n)}$  - the Hankel function of  $n$ :th kind and  $m$ :th order.

### FEM Model Description

For all the FEM computations the commercial software COMSOL Multiphysics® [7] is employed herein. The wave equation solved in a lossless medium herein, is known as the inhomogeneous Helmholtz equation:

$$\nabla \frac{1}{\rho} (\nabla p - q_d) - \frac{k^2 p}{\rho} = Q_m, \quad (7)$$

where

$p$  - acoustic pressure, Pa;

$k$  - the wave number,  $m^{-1}$ ;

$Q_m$  - a monopole source,  $s^{-2}$ ; and

$q_d$  - a dipole source,  $Nm^{-3}$ .

The main duct is assumed "sound hard" i.e. the wall boundary condition is set as:

$$-\mathbf{n}_r \left[ -\frac{1}{\rho} (\nabla p - q_d) \right] = 0, \quad (8)$$

where

$\mathbf{n}_r$  - the normal vector of the flow duct surface.

Along the silencer section the wall boundary is set as:

$$-\mathbf{n}_r \left[ -\frac{1}{\rho} (\nabla p - q_d) \right] = -p \frac{i\omega}{Z_{wall}\rho c}. \quad (9)$$

The wall (surface) impedance in Eq. 9 will be computed using Eqs. 1, 2, 3, 4, 5, 6, including the grazing flow effects.

In order, to determine the TL of the modeled silencer the input and output acoustic power has to be found. In order to do that it is convenient to use reflection free terminations in the axial direction (up/downstream), which is realized by requiring that [8]:

$$-\mathbf{n}_a \cdot \left[ -\frac{1}{\rho} (\nabla p - q_d) \right] + p \frac{ik}{\rho} + \nabla^2 p \frac{i}{2k\rho} = Q_m \quad (11)$$

at the up- and downstream terminations. Now assuming negligible reflected waves, the acoustic power ( $P_{out}$ ) at the outlet termination can be obtained by integrating the intensity over the cross-section.

For the inlet section an incident plane wave is prescribed using Eq. 11 and the incident power ( $P_{in}$ ) can be directly computed. When the input and output acoustic powers are available, the TL is computed according to its definition as:

$$TL = 10 \log_{10} \left( \frac{P_{in}}{P_{out}} \right). \quad (12)$$

The maximum and minimum frequencies were set to 50 Hz and 3300 Hz respectively and the solution computed with a step of 10 Hz. The upper limit is chosen just below the cut-on for the 1st non-plane wave in the main duct. The resulting model consisted of **824** grid elements which, for the **326** frequency points, took less than **2** minutes to run on an ordinary PC.

The solved acoustic pressure distribution for the prototype silencer at the design target frequency (2 kHz), is plotted for the modeling domain and presented in Fig. 4. The predicted TL spectrum is shown in comparison with the experimental data in Fig. 5.

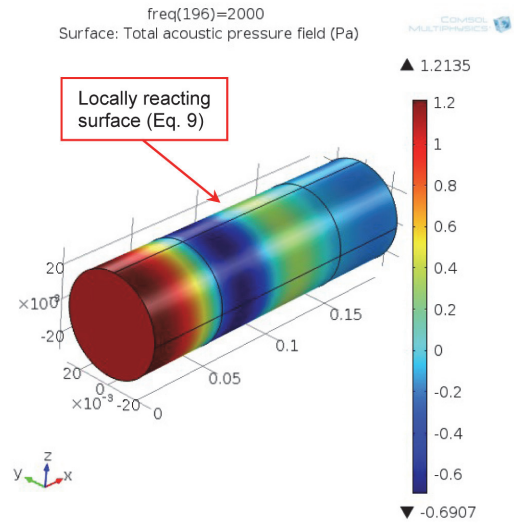


Figure 4. Acoustic pressure distribution at 2 kHz plotted on the FEM modeling domain for the prototype silencer with the standard MPP, i.e. not optimized.

## OPTIMIZATION

The TL performance of the locally reacting compact silencer is determined by its surface impedance formed by the MPP and the adjoining cavity. As a consequence, in order to control the TL performance, one has to optimize the surface impedance. Now the question arises, which complex acoustic impedance value would give the highest TL value? A similar problem was encountered by L. Cremer who in 1953 derived the surface impedance of maximum sound damping, assuming local reaction, achievable in an infinite rectangular duct [9], as:

$$Z_{Cr} = (0.91 - 0.76i) \frac{ka}{\pi}, \quad (13)$$

where

$Z_{cr}$  - the normalized surface impedance for theoretical maximum sound damping in an infinite rectangular duct; and

$a$  - rectangular duct cross-section height, m.

In 1973 B. J. Tester suggested an expression for optimal impedance for circular ducts and also included a correction for mean flow effects [10]:

$$Z_{cc} = (0.88 - 0.38i) \frac{kr}{\pi(1 + M)^2}, \tag{14}$$

where

$Z_{cc}$  - the normalized surface impedance for theor. maximum sound damping in a circular duct.

Assuming one could realize this Cremer impedance for each frequency, one can compute the theoretical maximum damping for the prototype silencer in Figure 3. This is shown as the red curve in Figure 5.

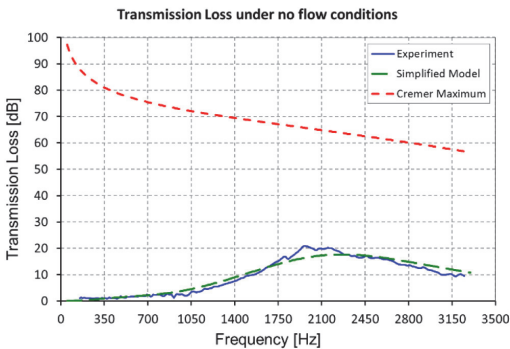


Figure 5. The results of experimental validation of sound transmission loss obtained by the simplified modeling approach (green and blue curves) for the prototype silencer (Figure 3). The red curve shows the theoretical maximum damping for the silencer using the so called Cremer impedance. All results are for no flow.

To see how a Cremer impedance can be created by the prototype silencer, one must first realize that the resistance of the total wall impedance (Eq. 1) is controlled by the MPP. Therefore, the resistive part of the MPP impedance has to match the real part of the Cremer impedance at the target frequency. In Figure 6 the Cremer resistance based on Eq. 14, and the resistance of a standard MPP, used for the prototype, plus one possible MPP choice that matches the Cremer resistance at 2000 Hz see Table 2, are shown.

Table 2. The geometrical parameters of the MPP slit type panels studied. The optimized MPP is designed to equal the Cremer resistance at 2 kHz for  $r = 30$  mm.

MPP panel	Thickness [mm]	Perforation ratio [1]	Averaged slit width [mm]
Standard	1	0.043	0.095
Optimized	1	0.062	0.210

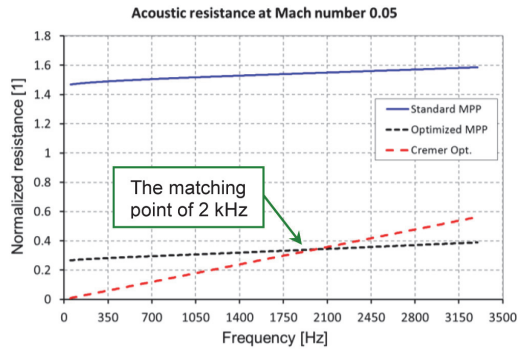


Figure 6. Comparison of acoustic resistance between a standard and an optimal MPP (with slits) and the Cremer resistance. Desired target frequency for maximum damping is 2000 Hz.

After the real part is fixed according to the Cremer impedance, it is necessary to address the imaginary part to achieve the desired optimum damping at the target frequency. The imaginary parts of the MPPs impedance, are compared with the optimum in Fig. 7.

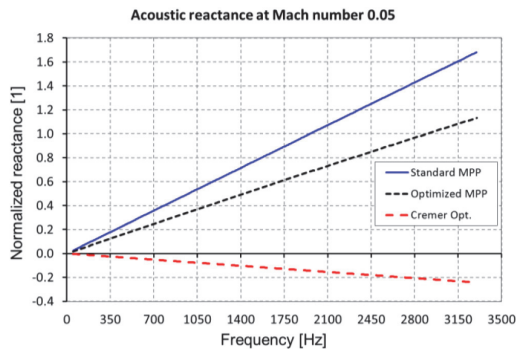


Figure 7. Comparison of acoustic reactance between a standard and an optimal MPP (with slits) and the Cremer reactance. To reach the Cremer optimum a cavity with the right amount of negative reactance must be added to the MPP positive ("mass") reactance.

Since the MPP reactance is always positive while the Cremer reactance is negative, the cavity must be used to reach the optimum reactance value. In addition, as the cavity impedance is a periodic function, there is more than one possible solution

for realizing the Cremer reactance at the target frequency. In Fig. 8 two possible alternatives are shown for the prototype silencer case and a target frequency of 2000 Hz.

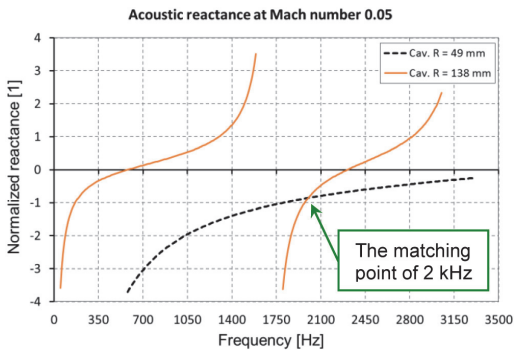


Figure 8. Acoustic reactance of two different cavities suitable for realizing the optimum reactance for the prototype silencer at 2000 Hz.

The best choice to get a compact silencer and to make the resulting damping curve more broad-band, is the smallest cavity radius which satisfies the optimum condition.

The predicted TL performance of the optimized compact silencer configuration with a cavity radius of 49 mm and the MPP data from Table 2, is presented in Fig. 9.

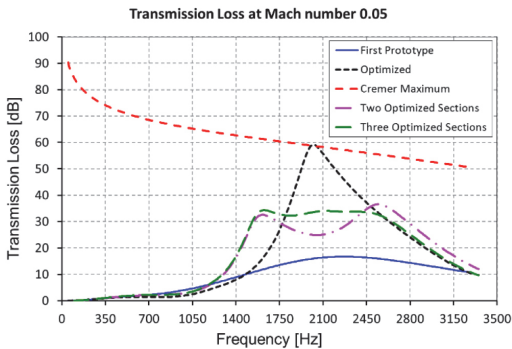


Figure 9. Predicted sound transmission loss for the prototype silencer for different configurations of MPP + cavity impedance. The optimized result is obtained by tuning the wall impedance based on Cremer's impedance at a target frequency 2000 Hz. By splitting the silencer in 2 or 3 sections tuned to 1500&2500 Hz and 1500&2000&2500 Hz, respectively, a more broad-band damping behavior is possible, see Table 3.

As expected the maximum TL value (Fig. 9) at the target frequency of 2 kHz coincides with Cremer's theoretical maximum which is approximately 60 dB. The peak TL of the optimized configuration is very high, but due to break-out radiation, flanking transmission etc. not practical. Therefore, it could be more effective to utilize the theoretical high damping per meter by dividing the locally reacting silencer into a few

separately optimized sections while keeping the total length of the silencer. The predicted TL for two such configurations are shown in Fig. 9 with the design data summarized in Tab. 3.

Table 3. Design constraints for the optimized sections shown in Figure 9.

Configuration name	Section 2		Section 1		Section 3	
	length, mm	freq., kHz	length, mm	freq., kHz	length, mm	freq., kHz
Optimized	-	-	96	2.0	-	-
Two optimized sections	48	1.5	-	-	48	2.5
Three optimized sections	48	1.5	20	2.0	28	2.5

As can be seen in Fig. 9 the compact silencer configuration with three separately optimized sections, while still ensuring local reaction of the cavity, will give approximately constant TL ( $32 \pm 2$  dB) in a wide frequency band around the target frequency. This type of behavior would provide a good and robust noise control solution which can handle varying operating conditions.

Furthermore, the division into separate small standalone sections is improving even more the packing possibilities in, e.g., an engine compartment of a car or truck, which makes it an attractive choice for limited space conditions.

## REALIZATION OF OPTIMAL DESIGN

The dimensions of the original cavity (See Fig. 2) does not meet the resulting requirements of  $R = 49$  mm from optimization at target frequency of 2 kHz. Therefore, the optimal perforation as well as the frequency of TL peak will be different for the original cavity.

Acustimet™ MPP with the thickness of 1 mm, perforation ratio of 6.5 and the slit width of 0.240 mm, was utilized with the prototype cavity (Fig. 2 and 3) in an acoustic performance investigation of such type of silencers, reported in [11]. This combination matches the Cremer impedance closely under Mach 0.05 mean flow conditions and a frequency of  $\approx 2.6$  kHz. Respective experimentally determined TL spectra is plotted in Fig. 10.

Expectedly this close to optimal configuration gives a very high and broad TL peak (Fig. 10) at a frequency determined by the Cremer impedance. As the damping in such a dissipative setup is length dependent of the locally reacting surface, and since the length is seen longer in upstream propagation, the TL spectra in that direction is noticeably higher.

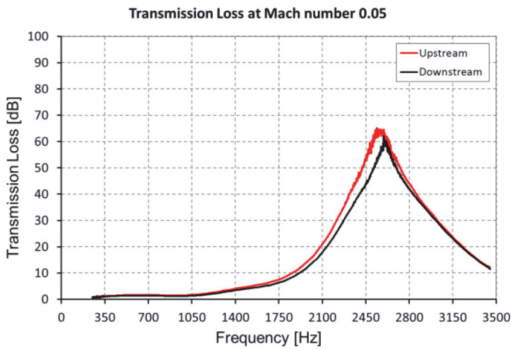


Figure 10. Experimental TL of the compact silencer configuration consisting of prototype cavity (Fig. 2 and 3) and close to optimal MPP under 0.05 Mach mean flow conditions at  $\approx 2.6$  kHz [11].

## SUMMARY AND CONCLUDING REMARKS

In the present work, a novel type of compact MPP silencer is discussed and it is demonstrated how the damping can be optimized using the so called Cremer impedance. This optimum can be used for all silencers systems that are locally reacting and ensures maximum dissipation of the fundamental (plane wave) mode. Despite its potential for reaching very high damping levels, several hundred dB/m, this possibility has rarely been used in practical silencer design. For medium and high frequencies the Cremer impedance will lead to dissipative type of silencers. But since the impedance is proportional to the Helmholtz-number, see Eq. 14, it goes to 0 for low frequencies, i.e., giving a reactive silencer or resonator.

The optimization results presented are based on a prediction model validated by experimental data. In addition to modelling results, the experimentally determined transmission loss curve of the existing prototype cavity equipped with approximately optimal Acustimet™ MPP under 0.05 Mach mean flow conditions has been presented. But still it remains to build and test more optimized silencers, in particular the effect of flow, high sound levels and separately optimized sections.

## REFERENCES

1. Regulation (EC) No 715/2007 of the European Parliament and of the Council of 20 June 2007 on type approval of motor vehicles with respect to emissions from light passenger and commercial vehicles (Euro 5 and Euro 6) and on access to vehicle repair and maintenance information, *Official Journal of the European Union* L171, 2007.
2. Allam, S., Åbom, M., "A New Type of Muffler Based on Microperforated Tubes," *Journal of Vibration and Acoustics* 133(03):1005, 2011, doi:10.1115/1.4002956.
3. Åbom, M. and Allam, S., "Dissipative Silencers Based on Micro-Perforated Plates," SAE Technical Paper 2013-24-0071, 2013, doi:10.4271/2013-24-0071.

4. Maa D.-Y., "Theory and design of micro perforated-panel sound-absorbing construction," *Science China Mathematics* XVIII:55-71, 1975.
5. Åbom, M., "Measurement of the Scattering-Matrix of Acoustical Two-Ports," *Mechanical Systems and Signal Processing* 5(2):89-104, 1991.
6. Guo, Y., Allam, S., Åbom, M., "Microperforated plates for vehicle applications," *Proceedings of Inter-Noise*, 2008.
7. COMSOL AB, "COMSOL Multiphysics®," [www.comsol.se](http://www.comsol.se).
8. Givoli, D., Neta, B., "High-order non-reflecting boundary scheme for time-dependent waves," *Journal of Computational Physics* 186:24-46, 2004.
9. Cremer, L., "Theory regarding the attenuation of sound transmitted by air in a rectangular duct with an absorbing wall, and the maximum attenuation constant produced during this process," *Acustica* 3:249-263, 1953.
10. Tester, B. J., "The propagation and attenuation of sound in lined ducts containing uniform or "plug" flow," *Journal of Sound and Vibration* 28(2):151-203, 1973.
11. Kabral, R., Auriemma, F., Knutsson, M., Åbom, M., "A New Type of Compact Silencer for High Frequency Noise," *Online Proceedings of the 9th International DAAAM Baltic Conference*, ISSN 2346-6138.

## CONTACT INFORMATION

Raimo Kabral  
Competence Center for Gas Exchange  
KTH-The Royal Institute of Technology  
Teknikringen 8, Stockholm, SE-10044, Sweden  
[kabral@kth.se](mailto:kabral@kth.se)

Mats Åbom  
The Marcus Wallenberg Laboratory  
KTH-The Royal Institute of Technology  
Teknikringen 8, Stockholm, SE-10044, Sweden  
[matsabom@kth.se](mailto:matsabom@kth.se)

## ACKNOWLEDGMENTS

The financial support from European Union (7th Framework program) through Marie Curie actions initial training network FlowAirS ([www.flowairs.eu](http://www.flowairs.eu)) is greatly acknowledged.

## DEFINITIONS/ABBREVIATIONS

**BPF** - Blade or lobe passing frequency

**FEM** - Finite element method

**MPP** - Micro-perforated panel

**IC** - Internal combustion

**TL** - Sound transmission loss



## Paper III

Kabral, R., Auriemma, F., Knutsson, M., Åbom, M.  
A new type of compact silencer for high frequency noise.  
*9th International DAAAM Baltic Conference,  
Tallinn, Estonia, April 24-26, 2014.*



## A NEW TYPE OF COMPACT SILENCER FOR HIGH FREQUENCY NOISE

Kabral, R., Auriemma, F., Knutsson, M., Åbom, M.

**Abstract:** *In modern IC engine design super-chargers are utilized to increase the fuel conversion efficiency. Nevertheless, these components are also recognized as strong high frequency noise sources in the engine compartment. For installations under such limited space and high sound pressure conditions innovative noise control concepts are essential.*

*To reduce this type of noise a new type of silencer based on micro-perforated plates and optimized using the so called Cremer's acoustic impedance is proposed and investigated experimentally. The experimental data is also used to validate modelling done on the new silencer.*

*Key words: Compact silencer, Micro-perforated, Acoustic impedance, Super-Charger.*

### 1. INTRODUCTION

Since 2015 the vehicle manufacturers have been obliged to implement engines complying the Euro 6 emission standard [1]. To this aim, the super-charging of the engine is almost un-avoidable, as it increases the indicated fuel conversion efficiency. On the other hand, additional concerns related with high frequency noise generation, will arise from compressors. Traditional solutions to reduce intake noise of the IC engine are based on the well-known Helmholtz resonator, which reflects sound generated back to the source. Moreover, sound reflections also occur at the opening of the duct termination (See e.g. [2] or [3]). Therefore, in such solutions, the noise dissipation relies on the source ability to absorb the reflected noise.

To overcome this dependence, and to design a robust noise control solution, the sound has to be dissipated by properly designed absorptive elements.

Traditionally, dissipative silencers are based on fibrous materials, which pollute the medium and, when integrated to the air inlet, can cause failure of the IC unit.

Therefore, producing acoustic absorption with non-fibrous materials is of interest.

The idea of producing acoustic resistance in room applications by employing the viscosity in circular small apertures (in order of acoustic boundary layer) is originated from D. Y. Maa [4]. Usually, producing such acoustic elements is a time consuming and expensive process. These issues can be overcome by using mass produced sound absorbing panels called Acustimet™ [5].

These panels were studied also as one possible noise control solution in vehicle applications (See e.g. [6]). In addition, a new type of silencer based on the micro-perforated panels (MPP) was proposed and studied by Allam and Åbom in [7]. In order to eliminate the drawback of having transmission loss minima at half-wave length multiples, the locally reacting limit was formulated by Åbom and Allam in [8]. The proposed design consists of straight-flow channel made of MPP that is adjoined to locally reacting cavity, thus resulting in a locally reacting surface.

Kabral et. al. proposed the optimization technique for such compact silencer in the [9]. The essence of the method is matching the acoustic wall impedance with the Cremer optimum impedance [10]. The latter was derived to obtain the highest sound damping in an infinite channel. The

concept was developed further by Tester in [11], who derived the expression for the circular cross-section, and also added the plug-flow correction as follows:

$$Z_{CC} = (0.88 - 0.38i) \frac{kr}{\pi(1 + M)^2}, \quad (1)$$

$Z_{CC}$  – the norm. surface impedance for theor. maximum sound damping in a circular duct;

$k$  – the wave number,  $m^{-1}$ ;

$r$  – the radius of the channel, m;

$M$  – the Mach number.

The investigation in [9] was carried out by employing simplified FEM model where the cavity and perforation of the compact silencer were defined as an acoustic impedance boundary condition. The model was been validated with hi-resistance configuration under no flow conditions.

The results indicated that, by implementing this optimization technique, very high controlled sound damping is achievable.

In the present work, a systematic validation of the modelling, and a detailed investigation of the sound damping mechanisms, will be performed. The same prototype cavity, used in [9], will be implemented in configuration with three different Acustimet™ MPPs (see Fig. 1). In addition, the same simplified FEM model is employed to compute acoustic quantities corresponding to the Cremer's optimum.

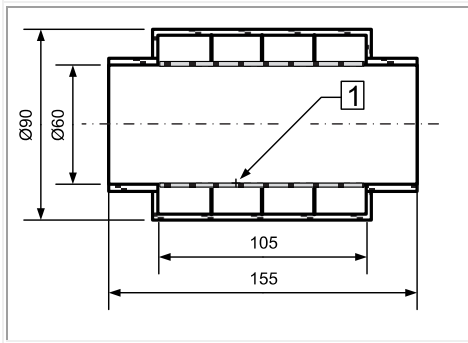


Fig.1. The sketch of the prototype silencer [9] with indicated MPP in field no. 1.

## 2. METHOD

In order to evaluate if the MPP and cavity combination is optimal, the acoustic impedance of the absorbing surface has to be determined and compared to the Cremer's optimum. In the compact silencer this impedance is formed by contributions from MPP and the locally reacting cavity as

$$Z_{surf} = Z_{MPP} + Z_{cav}, \quad (2)$$

where

$Z_{surf}$  – a normalized surface impedance;

$Z_{MPP}$  – the normalized MPP impedance;

$Z_{cav}$  – the normalized cavity impedance.

The geometrical parameters are known in case of two of the three MPP Acustimet included in the investigation (Tab. 1). As a consequence, the acoustic transfer impedance can be determined by means of existing semi-empirical models. On the other hand, exact parameters of the Acustimet panel with largest apertures are unknown, except the thickness, which is 1mm for all the panels. Therefore, the acoustic transfer impedance of this panel will be determined experimentally.

Name	Perforation Ratio	Slit width [mm]
Res. 0.05	Unknown	Unknown
Res. 0.25	6.5	0.240
Res. 1.50	4.3	0.095

Table 1. Geometrical parameters of Acustimet MPP's.

### 2.1 Acoustic impedance models

The comprehensive overview of the existing semi-empirical models for MPP transfer impedance has been given by Guo et. al. in [6]. The resulting model of slit type MPP, utilized also herein, was validated experimentally by testing different Acustimet™ panels.

The acoustic resistance  $Re(Z)$  and reactance  $Im(Z)$  of Acustimet MPP is being computed as:

$$r_s = \text{Re} \left\{ \frac{i\omega t}{\sigma c} \left[ 1 - \frac{\tanh(k\sqrt{i})}{k\sqrt{i}} \right]^{-1} \right\} + \frac{4R_s}{\sigma\rho c} + \frac{|u_h|}{\sigma c} + \beta \frac{M}{\sigma} \quad (3)$$

and

$$x_s = \text{Im} \left\{ \frac{i\omega t}{\sigma c} \left[ 1 - \frac{\tanh(k\sqrt{i})}{k\sqrt{i}} \right]^{-1} \right\}, \quad (4)$$

where

- $\omega$  – a radial frequency,  $s^{-1}$ ;
- $\rho$  – the density of the medium,  $kg/m^3$ ;
- $k$  – shear wave number,  $m^{-1}$ ;
- $t$  – the thickness of perforated panel, m;
- $\sigma$  – the porosity of the perf. surface;
- $\beta$  – a factor for grazing flow effects;
- $u_h$  – peak particle velocity in apertures, m/s; and
- $R_s$  – surface resistance, Pas/m.

The shear wave number which is used to relate the acoustic boundary layer thickness with the dimensions of the aperture, is defined as:

$$k = d \sqrt{\frac{\omega}{4\nu}}, \quad (5)$$

where

- $d$  – the slit width, m; and
- $\nu$  – the kinematic viscosity of medium,  $m^2/s$ .

The consequence of the oscillating motion of the fluid on the perforated surface is the increase of the acoustic resistance, which contribution is given by [6]:

$$R_s = \frac{1}{2} \sqrt{2\rho\omega\eta}, \quad (6)$$

where

- $\eta$  – the dynamic viscosity of the medium,  $kgm^2/s$ .

The equation for cavity impedance, implemented herein, was derived in [8] as:

$$Z_{cav} = \frac{i \left[ H_0^{(1)}(k_a r) - \frac{H_1^{(1)}(k_a R)}{H_1^{(2)}(k_a R)} H_0^{(2)}(k_a r) \right]}{H_1^{(1)}(k_a r) - \frac{H_1^{(1)}(k_a R)}{H_1^{(2)}(k_a R)} H_1^{(2)}(k_a r)}, \quad (7)$$

where

- $k_a$  – the axial wave number,  $m^{-1}$ ;
- $R$  – the radius of the expansion chamber, m;
- $r$  – the radius of main duct, m;
- $H_m^{(n)}$  – the Hankel function of n:th kind and m:th order.

## 2.2 Experiments

The experimental procedures in the present work is considering plane wave 0<sup>th</sup> duct mode and assuming time dependency of  $\exp(i\omega t)$ . Consequently, the well-known acoustic two-port model [12] for flow-duct elements is appropriate for the investigation.

Depending on the selection of acoustic state variables, the linear relation of the states between the ports are given though either acoustic scattering (Eq. 8) or transfer matrix (Eq. 9) [12]:

$$\begin{bmatrix} p_{a+}^I & p_{a+}^{II} \\ p_{b+}^I & p_{b+}^{II} \end{bmatrix} = \begin{bmatrix} R_a & T_b \\ T_a & R_b \end{bmatrix} \begin{bmatrix} p_{a-}^I & p_{a-}^{II} \\ p_{b-}^I & p_{b-}^{II} \end{bmatrix}, \quad (8)$$

$$\begin{bmatrix} p_a^I & p_a^{II} \\ q_a^I & q_a^{II} \end{bmatrix} = \begin{bmatrix} T_{11} & T_{12} \\ T_{21} & T_{22} \end{bmatrix} \begin{bmatrix} p_b^I & p_b^{II} \\ q_b^I & q_b^{II} \end{bmatrix}, \quad (9)$$

where  $p_{a+}^I$  and  $p_{b-}^{II}$  are complex acoustic pressure wave amplitudes at port a and b of the first and second set of state variables. The subscript + and – indicate the propagation direction;  $R$  and  $T$  are complex reflection and transmission coefficients.

$p_a^I$  and  $q_b^{II}$  are total acoustic pressure and acoustic volume flow at port a and b of first and second set of state variables.

By considering the number of unknowns in these matrixes, and by assuming not

symmetric setup, two sets of linearly independent state vectors have to be experimentally determined.

While the elements of scattering matrix are straightforward description of the wave interaction problem, the transfer matrix formulation is more appropriate for estimation of transfer properties, e.g. acoustic impedance. Moreover, one can be obtained from the other one by linear transformation of the state vectors.

In order to determine the necessary state vectors of two-port, the acoustic pressures at both branches are measured with duct wall mounted microphones. Finally, the wave decomposition is carried out according to technique described in [13].

For perforated elements, whose thickness is much smaller than the acoustic wave length, the air inside the apertures can be considered as lumped mass. In this case it can be shown that the transfer matrix elements (Eq. 9) become  $T_{11} = 1$ ,  $T_{21} = 0$ ,  $T_{22} = 1$  and  $T_{12} = Z_{MPP}\rho_0 c/A$ .

## 2.2 Performance parameters

The most common quantity used to evaluate the acoustic performance of a silencer is sound transmission loss (TL). The TL can be interpreted as the loss of acoustic power in sound transmission through the two-port element. This can be obtained from the transmission elements of the scattering matrix (Eq. 8) according to:

$$TL = 10 \log_{10} \left( \frac{1}{|T|^2} \right), \quad (10)$$

The Eq. 10 is valid in case of same cross-sectional area in both ports ( $a$  and  $b$ ), negligible flow pressure loss and temperature gradient.

The transmission loss is produced by the absorption and reflection of incident waves.

The latter is not favorable, in terms of robust noise control solution, since it relies on the ability of the source to absorb the reflected waves. Hence, the TL alone is not

sufficient to evaluate the silencers acoustic performance.

In addition to the TL, the absorption coefficient spectra are commonly studied to evaluate the silencer ability to absorb sound. This can be computed by utilizing the scattering matrix elements and normalizing the input sound power to 1W as:

$$A = 1 - |R|^2 \frac{(1 - M)^2}{(1 + M)^2} - |T|^2, \quad (11)$$

The absorption coefficient provides insight of how much incident sound power is absorbed. This is not adequate to evaluate the performance of the absorbing element of the silencer as soon as  $R$  becomes not negligible. In addition, the absorption coefficient is computed in linear domain while the sound perceived by the receiving person is in logarithmic scale.

Therefore, for optimization purposes, the sound actually entering the silencer has to be considered. This can be done by computing sound absorption (SA) instead of absorption coefficient as:

$$SA = 10 \log_{10} \left[ \frac{1 - |R|^2 \frac{(1 - M)^2}{(1 + M)^2}}{|T|^2} \right], \quad (12)$$

Also the sound reflected can be obtained in similar fashion as:

$$SR = -10 \log_{10} \left[ 1 - |R|^2 \frac{(1 - M)^2}{(1 + M)^2} \right], \quad (13)$$

The set of TL, SA and SR will give detailed description of the silencer acoustic performance and quantification of dampened, absorbed and reflected sound power. Hence, the set of these logarithmic quantities is adequate to evaluate the goodness of the optimized silencer.

### 3. RESULTS

The normalized acoustic resistance and reactance of locally reacting surface inside the compact silencer prototype has been computed by means of Eq. 3, 4 and 7 for Res. 0.25 and Res 1.50 MPPs (See Tab. 1).

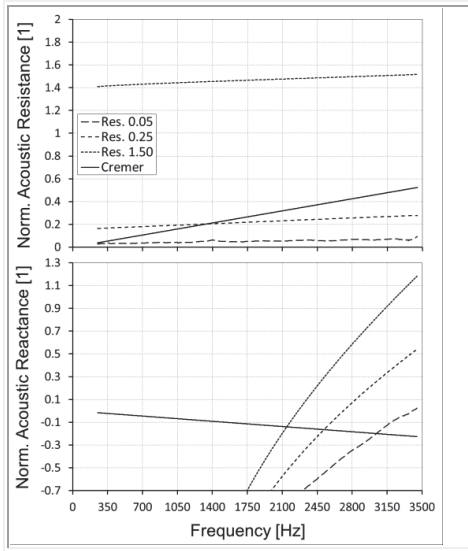


Fig. 2. Acoustic Impedance of the locally reacting surface inside the compact silencer prototype for no mean flow case.

The respective quantities of Res. 0.05 MPP are obtained by combining the experimentally determined transfer impedance with the Eq. 7 according to Eq. 2. These results are plotted in the comparison with the Cremer's optimum for no mean flow case in the Fig. 2.

In the Fig. 2 one can observe that, for none of the configurations, the total (Eq. 2) acoustic impedance is not matching exactly the Cremer's optimum. Nevertheless, the prototype provided with the MPP of Res. 0.25 is matching the above optimum at around 2.5 kHz, since the delivered normalized resistance is only 0.1 lower.

However, as the grazing flow on the surface of MPP generates additional contribution to the resistance (See Eq. 3), it is expected to match the Cremer condition

even better when a mean flow through the silencer is introduced.

In the Fig. 3 the acoustic surface impedance of the configuration with the Res. 0.25 MPP is computed and compared to the Cremer optimum in case of 0.05 Mach mean flow condition.

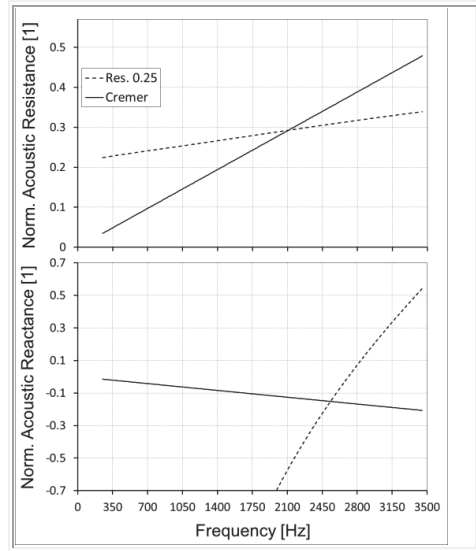


Fig. 3. Acoustic Impedance of the locally reacting surface inside the compact silencer prototype for 0.05 Mach mean flow case.

It can be seen in the plot (Fig. 3) that, in case of 0.05 Mach mean flow, the Cremer condition is closely fulfilled.

In the following figure (Fig. 4) the set of acoustic performance quantities (See Eq. 12 and 13) are plotted for the three compact silencer configurations in no mean flow conditions.

The wide and low TL peak of Res. 1.50 configuration in Fig. 4 indicates the absorptive type of damping which can be confirmed by observing the SA curve of the same configuration. In this setup the acoustic resistance is too large, i.e. the access to the cavity is restricted and, therefore, the cavity is not efficiently utilized.

Although this type of low reflection behavior (See the SR curve in the Fig. 4) is desirable in anechoic terminations, it is not

optimum in perspective of space, and hence it will not be considered further.

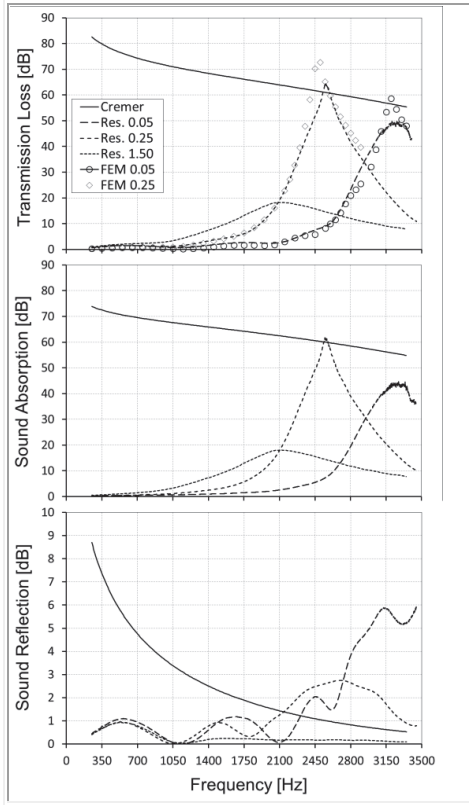


Fig. 4. Acoustic performance quantities under no mean flow conditions.

The other configurations in Fig.4 have both high TL peaks. For this reason, by looking only at the TL spectrums, it would be hard prefer one over another. Nevertheless, by studying the SA an SR spectrums, the mechanism on sound damping is revealed. One has to note that the cut-off of the peak of the configuration Res.0.05 is believed related with the experimental difficulties to realize the completely sealed cavities. This means that even higher reflection properties are expected.

The transfer impedance of the MPPs has been determined for planar elements, whereas the plates inside prototype are bended to tubular shape. Nevertheless, the

numerical results of simplified FEM model presented in [9] are validated reasonably well for both configurations in the Fig. 4.

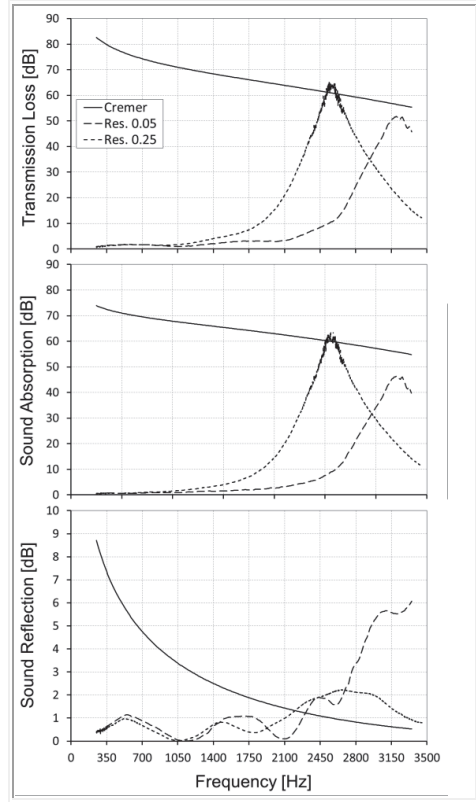


Fig. 5. Acoustic performance quantities under 0.05 Mach mean flow conditions.

Accordingly, this modelling technique can be efficiently utilized in the optimization process.

In the Fig.5 it is observable that the absorption properties of the prototype configurations are unaffected and the reflection of sound has been reduced further at the resonance frequency.

#### 4. CONCLUSIONS

In the present work a new type of compact silencer was proposed and experimentally investigated. In addition, the numerical model of this silencer has been validated.

It was shown that the sound transmission loss is not adequate for the acoustic performance assessment of the compact silencer.

To get better insight of the sound damping mechanism, another set of quantities, describing the sound power distribution, were derived and analyzed.

This enabled to evaluate whether in a certain configuration the absorption is optimal.

It was confirmed experimentally that the proposed compact silencer, optimized according to the Cremer's impedance, is a very effective solution for noise control.

## 5. REFERENCES

1. Regulation (EC) No 715/2007 of the European Parliament and of the Council, Official Journal of the European Union L171, 2007.
2. Rämmal, H.; Lavrentjev, J. "Sound reflection at an open end of a circular duct exhausting hot gas", *Noise Control Engineering Journal*, 2008, 56(2), 107-114.
3. Tiikoja, H.; Lavrentjev, J.; Rämmal, H.; Åbom, M. "Experimental Investigations of Sound Reflection from Hot and Subsonic Flow Duct Termination", *Journal of Sound and Vibration*, 2014, 333(3), 788 - 800.
4. Maa, D.-Y., "Theory and design of micro perforated-panel sound-absorbing construction," *Science China Mathematics* 1975, XVIII:55-71.
5. Knipstein, D., "Soundabsorbing element and procedure for manufacture of this element and use of this element", *European Patent No. EP0876539*, 23.01.1997.
6. Guo, Y., Allam, S., Åbom, M., "Microperforated plates for vehicle applications", *Proceedings of Inter-Noise*, 2008.
7. Allam, S., Åbom, M., "A New Type of Muffler Based on Microperforated Tubes", *Journal of Vibration and Acoustics*, 2011, 133(03):1005.

8. Åbom, M., Allam, S., "Dissipative Silencers Based on Micro-Perforated Plates", *SAE Technical Paper Series*, 2013, 2013-24-0071.

9. Kabral, R., Du, L., Åbom, M., Knutsson, M., "A Compact Silencer for the Control of Compressor Noise", *SAE Technical Paper Series*, 2014, 2014-01-2060.

10. Cremer, L., "Theory regarding the attenuation of sound transmitted by air in a rectangular duct...", *Acustica*, 1953, 3:249-263.

11. Tester, B. J., "The propagation and attenuation of sound in lined ducts containing uniform or "plug" flow," *Journal of Sound and Vibration*, 1973, 28(2):151-203.

12. Åbom, M., "Measurement of the Scattering-Matrix of Acoustical Two-Ports", *Mechanical Systems and Signal Processing*, 1991, 5(2):89-104.

13. Seybert, A., F., Ross, D., F., "Experimental Determination of Acoustic Properties Using a Two-Microphone Random-Excitation Technique", *Journal of Acoustical Society of America*, 1977, 61(5):1362-1370.

## 6. ADDITIONAL DATA ABOUT AUTHORS

Raimo Kabral, KTH, Tallinn University of Technology, [kabral@kth.se](mailto:kabral@kth.se).

Fabio Auriemma, Tallinn University of Technology.

Magnus Knutsson, Volvo Car Corporation.  
Mats Åbom, MWL KTH Royal Institute of Technology.

## 7. ACKNOWLEDGMENTS

The financial support from European Union (7th Framework program) through Marie Curie actions initial training network FlowAirS ([www.flowairs.eu](http://www.flowairs.eu)) is greatly acknowledged.

The financial support of the ERMOS programme (Co-funded by Marie Curie Actions) is acknowledged too.



## Paper IV

Kabral, R., Rammal, H., and Lavrentjev, J.  
Acoustic studies of micro-perforates for small engine silencers.  
*SAE Technical Paper Series*, 2012, Paper no. 2012-32-0107,  
doi:10.4271/2012-32-0107.

Reprinted with permission from SAE paper 2012-32-0107 Copyright © 2012 SAE International. This paper may not be reprinted, copied, distributed, or saved on any retrieval system without prior permission from SAE.



## Acoustic Studies of Micro-Perforates for Small Engine Silencers

2012-32-0107

20129107

Published

10/23/2012

Raimo Kabral  
TUT/KTH Royal Institute of Technology

Hans Rämmal and Jüri Lavrentjev  
Tallinn University of Technology

Copyright © 2012 SAE International and Copyright © 2012 SAE Japan

doi:10.4271/2012-32-0107

### **ABSTRACT**

To respond growingly strict environmental regulations the acousticians are challenging to develop novel types of silencing elements. There are different types of flow duct elements designed for silencing the pulsating gas flows into and out of fluid machines. The silencing effect is typically achieved by introducing acoustic reflection and absorption.

In order to achieve a good absorption in a wide frequency band, various fibrous materials e.g. wools are typically implemented. However, the physical properties of such materials do not often remain constant during the lifetime of a silencer. As the fibers tend to relocate and can partly be blown out to surroundings, acoustical performance may deteriorate. Therefore, it is in great interest to avoid fibrous materials in the design of the flow duct silencing elements.

The present work is focused on the modern type of absorptive acoustic element - a micro-perforated element. The absorption in micro perforated element is dominantly originating from the viscous effect inside the openings, non-linear acoustic vortex shedding and grazing flow iteration. To exert the advantages of this type of perforation, the opening dimensions have to be smaller than the thickness of the acoustic boundary layer i.e. in the sub millimeter range. Although different micro-perforated panels have been studied by several authors mainly for room acoustic applications, only a relatively few publications concerning the flow duct elements are currently available.

In this paper a number of different perforated elements including micro-perforates have been studied by varying the perforation shape and porosity. The studies have resulted in the development of micro perforated tubes with high absorptive properties. The micro-perforated tubes have successfully been implemented in the design of a Formula SAE racing silencer.

The scattering matrix elements, as well as the transmission loss are presented and analyzed for a variety of perforated tubes and the complete silencer.

The results exhibit a good potential for the micro-perforated elements developed. Also it has been demonstrated that this type of absorptive element can effectively substitute the conventional designs incorporating fibrous materials.

### **INTRODUCTION**

In order to offer an alternative to traditional fibrous and porous absorbers micro-perforated panels (MPP) have been investigated for almost four decades. The MPP-s have generally been found to be reliable and effective absorptive silencer solutions suitable for in-duct applications [1,2,3,4,5,6,7,8,9].

Generally MPP-s are installed at a small distance from a solid surface thus forming an adjoining cavity behind the panel (see Fig. 1). The sub millimeter pores coupled to a cavity behind form a series of small Helmholtz resonators enabling noise attenuation. In the past most of the MPP-s were designed to consist of groups of circular apertures. Already

more than 30 years ago, Maa [1, 2] developed a model to characterize the absorption properties of MPP absorbers having circular-shaped apertures. This model enables to calculate the absorption coefficient of MPP as a function of four parameters: pore diameter  $d$ , panel porosity  $\sigma$ , panel thickness  $t$ , and cavity depth  $D$ , see Fig. 1. One limitation of Maa's work however is that non-uniform pore size and shape is not taken into account.

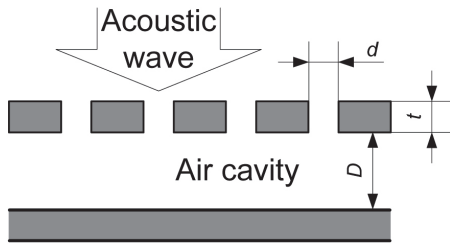


**Figure 1.** A schematic representation of MPP together with an adjoining air cavity.

The effective frequency range of MPP absorbers can be tuned by varying the pore diameter and porosity as well as the cavity depth. The effect of partitioning the air cavity has been noticed by several researchers. Yairi et al [3] first investigated the effect of subdivision of the adjoining air cavity on the MPP transmission loss properties. Hillereau et al. [4] considered a more complicated case where the subdivided cell walls were also made of porous material. They concluded that the variation of the porosity had a significant impact on the acoustic attenuation of the MPP. A parametric study of the MPP-s to investigate the impact of each of these parameters on the absorption coefficient can be found in [5, 6, 7]. Generally, the MPP offer a maximum absorption when the depth of the cavity is approximately one-quarter of wavelength, causing the highest acoustic particle velocity inside the pore.

Due to the described benefits, the MPP absorbers are being increasingly used in automotive applications, including silencers [8, 9]. Traditionally, different sound absorbing materials e.g. glass fiber or foams have been used in acoustic silencers in order to achieve desirable attenuation. Those porous absorbing materials however deteriorate over time and are typically non-renewable. Therefore the MPP absorbers have been found to be an attractive alternative to fibers and foams used in silencers. Ordinary perforates used in silencers are perforated to pore diameters in the order of millimeters with modest inherent acoustic resistance. The MPP absorbers typically have pore diameters ranging from 1 mm to as small as 0.1 mm, thus providing higher acoustic resistance and enabling improved sound attenuation. Due to the small pores and thin panels, remarkably high sound absorption coefficients can be achieved by relatively low material thickness compared to porous and fibrous absorbers.

Today, commercial MPP-s have in most cases been used in acoustic silencers. In the silencer applications the MPP-s however typically operate without the small cavity behind the panels. Therefore the theory by Maa's is not directly applicable for analytical determination of the absorption properties of the micro-perforated (MP) elements. Due to the lack of appropriate theoretical models experimental methods are widely implemented to investigate the acoustic performance of MPP-s. Currently advanced and accurate computer aided manufacturing technologies e.g. laser cutting, etching, and jetting can be employed to produce acoustic panels perforated by a variety of aperture geometries. The dimensions of circular pores or of any other aperture shapes can be designed to be uniform or varying across the panel.

Irregularly perforated apertures shapes can be designed in order to achieve higher absorption over a wider bandwidth. A combination of the MPP-s with different absorbing characteristics enables to design silencers offering high noise attenuation characteristics across a certain frequency range.

This paper presents an investigation of various custom made MP elements designed in different perforation aperture and porosity. The aim is to present a MP silencer element that offers high noise attenuation over wide frequency region and is applicable in small engine exhaust systems.

## EXPERIMENTS

The experimental investigations carried out in this paper are based on acoustic two-port model widely implemented for various flow duct elements. A detailed overview of this model is given in a recent paper by the authors of this work [10]. Hence only a brief description will follow herein.

Acoustic characteristics of the two-port can typically be described in the scattering matrix (S-matrix) form as follows:

$$\begin{bmatrix} p_{a+} \\ p_{b+} \end{bmatrix} = \begin{bmatrix} R_a & T_b \\ T_a & R_b \end{bmatrix} \begin{bmatrix} p_{a-} \\ p_{b-} \end{bmatrix}, \quad (1)$$

where  $p_+$  and  $p_-$  are complex pressure wave amplitudes propagating in the pipes coupled to the two-port (see Fig. 2),  $R$  is the reflection coefficient (RC) and  $T$  is the transmission coefficient (TC) of the two-port element studied. The subscripts a and b denote the inlet and outlet of the two-port element as exhibited in Fig. 2.

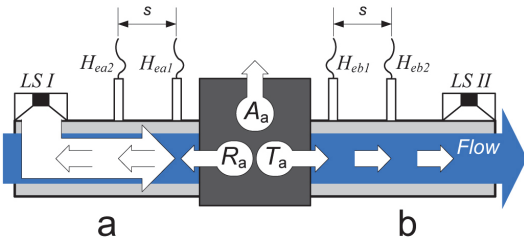


**Figure 2.** A simplified schematic layout of the measurement setup used in this paper to study the micro-perforated silencer elements and silencers. The white arrows represent the distribution of acoustic energy in case of activated loudspeaker (LS I).

The test samples investigated in this study are symmetrical perforated ( $l=100\text{mm}$ ) tubes (See Fig. 3). As the acoustic performance of these test tubes was believed to remain similar in both directions along the tube central axis in case of no flow conditions, only the coefficients characterizing the acoustic behavior in downstream direction i.e.  $R_a$  and  $T_a$  are treated in this paper (See Eq. 1). In order to simulate a realistic operating environment typically present inside a silencer chamber the samples were tested in a custom built measurement chamber (see Fig. 3) offering relatively high RC values.

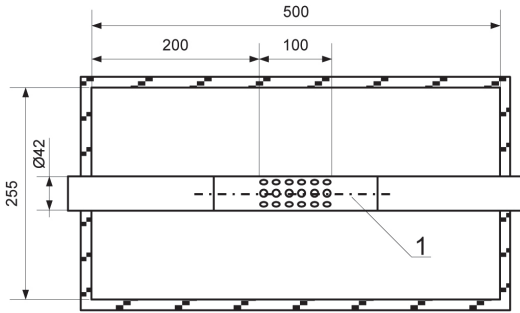


**Figure 3.** A measurement chamber incorporating a centrally positioned perforated test sample (1) (measurements are given in mm).

The RC and the TC of the test object can be determined by measuring the transfer functions between the loudspeaker (LS) excitation signal and the microphone signals obtained at four cross-sections of the pipes (See Fig. 2). In order to solve the equation system (Eq. 1) the source switching (or alternatively the load variation) techniques can be followed [11]. In this study the source switching is performed by activating the acoustic excitation (LS I and LS II) at side a and b respectively (See Fig. 2). The RC and the TC are then determined by implementing the following relations:

$$|R_a| = \frac{|H_{ea+}^{II} H_{eb-}^I - H_{ea+}^I H_{eb-}^{II}|}{|H_{ea-}^{II} H_{eb-}^I - H_{ea-}^I H_{eb-}^{II}|}, \quad (2)$$

$$|T_a| = \frac{|H_{eb+}^{II} H_{eb-}^I - H_{eb+}^I H_{eb-}^{II}|}{|H_{ea-}^{II} H_{eb-}^I - H_{ea-}^I H_{eb-}^{II}|}, \quad (3)$$

where

$$H_{ea+} = \frac{H_{ea1} \exp(ik_a s) - H_{ea2}}{\exp(ik_a s) - \exp(-ik_a s)},$$

$$H_{ea-} = \frac{-H_{ea1} \exp(-ik_a s) + H_{ea2}}{\exp(ik_a s) - \exp(-ik_a s)},$$

$$H_{eb+} = \frac{H_{eb1} \exp(ik_b s) - H_{eb2}}{\exp(ik_b s) - \exp(-ik_b s)},$$

$$H_{eb-} = \frac{-H_{eb1} \exp(-ik_b s) + H_{eb2}}{\exp(ik_b s) - \exp(-ik_b s)}, \quad (4)$$

$H_e$  is a transfer function respectively,  $M$  is the Mach number of the media flowing through the two-port element,  $k$  is the wave number and  $s$  is the microphone separation. The superscripts I and II denote the driving signal of the respective LS (See Fig. 2).

In order to characterize and compare the selected test samples primarily considering the ability to absorb acoustic energy, the absorption coefficient (AC) has been determined [12]. Typically, the AC describes the amount of the acoustic energy absorbed by material. In case of the two-port element incorporating an expansion chamber and quarter-wave resonators (See Fig. 3) the AC will be additionally affected by the interference between the incident and the reflected acoustic pressure waves inside the chamber. Therefore the AC can be regarded as an indicator that contributes the acoustic energy lost by two relevant mechanisms: the sound absorption and the interference effects taking place inside the silencer structures. As the characterization and development of highly absorptive MP in-duct elements was aimed, the AC was found to be a key parameter considered in this study.

The AC can be calculated by implementing the RC and the TC as follows [12]:

$$A_a = 1 - \left[ |R_a| \left( \frac{1 - M_a}{1 + M_a} \right) \right]^2 - \left[ |T_a| \left( \frac{1 + M_b}{1 + M_a} \right) \right]^2. \quad (5)$$

To compare the acoustic performance of the complete silencers the transmission loss (TL), as a widely used engineering parameter, was utilized. Being a ratio of the

incident and transmitted sound power, the transmission loss can be calculated by the following relationship:

$$TL_a = 10 \log \left[ \frac{A_a \cdot \rho_b \cdot c_b \cdot (1 + M_a)^2}{A_b \cdot \rho_a \cdot |T_a|^2 \cdot c_a \cdot (1 + M_b)^2} \right], \quad (6)$$

where  $A$  is the cross sectional area of the flow-channel,  $\rho$  is the density of the flowing media and  $c$  is the speed of sound [13].

The experiments were performed by using a dedicated hot flow test-rig technically described in a previous study, reported in [10]. However, all the measurements in this work have been carried out at the ambient temperature. A measurement section of the test rig set up for the characterization of micro-perforated silencer elements is presented in Fig. 4.

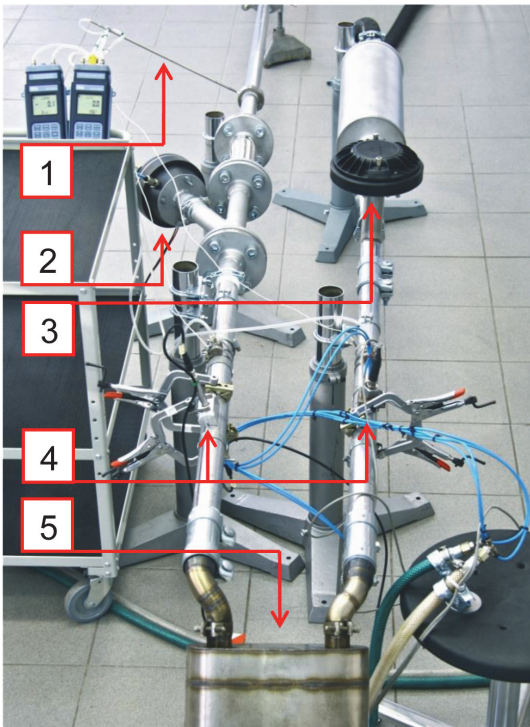


**Figure 4. A measurement section of the test-rig incorporating the following main parts: Pitot tube (1), loud speaker I (2) and II (3), microphones (4), object under test (5).**

The losses of acoustic energy in the apertures of the micro-perforated elements have been found [14] to be directly related to the particle velocity of the elastic media inside the apertures. Therefore, to achieve relatively high particle

velocity, a white noise excitation was chosen with average sound pressure level exceeding 110 dB.

Technically the perforations can be defined by the geometrical shape of the apertures and by the porosity. In this paper the effect of aperture geometry, particularly of the ratio between the perimeter and area (PA Ratio), has been investigated focusing on the acoustic losses. Additionally, the influence of the porosity has been studied experimentally.

Tubular test samples offering various PA Ratio-s and porosity (see Table 1) were manufactured. Traditional circular apertures, triangular and slit-type perforations were designed.

**Table 1. A technical description of the perforated samples investigated.**

Name	Aperture Sketch (mm)	P/A Rat.	Photo	Porosity
Sample 1		4.0		10%
Sample 2		5.1		10%
Sample 3		13.4		10%
Sample 4		13.4		2%
Sample 5		13.4		2%

The samples were produced of stainless steel pipes by employing a CNC laser tool. The minimum dimension of the perforated apertures was limited by the diameter of the laser beam (approximately 0.15mm). Due to technological issues (structural stability, material melting and etc.) the maximum porosity of the perforated samples was limited to 10% in this study. The higher porosity would believably provide an increase in the RC values. However, the porosities commonly treated by other authors for micro-perforated room acoustic applications remain in a region of 1...2 percent [see e.g. 15].

Additionally to the tests on the geometry and porosity of the perforations, the directionality in respect to the direction of the sound propagation and fluid flow was varied in the case of slit shaped apertures.

In order to provide comparison data of highly reflective and absorptive silencer configurations an empty measurement box (perforation ratio 100%) and a traditionally perforated absorptive pipe element (35% perforation ratio, 3mm circular aperture diameter and 20mm thick fibrous material wrapped around the element) were tested. After the determination of comparison data, the perforated samples described in [Table 1](#) were tested.

The challenge of the study was to find an aperture shape which provides the highest AC spectrum across the frequency range of interest (below 1,8kHz). The next step was to investigate the effect of perforation ratio (porosity) to the characteristics of the AC and the RC spectrums.

In order to simulate the estimated realistic conditions the element was designed for, the tests were additionally performed in 30m/s mean flow velocity conditions. In [\[10\]](#) it was found that the flow noticeably reduces the RC when passing through the straight-flow type of silencer. Hereby, a sample with relatively high RC value was found to be suitable for testing the flow effects. In case of a tubular perforated in duct element the perforated pores are expected to work in grazing flow conditions. Naturally, the grazing flow will produce vortex shedding around the perforated surface resulting in higher acoustic impedance, which in turn will believably cause a higher AC.

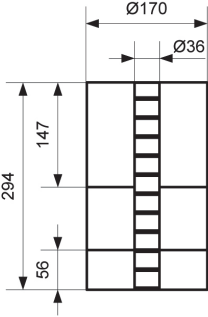
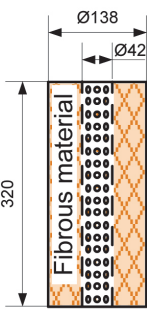
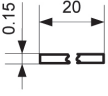
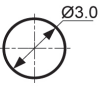
In addition to the acoustical performance of the in-duct silencer elements there is another important measure to be considered: the pressure drop (PD). In this study the PD was determined for all the perforated samples treated.

Based on the experimental results a suitable MPP configuration was developed for implementation in a small engine straight-flow silencer prototype.

In the present paper the novel prototype silencer equipped by the MP element developed is compared with the previous silencer (incorporating traditional 3mm perforations and fibrous materials) by considering the weight and TL in realistic flow velocity conditions. The acoustical characteristics of the previous silencer, successfully used during the last season, are provided by the authors in [\[10\]](#) in the S-matrix form.

Characteristic technical data of the silencers studied is presented in [Table 2](#).

**Table 2. A technical description of the micro-perforated prototype silencer and the conventionally perforated and fibrous material filled silencer.**

Name	Prototype	Conventional Silencer
Simplified Sketch		
Photo		
Aperture Sketch		
Porosity	10%	35%
Mass	1.43kg	1.81kg

## RESULTS AND DISCUSSION

In [Fig. 5](#) results of the preliminary experiments is presented.

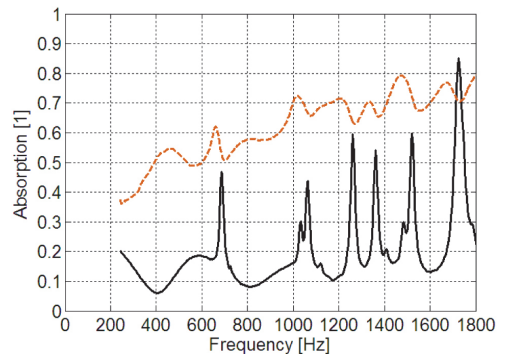


**Figure 5. The absorption coefficient of the empty test box (black solid) and the conventional perforation surrounded by fibrous material (orange dashed).**

In case of an empty measurement box a very resonant behavior can be noticed (see [Fig. 5](#)). Considering standing wave resonances inside the cavity this is natural. By adding a

conventionally perforated (3mm aperture diameter) element covered by 20mm thick fibrous material, a remarkable increase in AC over a wide frequency range was introduced. However, a majority of the characteristic resonance peaks that dominated the spectrum of empty box are still preserved.

The results of the perforated samples with different aperture geometries are compared with the conventional perforation together with fibrous material filling in the Fig. 6. For clarity the AC curve of the empty measurement box is excluded (See Fig. 5).

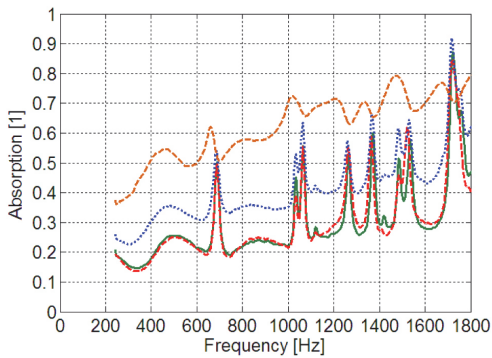


**Figure 6.** The absorption coefficient of sample 1 (red dashed), sample 2 (green solid), sample 3 (blue dotted) and conventional setup with wool (orange dashed).

As can be seen in the Fig. 6 the AC curves of the perforation samples 1 and 2 (See Tab. 1) appeared to be similar. The AC of sample 3 is noticeable higher in a wide frequency range exhibiting a generation of wideband losses originating from the micro-perforation. One can note that the samples 1 and 2 are both perforated to relatively similar PA Ratio compared to the sample 3 (See Tab. 1). This result enables to conclude that for an in-duct MP element the ability to absorb sound depends on the PA Ratio and a broad band attenuation improves by increasing the PA Ratio.

In the following Fig.-s 7 and 8 the AC and the RC of the samples with different porosities and aperture orientations are compared together with the comparison curves from Fig. 6.

The effect of smaller porosity value causes an upward shift of the AC curve can be observed in Fig. 7 in case of the samples 3 and 4. In Fig. 8 the opposite trend can be observed for the RC indicating higher reflections of sound with higher porosity. Practically this shows that the micro-perforated element with higher porosity is appropriate in reflective conditions (e.g. in reactive chamber type silencers) and vice versa.

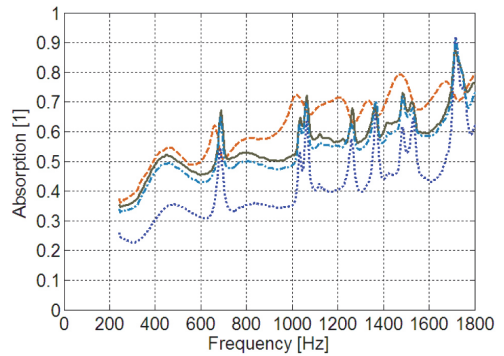


**Figure 7.** The absorption coefficient of sample 3 (blue dotted), sample 4 (light blue dash-dotted) and, sample 5 (gray solid) compared to the conventional setup with fibrous material (orange dashed).

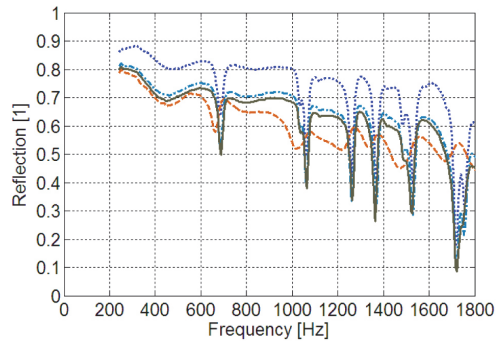


**Figure 8.** The reflection coefficient of sample 3 (blue dotted), sample 4 (light blue dash-dotted), sample 5 (gray solid) and the conventional setup with fibrous material (orange dashed).

The orientation of the aperture shape respectively to the propagation of sound waves affects the RC curve as can be seen in Fig. 8 in case of samples 4 and 5. However, despite of slightly favoring the longitudinally perforated element (Sample 4), the discrepancy between the results is relatively little. One should also mention that while the values of the RC remained relatively similar, the laterally perforated element (Sample 5) offers more AC (see Fig. 7) making this orientation a preferable solution for a flow duct.

Fig. 9 presents the results of the PD measurements. The most absorptive samples with different porosity and aperture orientations are compared.

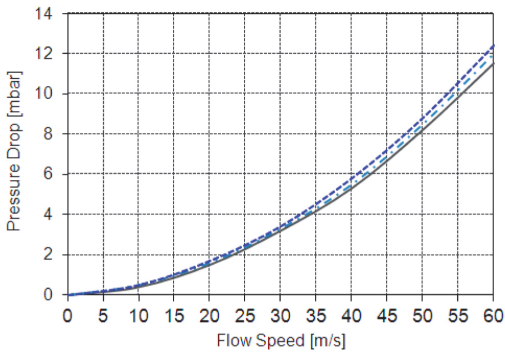


**Figure 9.** The pressure drop of the Sample 3 (blue dotted), the Sample 4 (light blue dash-dotted) and the Sample 5 (gray solid) measured in 25°... 28°C temperature range.

Although the PD difference for the relatively short tubular samples appears to be almost negligible one can notice that the higher perforation ratio expectedly tends to cause an increase in PD. At higher flow velocities the longitudinally oriented perforation also tends to increase flow resistance causing a minor PD growth.

For sample 4 the effect of flow velocity on the AC and RC is presented in Fig-s. 10 and 11.

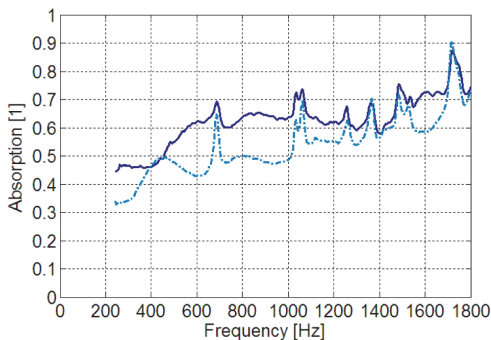


**Figure 10.** The absorption coefficient of the sample 4 in the absence of flow (light blue dash-dotted) and in 30m/s (dark blue solid) mean flow conditions.

As can be seen both the AC (Fig. 10) and RC (Fig. 11) are remarkably influenced by the flow velocity. While a broadband increase of the AC can clearly be observed in higher flow velocity conditions a broadband decrease was measured for the RC spectrum. This behavior can be explained by the appearance of higher acoustic impedance originating from the vortices generated by the grazing flow around the perforated surface.

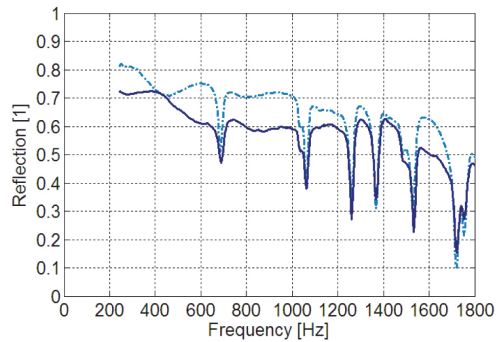


**Figure 11.** The reflection coefficient of the sample 4, measured in the absence of flow (light blue dash-dotted) and in 30m/s mean flow conditions (dark blue solid).

In practice, when implementing a MP element with high porosity in a relatively reflective setup, this result means that higher RC can be achieved by reducing the flow speeds around the perforation. This can for instance be technically solved by designing larger flow duct diameters.

The TL of the new prototype silencer is compared to the conventional silencer (see Table 2) in Figures 12 and 13. In order to study the effect of mean flow the results are presented in no flow (Fig. 12) and in 20m/s flow velocity conditions (Fig 13).

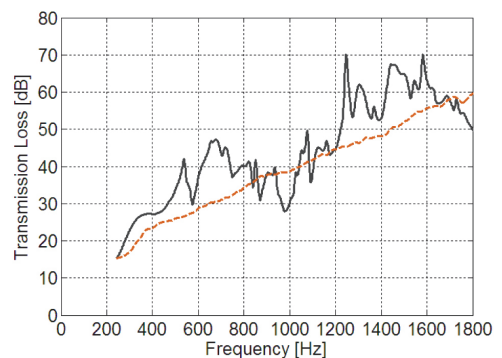


**Figure 12.** The transmission loss of the Prototype silencer (gray solid) and conventional straight-flow silencer (orange dashed) measured in the absence of flow.

In Fig-s. 12 and 13 the TL advantage of the MP element based prototype muffler can clearly be seen almost across the whole frequency range. By assuming the dominant noise generation at the first harmonics of the firing frequencies (typically occurring below 500Hz) the most important gain in TL (up to around 18dB at 650Hz), regarding noise control, takes place in the low frequency region. As can be noticed the

silencers expectedly represent clearly different silencing characteristics. The TL spectrum of the MP silencer is more resonant offering more reactive type of noise cancellation while the conventional configuration follows the expected character of an absorptive silencer. The results demonstrate that by choosing an appropriate configuration of a MP element perforation ratio and geometry, an efficient silencer can be designed that combines the sound absorption in perforated pores with the reactive effect of the chambers.

Based on the conclusions in a previous study [10] where the chamber wall vibrations were found to affect the acoustical performance of muffler, especially at the dominant high frequency resonances, the scattering around the TL peaks of the MP silencer, is believed to originate from the shell vibrations.

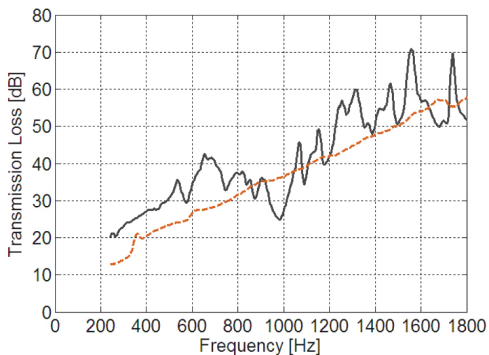


**Figure 13. The transmission loss of the prototype silencer (gray solid) and conventional straight-flow silencer (orange dashed) in 20m/s mean flow conditions.**

In case of the mean flow (see Fig. 13) the general trend discussed remains. Moreover, at very low frequencies (at around 250Hz) the MP prototype silencer introduces an extra attenuation when exposed to the mean flow conditions. The reason for this increase in low frequency attenuation can be explained by the vortex shedding around the apertures of the perforated element surface faced to a grazing flow as discussed earlier.

It should also be mentioned that, as opposed to the conventional perforation design, no whistling (characteristic tonal noise) was generated when testing the developed MP element in flow.

## CONCLUSIONS

A number of different perforations have been studied in this paper for the application in flow duct silencers. The experimentally determined acoustical results have been presented and analyzed as the absorption and reflection coefficient spectrums.

It was found that for the micro-perforated panels the ability to absorb acoustical energy could be improved by providing higher aperture perimeter to area ratio.

The results exhibit that micro-perforated elements with higher porosity would be favorable for applications in reactive silencer chambers.

The higher mean flow velocity was found to increase the low frequency absorption and decrease the reflection properties of the micro-perforated element.

As the primary result of this study an effective micro-perforated element has been developed and successfully implemented in a Formula SAE prototype silencer.

It has been demonstrated that an appropriately designed micro-perforated element can effectively substitute the conventional straight flow silencer filled by fibrous materials. Moreover, the absence of fibrous materials in combination with high attenuation abilities allow the micro-perforated silencers to provide a clear mass advantage (See Tab. 2).

## REFERENCES

1. Maa, D.Y., Theory and design of Microperforated-panel sound-absorbing construction. *Sci Sin*, XVIII (1975), pp. 55-71.
2. Maa, D.Y., Potential of microperforated panel absorber. *J Acoust Soc Am*, 104 (5) (1998), pp. 2861-2866.
3. Yairi, M, Sakagami, K, Morimoto, M, Minemura, A. Acoustical properties of microperforated panel absorbers with various configurations of the back cavity. In: *Proceeding of ICSV12, Lisbon, Portugal*; (2005).
4. Tao, Z., Zhang, B., Herrin, D., and Seybert, A., "Prediction of Sound-Absorbing Performance of Micro-Perforated Panels Using the Transfer Matrix Method," SAE Technical Paper 2005-01-2282, 2005, doi: [10.4271/2005-01-2282](https://doi.org/10.4271/2005-01-2282).
5. Toyoda, M., Takahashi, D., Sound transmission through a microperforated-panel structure with subdivided air cavities. *J Acoust Soc Am*, 124 (6) (2008), pp. 3594-3603.
6. Liu, J., Herrin, D.W., Enhancing micro-perforated panel attenuation by partitioning the adjoining cavity. *Applied Acoustics*, 71 (2), (2010) p 120-127.
7. Hillereau, Syed, A.A., Gutmark, E.J., Measurements of the acoustic attenuation by single layer acoustic liners constructed with simulated porous honeycomb cores. *J Sound Vib*, 286 (1-2) (2005), pp. 21-36
8. Wu, M.Q., Micro-perforated panels for duct silencing. *Noise Control Eng J*, 45 (2) (1997), pp. 69-77.
9. Allam, S., Abom, M., A New Type of Muffler Based on Microperforated Tubes, *J. Vib. Acoust.*, (2011), 133 (3), 8 pp.

10. Auriemma, F., Kabral, R., Rämmal, H., Lavrentjev, J. et al., "Acoustic Studies on Small Engine Silencer Elements," SAE Technical Paper [2011-32-0514](#), 2011, doi: [10.4271/2011-32-0514](#).

11. Bodén, H., Åbom, M., Modelling of fluid machines as sources of sound in duct and pipe systems, *Acta Acustica* 3 (1995) 549-560.

12. Lavrentjev, J., Rämmal, H., and Tiikoja, H., "The Passive Acoustic Effect of Automotive Catalytic Converters," SAE Technical Paper [2011-24-0219](#), 2011, doi: [10.4271/2011-24-0219](#).

13. Åbom, M., An Introduction to Flow Acoustics, 164 (2004).

14. Maa, D. Y., Microperforated panel at high sound intensity, *Proc. Internoise* 94 (1994).

15. Zou, J., Shen, Y., Yang, J., Qiu, X., A note on the prediction method of reverberant absorption coefficient of double layer micro-perforated membrane, *Applied Acoustics* 67 (2006).

## **CONTACT INFORMATION**

Raimo Kabral  
Department of Automotive Engineering  
Tallinn University of Technology  
Ehitajate tee 5, Tallinn, 19086, Estonia  
[kabral@kth.se](mailto:kabral@kth.se)  
phone: +372 50 24 992;

Dr. Hans Rämmal  
Department of Automotive Engineering  
Tallinn University of Technology  
Ehitajate tee 5, Tallinn, 19086, Estonia  
[hansra@kth.se](mailto:hansra@kth.se)  
phone: +372 56 465 738;

Prof. Jüri Lavrentjev  
Department of Automotive Engineering  
Tallinn University of Technology  
Ehitajate tee 5, Tallinn, 19086, Estonia  
[juri.lavrentjev@ttu.ee](mailto:juri.lavrentjev@ttu.ee)  
phone: +372 6 203 262.

## **ACKNOWLEDGMENTS**

The authors would like to acknowledge technical consultancy companies Lettore and Triple Seven for successful co-operation including financial, technical and technological support. In addition, the support from Estonian Science Foundation (Grant No. 7913), "DoRa" program of Archimedes Foundation and FP-7 PEOPLE Program (Marie Curie Actions) is acknowledged.

## **DEFINITIONS/ABBREVIATIONS**

**MPP** - micro-perforated panel

**MP** - micro-perforated

**RC** - reflection coefficient

**TC** - transmission coefficient

**LS** - loud speaker

**AC** - absorption coefficient

**TL** - transmission loss

**PA Ratio** - perimeter to area ratio

**PD** - pressure drop

---

The Engineering Meetings Board has approved this paper for publication. It has successfully completed SAE's peer review process under the supervision of the session organizer. This process requires a minimum of three (3) reviews by industry experts.

All rights reserved. No part of this publication may be reproduced, stored in a retrieval system, or transmitted, in any form or by any means, electronic, mechanical, photocopying, recording, or otherwise, without the prior written permission of SAE.

ISSN 0148-7191

Positions and opinions advanced in this paper are those of the author(s) and not necessarily those of SAE. The author is solely responsible for the content of the paper.

**SAE Customer Service:**  
Tel: 877-606-7323 (inside USA and Canada)  
Tel: 724-776-4970 (outside USA)  
Fax: 724-776-0790  
Email: [CustomerService@sae.org](mailto:CustomerService@sae.org)  
**SAE Web Address:** <http://www.sae.org>  
**Printed in USA**



# Curriculum Vitae

## 1. Personal data

Raimo Kabral  
1983.07.22, Tallinn, Estonia  
kabral@kth.se

## 2. Education

Educational institution	Graduation year	Education (field of study/degree)
Tallinn University of Technology	(2011)...	Technical acoustics / PhD studies
Tallinn University of Technology	2010	Product development and production engineering / MSc

## 3. Language competence/skills (fluent, average, basic skills)

Language	Level
Estonian	Native language
English	Fluent
Swedish	Basic

## 4. Research activity, including honors and thesis supervised

### Publications

Kabral, R., Abom, M., Bodén H., 7.6 Use of two-port acoustic data to investigate turbo-compressor surge, in: Aeroacoustics research in Europe: The CEAS-ASC report on 2013 highlights, *Journal of Sound and Vibration*, 2015, 340, 56.

Åbom, M., Kabral, R. Turbocharger noise - generation and control. *SAE Technical Paper Series*, 2014, Paper no. 2014-10-25.

Kabral, R., Åbom, M. Investigation of flow-acoustic interaction in automotive turbocharger. *International Conference on Noise and Vibration Engineering ISMA 2014, Leuven, Belgium, September 15-17, 2014*.

Kabral, R., Bodén, H., Elnady, T. Determination of liner impedance under high temperature and grazing flow conditions. *American Institute of Aeronautics and Astronautics conference Aviation 2014, Atlanta, USA, June 16-20, 2014.*

Kabral, R., Du, L., Åbom, M., Knutsson, M. A compact silencer for the control of compressor noise. *SAE Int. Journal of Engines*, 2014, 7(3), 1572-1578, doi:10.4271/2014-01-2060.

Kabral, R., Åbom, M. Ongoing acoustics research in the KTH-Competence Centre for Gas Exchange. *Baltic-Nordic Acoustic Meeting 2014, Tallinn, Estonia June 2-4, 2014.*

Kabral, R., Auriemma, F., Knutsson, M., Åbom, M. A new type of compact silencer for high frequency noise. *9th International DAAAM Baltic Conference, Tallinn, Estonia, April 24-26, 2014.*

Kabral, R., Rammal, H., and Abom, M. Acoustical methods for investigating turbocharger flow instabilities. *SAE Technical Paper*, 2013, Paper no. 2013-01-1879, doi:10.4271/2013-01-1879.

Kabral, R., Rammal, H., Auriemma, F., Luppin, J. et al. A novel design for cruiser type motorcycle silencer based on micro-perforated elements. *SAE Technical Paper*, 2012, Paper no. 2012-32-0109, doi:10.4271/2012-32-0109.

Kabral, R., Rammal, H., and Lavrentjev, J. Acoustic studies of micro-perforates for small engine silencers. *SAE Technical Paper*, 2012, Paper no. 2012-32-0107, doi:10.4271/2012-32-0107.

Kabral, R., Rammal, H., Lavrentjev, J., and Auriemma, F. Acoustic Studies on Small Engine Silencer Elements. *SAE Technical Paper*, 2011, Paper no. 2011-32-0514, doi:10.4271/2011-32-0514.

#### Scholarships and awards

2012.04...2015.04 Early state researcher in the Marie Curie initial training network of "FlowAirS" ([www.flowairs.eu](http://www.flowairs.eu)).

2009 The "Silberauto AS" MSc studies scholarship in Tallinn University of Technology for excellent study results.

# Elulookirjeldus

## 1. Isikuandmed

Raimo Kabral  
1983.07.22 Tallinn Eesti  
Eesti kodakondsus  
raimo.kabral@mail.ee

## 2. Hariduskäik

Õppeasutus (nimetus lõpetamise ajal)	Lõpetamise aeg	Haridus (eriala/kraad)
Tallinna Tehnikaülikool	(2011)...	Tehniline akustika / doktoriõpe
Tallinna Tehnikaülikool	2010	Tootarendus ja tootmistehnika / magistrikraad

## 3. Keelteoskus (alg-, kesk- või kõrgtase)

Keel	Tase
Eesti	emakeel
Inglise	kõrgtase
Rootsi	algtase

## 4. Teadustegevus, sh tunnustused ja juhendatud lõputööd

### Publikatsioonid

Kabral, R., Abom, M., Bodén H., 7.6 Use of two-port acoustic data to investigate turbo-compressor surge, sisaldub artiklis: Aeroacoustics research in Europe: The CEAS-ASC report on 2013 highlights, *Journal of Sound and Vibration*, 2015, 340, 56.

Åbom, M., Kabral, R. Turbocharger noise - generation and control. *SAE Technical Paper Series*, 2014, 2014-10-25.

Kabral, R., Åbom, M. Investigation of flow-acoustic interaction in automotive turbocharger. *International Conference on Noise and*

*Vibration Engineering ISMA 2014, Louvain, Belgia, September 15-17, 2014.*

Kabral, R., Bodén, H., Elnady, T. Determination of liner impedance under high temperature and grazing flow conditions. *American Institute of Aeronautics and Astronautics conference Aviation 2014, Atlanta, USA, Juuni 16-20, 2014.*

Kabral, R., Du, L., Åbom, M., Knutsson, M. A compact silencer for the control of compressor noise. *SAE Int. Journal of Engines*, 2014, 7(3), 1572-1578, doi:10.4271/2014-01-2060.

Kabral, R., Åbom, M. Ongoing acoustics research in the KTH-Competence Centre for Gas Exchange. *Baltic-Nordic Acoustic Meeting 2014, Tallinn, Eesti Juuni 2-4, 2014.*

Kabral, R., Auriemma, F., Knutsson, M., Åbom, M. A new type of compact silencer for high frequency noise. *9th International DAAAM Baltic Conference, Tallinn, Eesti, Aprill 24-26, 2014.*

Kabral, R., Rammal, H., and Abom, M. Acoustical methods for investigating turbocharger flow instabilities. *SAE Technical Paper*, 2013, 2013-01-1879, doi:10.4271/2013-01-1879.

Kabral, R., Rammal, H., Auriemma, F., Luppin, J. et al. A novel design for cruiser type motorcycle silencer based on micro-perforated elements. *SAE Technical Paper*, 2012, 2012-32-0109, doi:10.4271/2012-32-0109.

Kabral, R., Rammal, H., and Lavrentjev, J. Acoustic studies of micro-perforates for small engine silencers. *SAE Technical Paper*, 2012, 2012-32-0107, doi:10.4271/2012-32-0107.

Kabral, R., Rammal, H., Lavrentjev, J., and Auriemma, F. Acoustic Studies on Small Engine Silencer Elements. *SAE Technical Paper*, 2011, 2011-32-0514, doi:10.4271/2011-32-0514.

### Stipendiumid

2012.04...2015.04 Noorteadur Euroopakomisjoni Marie Curie teadusvõrgustikus "FlowAirS" ([www.flowairs.eu](http://www.flowairs.eu)).

2009 AS Silberauto magistriõppe stipendium Tallinna Tehnikaülikooli Arengufondis eeskujulike õppetulemuste eest.

**DISSERTATIONS DEFENDED AT  
TALLINN UNIVERSITY OF TECHNOLOGY ON  
*MECHANICAL ENGINEERING***

1. **Jakob Kübarsepp**. Steel-Bonded Hardmetals. 1992.
2. **Jakub Kõo**. Determination of Residual Stresses in Coatings & Coated Parts. 1994.
3. **Mart Tamre**. Tribocharacteristics of Journal Bearings Unlocated Axis. 1995.
4. **Paul Kallas**. Abrasive Erosion of Powder Materials. 1996.
5. **Jüri Pirso**. Titanium and Chromium Carbide Based Cermets. 1996.
6. **Heinrich Reshetnyak**. Hard Metals Serviceability in Sheet Metal Forming Operations. 1996.
7. **Arvi Kruusing**. Magnetic Microdevices and Their Fabrication methods. 1997.
8. **Roberto Carmona Davila**. Some Contributions to the Quality Control in Motor Car Industry. 1999.
9. **Harri Annuka**. Characterization and Application of TiC-Based Iron Alloys Bonded Cermets. 1999.
10. **Irina Hussainova**. Investigation of Particle-Wall Collision and Erosion Prediction. 1999.
11. **Edi Kulderknup**. Reliability and Uncertainty of Quality Measurement. 2000.
12. **Vitali Podgurski**. Laser Ablation and Thermal Evaporation of Thin Films and Structures. 2001.
13. **Igor Penkov**. Strength Investigation of Threaded Joints Under Static and Dynamic Loading. 2001.
14. **Martin Eerme**. Structural Modelling of Engineering Products and Realisation of Computer-Based Environment for Product Development. 2001.
15. **Toivo Tähemaa**. Assurance of Synergy and Competitive Dependability at Non-Safety-Critical Mechatronics Systems design. 2002.
16. **Jüri Resev**. Virtual Differential as Torque Distribution Control Unit in Automotive Propulsion Systems. 2002.
17. **Toomas Pihl**. Powder Coatings for Abrasive Wear. 2002.
18. **Sergei Letunovitš**. Tribology of Fine-Grained Cermets. 2003.
19. **Tatyana Karaulova**. Development of the Modelling Tool for the Analysis of the Production Process and its Entities for the SME. 2004.
20. **Grigori Nekrassov**. Development of an Intelligent Integrated Environment for Computer. 2004.

21. **Sergei Zimakov.** Novel Wear Resistant WC-Based Thermal Sprayed Coatings. 2004.
22. **Irina Preis.** Fatigue Performance and Mechanical Reliability of Cemented Carbides. 2004.
23. **Medhat Hussainov.** Effect of Solid Particles on Turbulence of Gas in Two-Phase Flows. 2005.
24. **Frid Kaljas.** Synergy-Based Approach to Design of the Interdisciplinary Systems. 2005.
25. **Dmitri Neshumayev.** Experimental and Numerical Investigation of Combined Heat Transfer Enhancement Technique in Gas-Heated Channels. 2005.
26. **Renno Veinthal.** Characterization and Modelling of Erosion Wear of Powder Composite Materials and Coatings. 2005.
27. **Sergei Tisler.** Deposition of Solid Particles from Aerosol Flow in Laminar Flat-Plate Boundary Layer. 2006.
28. **Tauno Otto.** Models for Monitoring of Technological Processes and Production Systems. 2006.
29. **Maksim Antonov.** Assessment of Cermets Performance in Aggressive Media. 2006.
30. **Tatjana Barashkova.** Research of the Effect of Correlation at the Measurement of Alternating Voltage. 2006.
31. **Jaan Kers.** Recycling of Composite Plastics. 2006.
32. **Raivo Sell.** Model Based Mechatronic Systems Modeling Methodology in Conceptual Design Stage. 2007.
33. **Hans Rämmal.** Experimental Methods for Sound Propagation Studies in Automotive Duct Systems. 2007.
34. **Meelis Pohlak.** Rapid Prototyping of Sheet Metal Components with Incremental Sheet Forming Technology. 2007.
35. **Priidu Peetsalu.** Microstructural Aspects of Thermal Sprayed WC-Co Coatings and Ni-Cr Coated Steels. 2007.
36. **Lauri Kollo.** Sinter/HIP Technology of TiC-Based Cermets. 2007.
37. **Andrei Dedov.** Assessment of Metal Condition and Remaining Life of In-service Power Plant Components Operating at High Temperature. 2007.
38. **Fjodor Sergejev.** Investigation of the Fatigue Mechanics Aspects of PM Hardmetals and Cermets. 2007.
39. **Eduard Ševtšenko.** Intelligent Decision Support System for the Network of Collaborative SME-s. 2007.

40. **Rünno Lumiste**. Networks and Innovation in Machinery and Electronics Industry and Enterprises (Estonian Case Studies). 2008.
41. **Kristo Karjust**. Integrated Product Development and Production Technology of Large Composite Plastic Products. 2008.
42. **Mart Saarna**. Fatigue Characteristics of PM Steels. 2008.
43. **Eduard Kimmari**. Exothermically Synthesized B<sub>4</sub>C-Al Composites for Dry Sliding. 2008.
44. **Indrek Abiline**. Calibration Methods of Coating Thickness Gauges. 2008.
45. **Tiit Hindreus**. Synergy-Based Approach to Quality Assurance. 2009.
46. **Karl Raba**. Uncertainty Focused Product Improvement Models. 2009.
47. **Riho Tarbe**. Abrasive Impact Wear: Tester, Wear and Grindability Studies. 2009.
48. **Kristjan Juhani**. Reactive Sintered Chromium and Titanium Carbide-Based Cermets. 2009.
49. **Nadežda Dementjeva**. Energy Planning Model Analysis and Their Adaptability for Estonian Energy Sector. 2009.
50. **Igor Krupenski**. Numerical Simulation of Two-Phase Turbulent Flows in Ash Circulating Fluidized Bed. 2010.
51. **Aleksandr Hlebnikov**. The Analysis of Efficiency and Optimization of District Heating Networks in Estonia. 2010.
52. **Andres Petritšenko**. Vibration of Ladder Frames. 2010.
53. **Renee Joost**. Novel Methods for Hardmetal Production and Recycling. 2010.
54. **Andre Gregor**. Hard PVD Coatings for Tooling. 2010.
55. **Tõnu Roosaar**. Wear Performance of WC- and TiC-Based Ceramic-Metallic Composites. 2010.
56. **Alina Sivitski**. Sliding Wear of PVD Hard Coatings: Fatigue and Measurement Aspects. 2010.
57. **Sergei Kramanenko**. Fractal Approach for Multiple Project Management in Manufacturing Enterprises. 2010.
58. **Eduard Latõsov**. Model for the Analysis of Combined Heat and Power Production. 2011.
59. **Jürgen Riim**. Calibration Methods of Coating Thickness Standards. 2011.
60. **Andrei Surzhenkov**. Duplex Treatment of Steel Surface. 2011.
61. **Steffen Dahms**. Diffusion Welding of Different Materials. 2011.

62. **Birthe Matsi**. Research of Innovation Capacity Monitoring Methodology for Engineering Industry. 2011.
63. **Peeter Ross**. Data Sharing and Shared Workflow in Medical Imaging. 2011.
64. **Siim Link**. Reactivity of Woody and Herbaceous Biomass Chars. 2011.
65. **Kristjan Plamus**. The Impact of Oil Shale Calorific Value on CFB Boiler Thermal Efficiency and Environment. 2012.
66. **Aleksei Tšinjan**. Performance of Tool Materials in Blanking. 2012.
67. **Martinš Sarkans**. Synergy Deployment at Early Evaluation of Modularity of the Multi-Agent Production Systems. 2012.
68. **Sven Seiler**. Laboratory as a Service – A Holistic Framework for Remote and Virtual Labs. 2012.
69. **Tarmo Velsker**. Design Optimization of Steel and Glass Structures. 2012.
70. **Madis Tiik**. Access Rights and Organizational Management in Implementation of Estonian Electronic Health Record System. 2012.
71. **Marina Kostina**. Reliability Management of Manufacturing Processes in Machinery Enterprises. 2012.
72. **Robert Hudjakov**. Long-Range Navigation for Unmanned Off-Road Ground Vehicle. 2012.
73. **Arkadi Zikin**. Advanced Multiphase Tribo-Functional PTA Hardfacings. 2013.
74. **Alar Konist**. Environmental Aspects of Oil Shale Power Production. 2013.
75. **Inge Roos**. Methodology for Calculating CO<sub>2</sub> Emissions from Estonian Shale Oil Industry. 2013.
76. **Dmitri Shvarts**. Global 3D Map Merging Methods for Robot Navigation. 2013.
77. **Kaia Lõun**. Company's Strategy Based Formation of e-Workplace Performance in the Engineering Industry. 2013.
78. **Maido Hiiemaa**. Motion Planner for Skid-Steer Unmanned Ground Vehicle. 2013.
79. **Dmitri Goljandin**. Disintegrator Milling System Development and Milling Technologies of Different Materials. 2013.
80. **Dmitri Aleksandrov**. Light-Weight Multicopter Structural Design for Energy Saving. 2013.
81. **Henrik Herranen**. Design Optimization of Smart Composite Structures with Embedded Devices. 2014.

82. **Heiki Tiikoja**. Experimental Acoustic Characterization of Automotive Inlet and Exhaust System. 2014.
83. **Jelena Priss**. High Temperature Corrosion and Abrasive Wear of Boiler Steels. 2014.
84. **Aare Aruniit**. Thermoreactive Polymer Composite with High Particulate Filler Content. 2014.
85. **Dmitri Gornostajev**. Development of the Calculation Method for Barge Hull. 2014.
86. **Liina Lind**. Wear of PVD Coatings on Fineblanking Punches. 2014.
87. **Nikolai Voltšihhin**. Design and Technology of Oxides-Containing Ceramic-Based Composites. 2014.
88. **Aleksander Šablinski**. RANS Numerical Modelling of Turbulent Polydispersed Flows in CFB Freeboard. 2015.
89. **Tanel Aruväli**. Wireless Real-time Monitoring of Machining Processes. 2015.
90. **Andrei Bogatov**. Morphological Changes on Diamond and DLC Films During Sliding Wear. 2015.